

UNCLASSIFIED

AD NUMBER
ADB017905
NEW LIMITATION CHANGE
TO Approved for public release, distribution unlimited
FROM Distribution authorized to U.S. Gov't. agencies only; Specific authority; Marc 1976. Other requests shall be referred to Air Force Armament Labaoratory [DLJW], Eglin AFB, Florida 32542.
AUTHORITY
DoDD 5230.24, 18 Mar 1987.

THIS PAGE IS UNCLASSIFIED

(2)



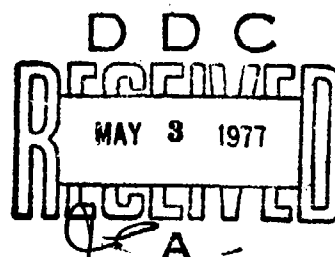
AFATL-TR-76-33

AD B017905

DICE-FAE ANALYSIS OF FUEL DISPERSAL AND DETONATION FROM A FUEL-AIR-EXPLOSIVE DEVICE

CALIFORNIA RESEARCH & TECHNOLOGY, INC.
6269 VARIEL AVENUE, SUITE 200
WOODLAND HILLS, CALIFORNIA 91367

MARCH 1976



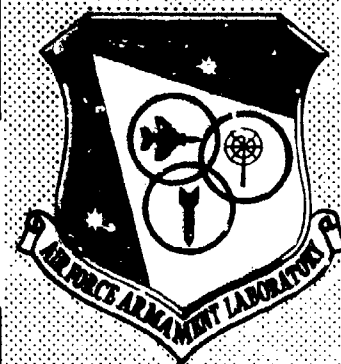
FINAL REPORT: OCTOBER 1975 - FEBRUARY 1976

Distribution limited to U. S. Government agencies only;
this report documents test and evaluation; distribution
limitation applied March 1976 . Other requests for
this document must be referred to the Air Force Armament
Laboratory (DLJW), Eglin Air Force Base, Florida 32542.

AIR FORCE ARMAMENT LABORATORY

AIR FORCE SYSTEMS COMMAND • UNITED STATES AIR FORCE

EGLIN AIR FORCE BASE, FLORIDA



AD No.
DDC FILE COPY

UNCLASSIFIED

SECURITY CLASSIFICATION OF THIS PAGE (When Data Entered)

REPORT DOCUMENTATION PAGE		READ INSTRUCTIONS BEFORE COMPLETING FORM	
1. REPORT NUMBER AFATL-TR-76-33	2. GOVT ACCESSION NO.	3. RECIPIENT'S CATALOG NUMBER	
4. TITLE (and Subtitle) DICE-FAE ANALYSIS OF FUEL DISPERSAL AND DETONATION FROM A FUEL-AIR-EXPLOSIVE DEVICE.		5. TYPE OF REPORT & PERIOD COVERED Final Report, 25 Oct 1975 to 25 Feb 1976	
6. AUTHOR(s) Martin Rosenblatt, Gordon E. Eggum, Kenneth N. Kreyenhagen		7. PERFORMING ORG. REPORT NUMBER 5080-1	
8. PERFORMING ORGANIZATION NAME AND ADDRESS California Research & Technology, Inc. 6269 Variel Avenue, Suite 200 Woodland Hills, California 91367		9. CONTRACT OR GRANT NUMBER(s) F08635-76-C-0082	
10. CONTROLLING OFFICE NAME AND ADDRESS Air Force Armament Laboratory Bombs and Warheads Branch Armament Development and Test Center Eglin AFB, Florida 32542		11. PROGRAM ELEMENT, PROJECT, TASK AREA & WORK UNIT NUMBER 25130714 Program Element 62602F	
12. MONITORING AGENCY NAME & ADDRESS (if different from Controlling Office) (12) 143 P.		13. REPORT DATE Mar 1976	
		14. NUMBER OF PAGES 136	
		15. SECURITY CLASS. (of this report) Unclassified	
		15a. DECLASSIFICATION/DOWNGRADING SCHEDULE	
16. DISTRIBUTION STATEMENT (of this Report) Distribution limited to U. S. Government agencies only; this report documents test and evaluation; distribution limitation applied March 1976. Other requests for this document must be referred to the Air Force Armament Laboratory (DLJW), Eglin Air Force Base, Florida 32542.			
17. DISTRIBUTION STATEMENT (of the abstract entered in Block 20, if different from Report)			
18. SUPPLEMENTARY NOTES Available in DDC.			
19. KEY WORDS (Continue on reverse side if necessary and identify by block number) Fuel-air-explosion Computational technique Detonation Particle break-up			
20. ABSTRACT (Continue on reverse side if necessary and identify by block number) Using the DICE-FAE code, a numerical solution was generated of both the dispersal and detonation phases for a BLU-73 liquid Fuel-Air-Explosive device. DICE-FAE is a two-dimensional, implicit, Eulerian, finite difference code which treats fuel-air mixtures, fuel droplet break-up, fuel phase changes, and fuel-air detonation dynamics. The fuel droplets flow through the air and interact with the air through drag and heat exchange mechanisms.			

DD FORM 1 JAN 73 1473 EDITION OF 1 NOV 65 IS OBSOLETE

UNCLASSIFIED

SECURITY CLASSIFICATION OF THIS PAGE (When Data Entered)

391223

UNCLASSIFIED

SECURITY CLASSIFICATION OF THIS PAGE(When Data Entered)

The cloud dispersal analysis started with initial conditions representing the fuel mass and burster products just after canister break-up. The FAE detonation analysis commenced with the calculated dispersed cloud fuel-air characteristics and with second event initiation by a centrally-located explosive charge.

Detailed comparisons from the DICE-FAE results and experimental data have not been completed, but the final calculated cloud dimensions and peak detonation pressures appear reasonable. The computational results also provide a detailed prediction in terms of space and time of the fuel concentrations during the dispersal phase and of the pressures and temperatures during the detonation phase.

UNCLASSIFIED

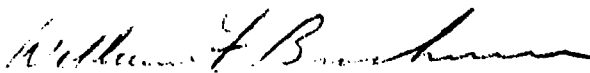
SECURITY CLASSIFICATION OF THIS PAGE(When Data Entered)

PREFACE

This final report describes analytical studies of the dispersal and detonation of liquid fuel-air devices, carried out by California Research & Technology, Inc., 6269 Variel Avenue, Suite 200, Woodland Hills, California 91367, under Contract F08635-76-C-0082 with the Air Force Armament Laboratory, Eglin Air Force Base, Florida 32542, from 25 October 1975 to 25 February 1976. The Air Force Armament Laboratory Project Officer was 1st Lieutenant Ronald S. Fry (DLJW).

This technical report has been reviewed and is approved for publication.

FOR THE COMMANDER



WILLIAM F. BROCKMAN, Colonel, USAF
Chief, Munitions Division

ADDITIONAL	
DTIC	White Section <input type="checkbox"/>
DDC	Buff Section <input checked="" type="checkbox"/>
UNANNOUNCED	<input type="checkbox"/>
JUSTIFICATION.....	
BY.....	
DISTRIBUTION/AVAILABILITY CODES	
Dist.	AVAIL. and/or SPECIAL
B	

TABLE OF CONTENTS

Section	Title	Page
I	SECTION I - INTRODUCTION	1
	1 Background and Objectives	1
	2 Summary of Results.	2
II	SECTION II- BASIC NUMERICAL METHOD AND ADAPTATIONS.	10
III	SECTION III-ANALYSIS OF FUEL CLOUD DISPERSION. . .	11
	1 DICE-FAE Initial Conditions	11
	2 Material Properties	16
	3 Fuel Droplet Breakup Model.	16
	4 Development of Cloud.	17
	5 Cloud Characteristics at End of Dispersal Phase (60 msec)	22
IV	SECTION IV - ANALYSIS OF FUEL CLOUD DETONATION. . .	25
	1 Model for Burning and Detonation.	25
	2 Initial Conditions for Detonation Phase . . .	30
	3 Cloud Detonation Processes.	30
V	SECTION V - CONCLUSIONS AND RECOMMENDATIONS. . .	48
	APPENDIX A - DETERMINATION OF THE INITIAL RELATIVE DENSITIES OF THE FUEL DROP GROUPS IN THE DICE-FAE SOLUTIONS.	50
	APPENDIX B - PROPERTIES OF AIR AND PROPYLENE OXIDE . .	53
	APPENDIX C - DROP BREAKUP MODEL.	38
	APPENDIX D - DENSITY CONTOUR PLOTS AND PARAMETER VERSUS TIME PLOTS FOR SOLUTION 5A PRIOR TO THE SECOND EVENT DETONATION.	65
	APPENDIX E - DENSITY CONTOUR PLOTS AND PARAMETER VERSUS TIME PLOTS FOR SOLUTION 5A SUBSEQUENT TO THE SECOND EVENT DETONATION.	87
	APPENDIX F - DICE-FAE SOLUTION 5B.	125
	APPENDIX G - DICE-FAE SOLUTION 5C.	132
	REFERENCES	135

LIST OF FIGURES

Figure	Title	Page
1	Air Velocity Vectors in Fuel Cloud at 30 msec. . . .	3
2	Total Fuel Density versus Radius at 3.8 ft Height. .	3
3	Total Fuel Density versus Height at 8.75 ft Radius .	3
4	Fuel Group 1 (0.01 cm diameter drops) Density Contours for DICE-FAE Case 5A at 60.0 msec	4
5	Pre-Detonation Fuel Cloud Dimensions for the DICE-FAE Solutions, and for the Experimental Work of Zabelka ¹ using an 83 lb Device	5
6	Distribution of Fuel in Different Droplet Sizes and as Vapor	6
7	Maximum Pressure Applied to the Ground Surface by the FAE Detonation as a Function of Radius. . . .	8
8	Impulse/Area Delivered by the SE Detonation to the Ground Surface by 77 msec (17 msec after the SE Detonation)	9
9	Schematic Diagram of the BLU-73 Canister Used in the DICE-FAE Solutions.	12
10	Initial Configuration for Problem FAE-5A	13
11	Air Velocity Vectors for DICE-FAE Case 5A at 5.0 msec.	18
12	Air Velocity Vectors for DICE-FAE Case 5A at 10.0 msec	19
13	Distribution of Fuel Drop Diameters in the Ex- panding Fuel Cloud Prior to the Second Event Detonation at 60 msec.	21

LIST OF FIGURES (CONTINUED)

Figure	Title	Page
14	Air Velocity Vectors for DICE-FAE Case 5A at 60.0 msec	23
15	Fuel to Air Ratio vs Radius in the Fuel Cloud at 60 msec (just prior to SE initiation) for Heights of .25 ft, 2.75 ft, 4.25 ft, and 5.75 ft . .	24
16	Pressure and Temperature of the Detonation Shock in a Propylene Oxide-Air Mixture, as a Function of the Percent Propylene Oxide (TIGER code data).	26
17	Energy Released in Burning per Gram of Propylene Oxide Mixture vs the Fuel Air Ratio from TIGER Output and as Assumed in the DICE Model.	27
18	Air Velocity Vectors for DICE-FAE Case 5A at 61.5 msec.	31
19	Air Velocity Vectors for DICE-FAE Case 5A at 64.0 msec.	32
20	Air Velocity Vectors for DICE-FAE Case 5A at 68.0 msec.	33
21	Air Velocity Vectors for DICE-FAE Case 5A at 77.0 msec.	34
22	Density History During the Second Event Deton- ation of the 100 μ Fuel Drops and the Fuel Vapor, Taken at a Height of 4 ft and a Radius of 5 ft . .	36
23	Fuel Drop Density Contours for DICE-FAE Case 5A at 61.5 msec	37
24	Air Temperature Contours for DICE-FAE Case 5A at 61.5 msec	38
25	Fuel Vapor Density Contours for DICE-FAE Case 5A at 61.5 msec, Showing the Regions of Activity Associated with the Detonation Front .	39
26	Fuel Vapor Density Contours for DICE-FAE Case 5A at 77.0 msec	40

LIST OF FIGURES (CONCLUDED)

Figure	Title	Page
27	Distribution of Fuel Drop Diameters in the Fuel Cloud Subsequent to the Second Event Initiation at 60 msec	41
28	Ground Level Pressures at 1, 5, and 10 Ft Radius Versus Time Following the Second Event Initiation at 60 msec . . .	43
29	Ground Level Pressures at 15, 20, and 25 Ft Radius Versus Time Following the Second Event Initiation at 60 msec . . .	44
30	Ground Level Pressures at 30, 35, 40, and 50 Ft Radius Versus Time Following the Second Event Initiation at 60 msec	45
31	Peak Pressure in the Detonation Front vs Radius for DICE Solution 5A Compared to an Estimate of These Pressures Based on Output from the TIGER Code	46

LIST OF TABLES

Table	Title	Page
1	Initial Distribution of Energy for the DICE-FAE Analysis.	14
2	Fuel Particle Size Groups.	15

SECTION I

INTRODUCTION

1. BACKGROUND AND OBJECTIVES

Liquid FAE (Fuel-Air-Explosive) devices are weapons which disperse a liquid fuel into a relatively extensive cloud using a small explosive charge. After the cloud has expanded enough to provide a suitable fuel/air mixture ratio, it is detonated. The fuel is initially contained in a canister with the dispersing explosive (burster charge) at the center. The detonation of the cloud (usually referred to as the second event, or SE) is initiated by one or more small explosive charges injected into the cloud. Ideally, the dispersed fuel should be totally consumed in the FAE detonation. Fuel-rich areas (in which some of the fuel doesn't burn because the oxygen is exhausted) or fuel-lean areas (with low fuel/air ratios) within the cloud are undesirable.

Developmental work on FAE devices to date has been generally confined to experimental programs, with computer modeling of the process having been attempted only for very specialized cases.

The purpose of the present exploratory effort has been to develop and use numerical simulation models to examine the processes involved in both the cloud dispersion and cloud detonation (second event) phases of a specific FAE event.

2. SUMMARY OF RESULTS

Using the DICE-FAE code, solutions were generated of both the fuel cloud dispersal and detonation phases for an FAE device simulating the BLU-73. DICE-FAE is a two-dimensional, implicit, Eulerian, finite difference code capable of treating air-fuel droplet mixtures, fuel droplet breakup, and fuel-air detonation.

The cloud dispersal analysis started with initial conditions representing the fuel mass and burster products just after canister breakup, and followed the subsequent cloud dispersal until 60 msec. The cloud detonation analysis started with the cloud characteristics at 60 msec and with second event initiation by a centrally-located explosive charge at that time. This analysis extended through cloud detonation and to 77 msec.

The principal results and conclusions are summarized here.

- (a) *The flow field within the expanding fuel cloud leads to severe variations in the fuel droplet density. Figure 1 shows the air velocity field at 30 msec. Rapid radial expansion of the fuel mass near the meridian plane of the device causes vortices to form above and below this plane. Figures 2 and 3 show the total fuel density along planes or surfaces which pass between and through the vortices. Fuel within the vortices cannot escape because of the circular flow. Consequently these are regions of high fuel concentration. Fuel between the vortices is swept to larger radii by the rapid flow. This causes an accumulation of fuel at the larger radii, forming a third region of high fuel concentration. Figure 4 shows density contours for the 90 percent of the fuel mass which consists of small droplets (0.01 cm) at the end of the fuel dispersal phase at 60 msec. Large gradients are seen to persist.*
- (b) *Cloud dimensions predicted by DICE-FAE at the end of the fuel dispersal phase compare favorably with experimental observations. Figure 5 compares the DICE-FAE cloud dimensions for the 72-lb BLU-73 FAE device with Zabelka's (Reference 1) experimental observations for an 83-lb device. Good agreement is seen.*
- (c) *Fuel drop breakup by aerodynamic shattering is effective in reducing all but the very largest fuel drops to small (0.01 cm) droplets. Figure 6 plots the time-history of distribution of fuel mass in drops of different size ranges (and in fuel vapor). By 10 msec all fuel drops with initial diameters smaller than 1 cm have been completely shattered into 0-0.2 cm droplets. At the time of the second event initiation (60 msec) 90 percent of the fuel mass in the cloud consists of 0-0.2 cm droplets. About 3 lbs of the fuel has impacted the ground.*
- (d) *A relatively large, centrally-located second event initiator charge is required to detonate the cloud, since fuel concentrations near the axis are relatively low at 60 msec. A 70 gr initiator proved inadequate, and the detonation would not propagate through the cloud. A 350 gr initiator was then used, and the cloud was successfully detonated.*

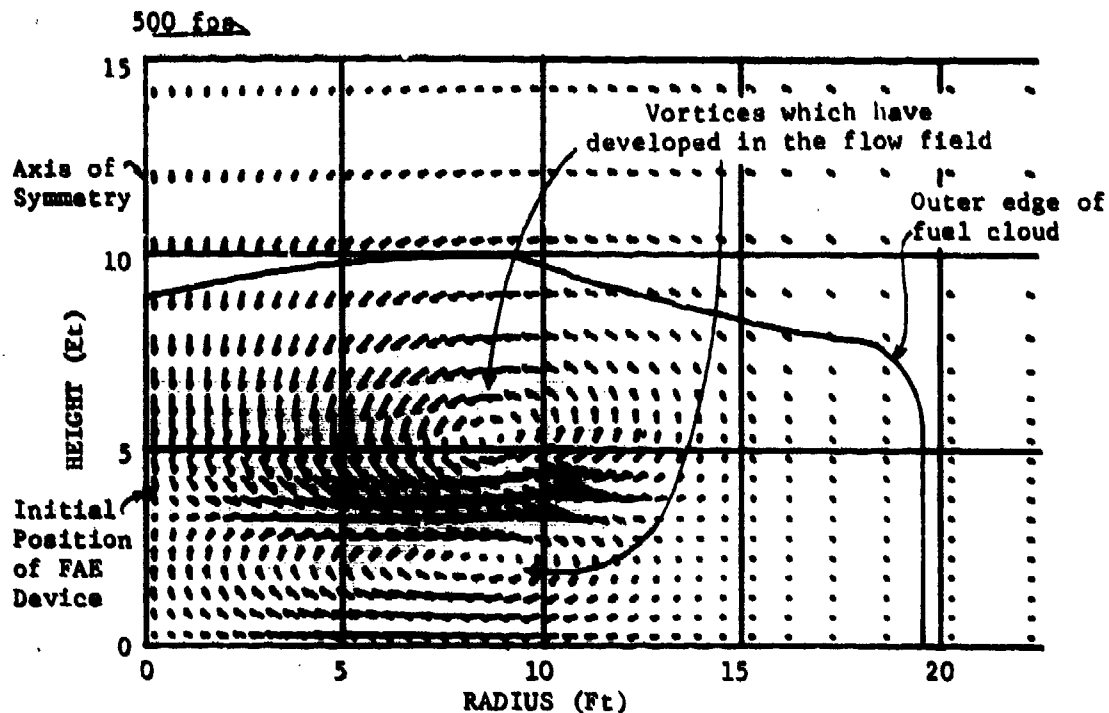


Figure 1. Air Velocity Vectors in Fuel Cloud at 30 msec

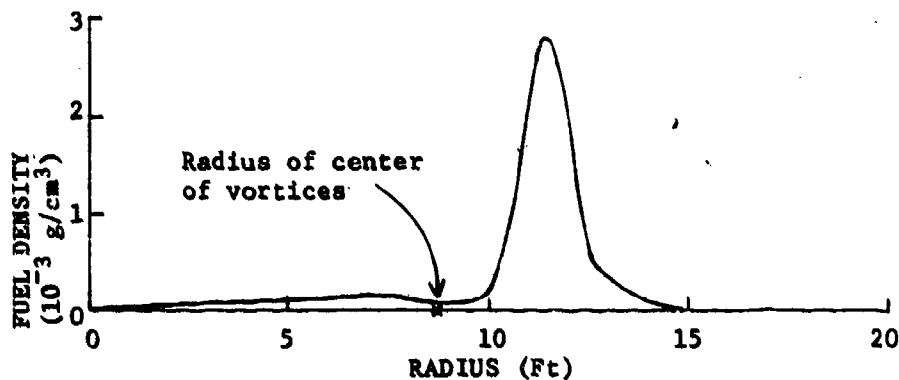


Figure 2. Total Fuel Density versus Radius at 3.8-ft Height

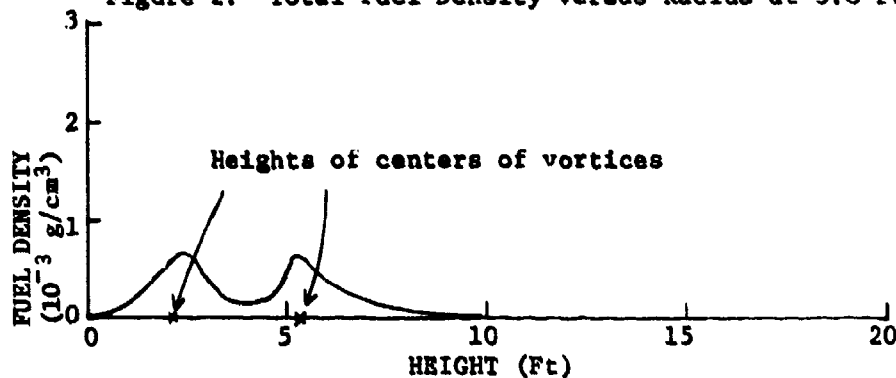


Figure 3. Total Fuel Density versus Height at 8.75-ft Radius

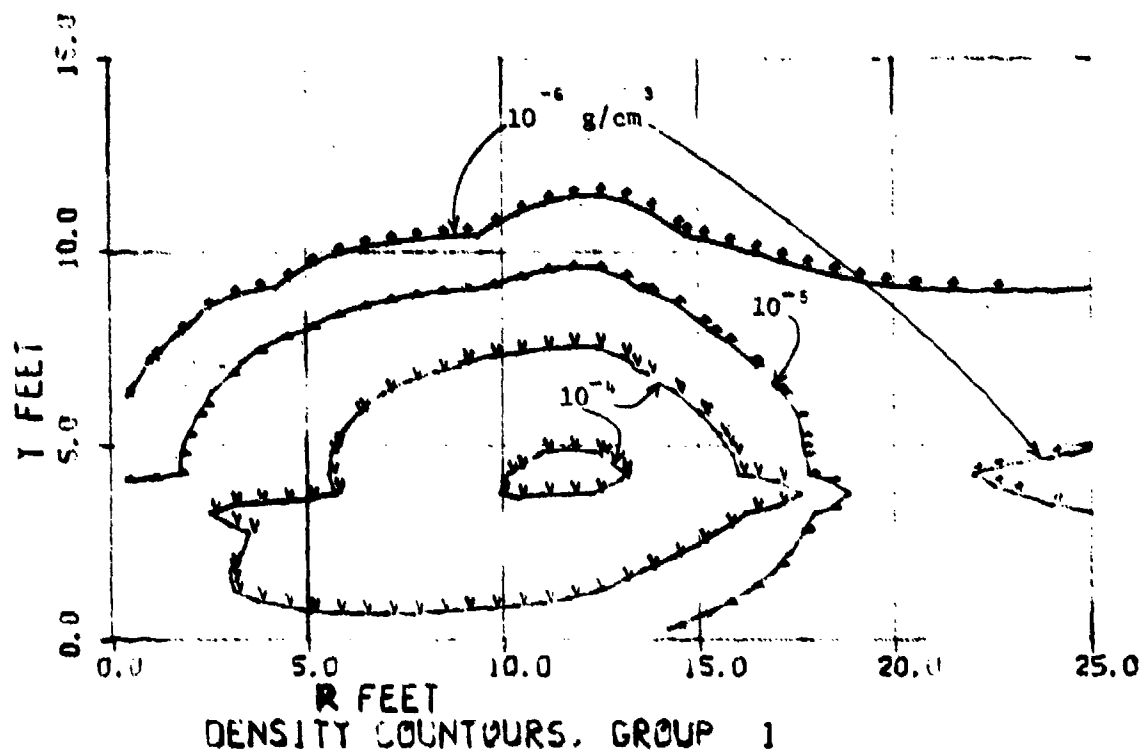


Figure 4. Fuel Group 1 (0.01 cm Diameter Drops) Density Contours
for DICE-FAE Case 5A at 60.0 msec

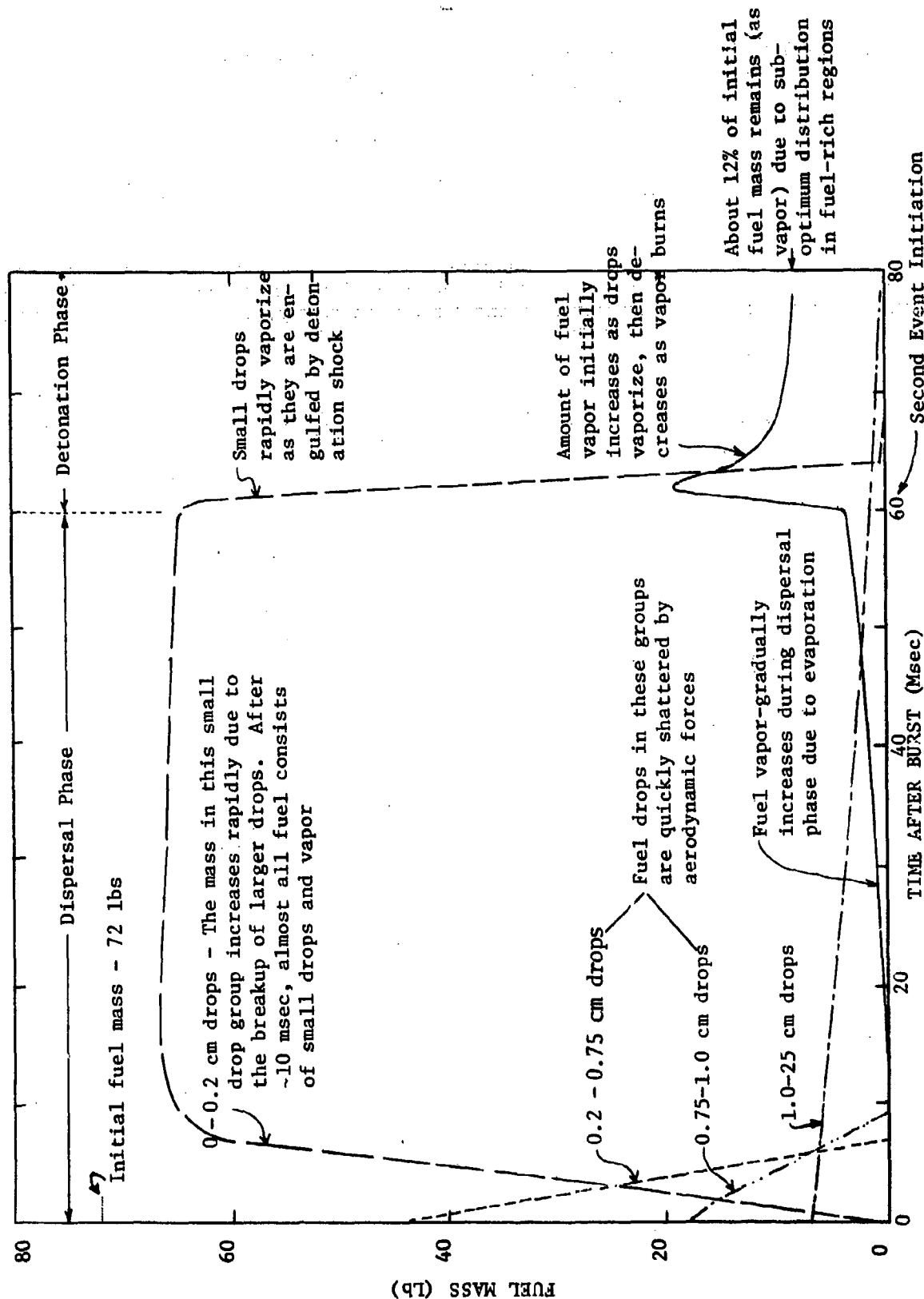


Figure 6. Distribution of Fuel in Different Droplet Sizes and as Vapor

- (e) *During cloud detonation, fuel droplets are first vaporized as the detonation shock arrives; detonation then occurs until the locally available fuel or oxygen is exhausted. The portion of Figure 6 after 60 msec shows the rapid vaporization of fuel droplets during the period from 60 to 63 msec. The vapor burns rapidly; the detonation is complete by about 67 msec, although residual fuel continues to burn more slowly as oxygen subsequently flows into the cloud. The following tabulation shows the disposition of the initial 72 lbs of fuel in the FAE device:*

59.4 lbs	(83 percent)	- detonates or rapidly burns by 77 msec
3.1 lbs	(4 percent)	- impacts on ground
0.6 lb	(1 percent)	- remains as large (>1 cm) drops
8.9 lbs	(12 percent)	- remains as fuel vapor

(The remaining fuel vapor may continue to burn.)

- (f) *The maximum pressure experienced on the ground during the FAE detonation was 200 psi at about 10-ft radius; impulse delivered to the ground was a maximum at the axis and dropped sharply with increasing radius. Figures 7 and 8 show the peak pressure and impulse on the ground versus radius.*
- (g) *DICE-FAE can be a cost-effective aid in the development and evaluation of improved FAE devices and concepts. While more definitive experimental comparisons are desirable to improve and validate the models, the existing DICE-FAE code provides credible predictions of the complex, interacting processes involved in an FAE event. As such, the technique can be used to examine the effects on cloud dispersal and detonation of major design variables, such as*
- fuel-to-burster ratio
 - early-time fuel droplet size distribution
 - altitude and velocity of canister at time of burst
 - properties of fuel which affect breakup and vaporization
 - location and time of SE initiation
 - properties of SE initiator

The technique can also be used to model and evaluate innovative new FAE concepts, such as those involving simultaneous initiation of the cloud everywhere throughout its volume.

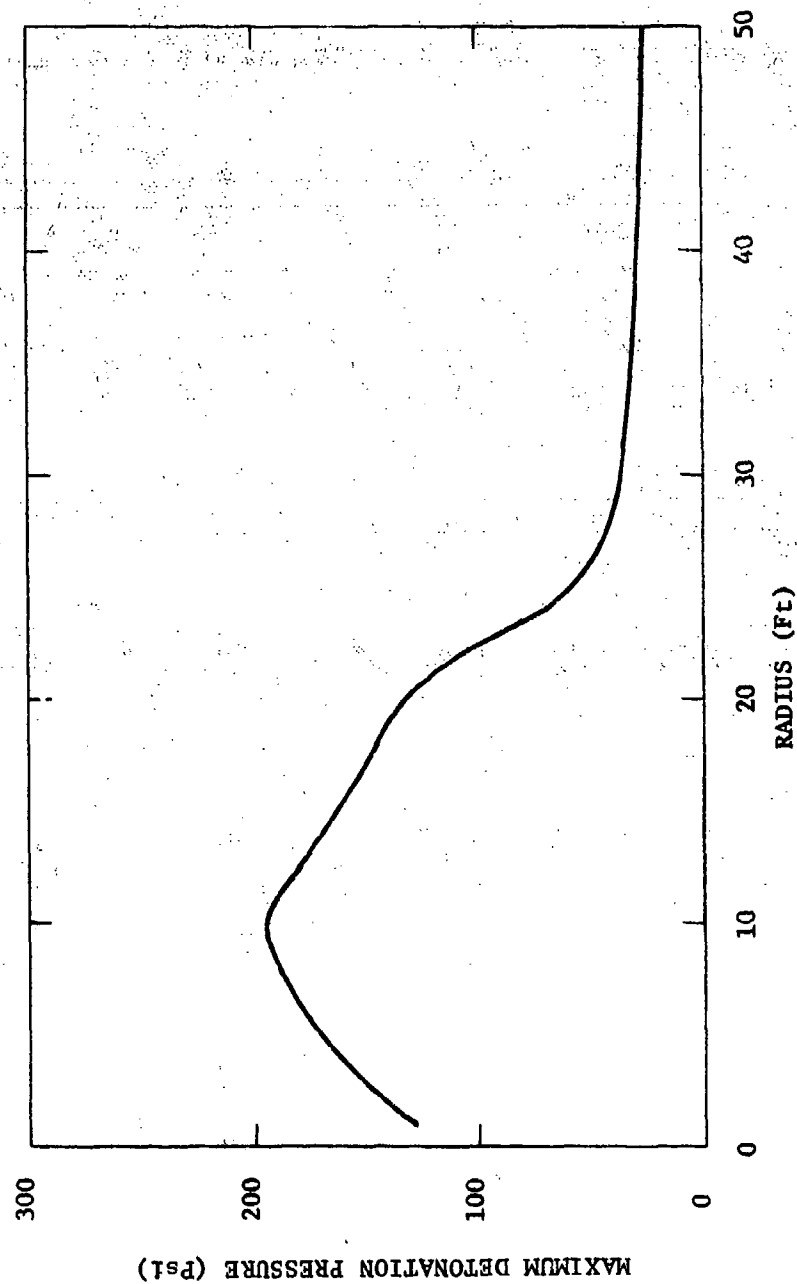


Figure 7. Maximum Pressure Applied to the Ground Surface by the FAE Detonation as a Function of Radius

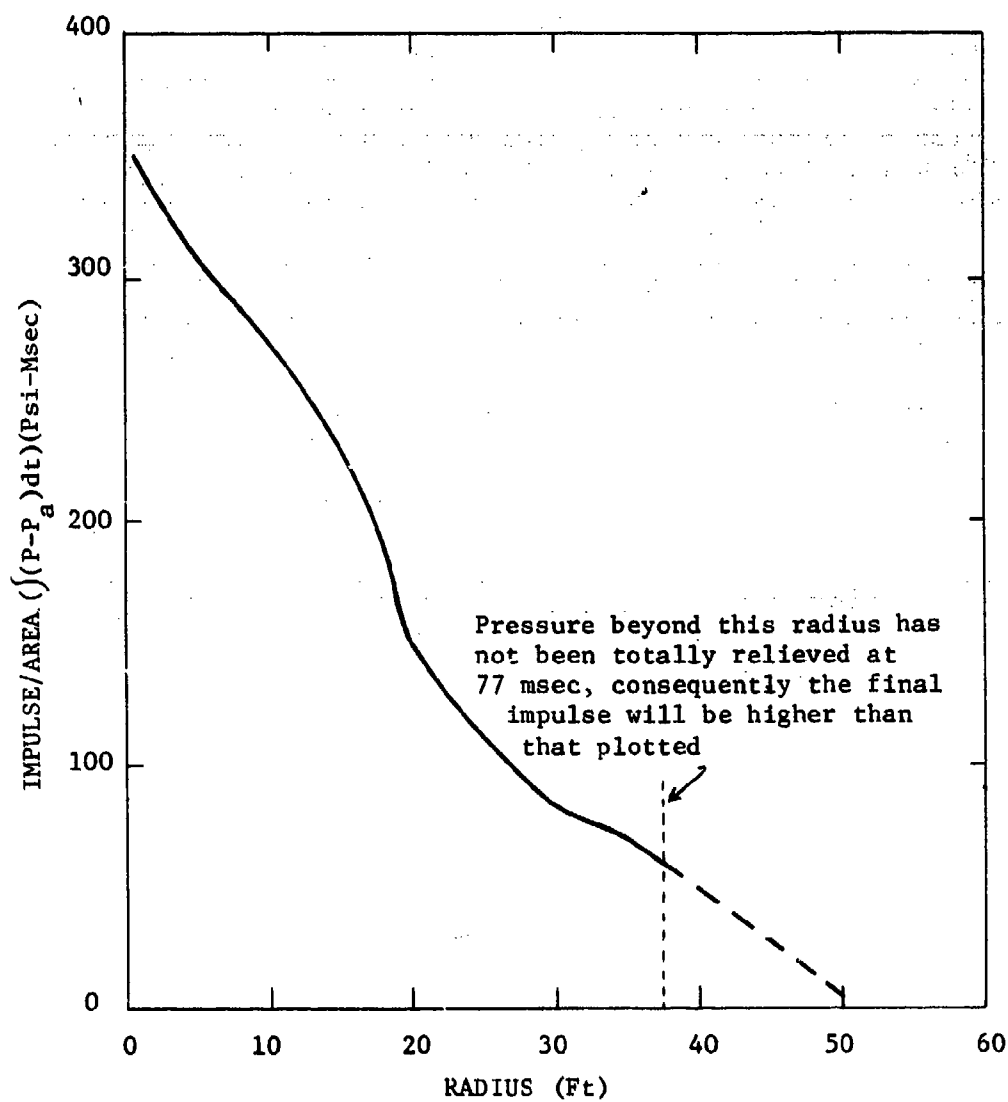


Figure 8. Impulse/Area Delivered by the SE Detonation to the Ground Surface by 77 msec (17 msec after the SE Detonation)

SECTION II

BASIC NUMERICAL METHOD AND ADAPTATIONS

The basic numerical code used for the FAE analysis was DICE-II, a 2-D implicit Eulerian finite difference technique which treats fluid-particle mixtures. DICE-II was originally developed (under sponsorship of the Defense Nuclear Agency) to provide a method for analyzing the dynamics of the lofted dust and water droplet clouds which develop from nuclear explosions on or near the surface. DICE-II treats particle size groups as continua which can flow independently through the Eulerian grid. Mutual momentum and thermal interactions between the particles and the air are treated through drag and heat exchange models. Phase changes (solid-liquid-vapor) can take place.

For application to FAE analyses, adaptations were made in the basic DICE-II code to allow treatment of:

- (1) stripping or breakup of liquid drops into smaller droplets as they are acted on by aerodynamic forces, and
- (2) burning of the fuel, with development of a detonation wave if the local energy release rate is sufficient.

SECTION III

ANALYSIS OF FUEL CLOUD DISPERSION

Three DICE-FAE analyses of an FAE event were performed. These are designated as Solutions 5A, 5B, and 5C. This report is primarily devoted to Solution 5A, which treats the fuel cloud expansion, the second event initiation at 60 msec, and the subsequent detonation of the fuel cloud. Solution 5B is a partial solution which treats the initiation of the second event by a smaller (less energetic) initiator. This smaller initiator proved inadequate, and the detonation did not propagate. Solution 5C used a second-order numerical differencing scheme in treating the dispersion of the fuel. Solutions 5B and 5C are discussed in Appendices F and G.

1. DICE-FAE INITIAL CONDITIONS

The DICE-FAE solutions analyzed the functioning of the BLU-73 FAE device which is shown schematically in Figure 9. The canister was assumed to be stationary, in a vertical orientation, with its base 3 ft off the ground.

The solutions begin at a point in the FAE event when the canister has fragmented and the fuel has expanded to the point where it is no longer a continuous mass, but rather can be considered to be a closely packed collection of fuel drops. Figure 10 shows the initial conditions used to describe the fuel disposition and velocity at the beginning of the DICE-FAE analysis. There are three regions.

Region I, which corresponds to the burster detonation products, was given an initial density of 0.0019 g/cm^3 . This density gives a total mass of the simulated detonation products of 0.72 lb (the initial weight of the burster).

The main mass of the fuel charge is in Region II, which has a volume of $4.2 \times 10^4 \text{ in}^3$. Since the fuel charge in the canister had an original volume of approximately 3300 in^3 , the average fuel density at the beginning of the DICE-FAE solution would have dropped by a factor of about $\frac{4.2 \times 10^4}{3300} = 13$.

It is reasonable to assume that this much expansion would be associated with complete "break up" of the fuel into drops.

Region III is a transition region around the main mass of fuel. It consists of air and fuel in a mixture of declining richness.

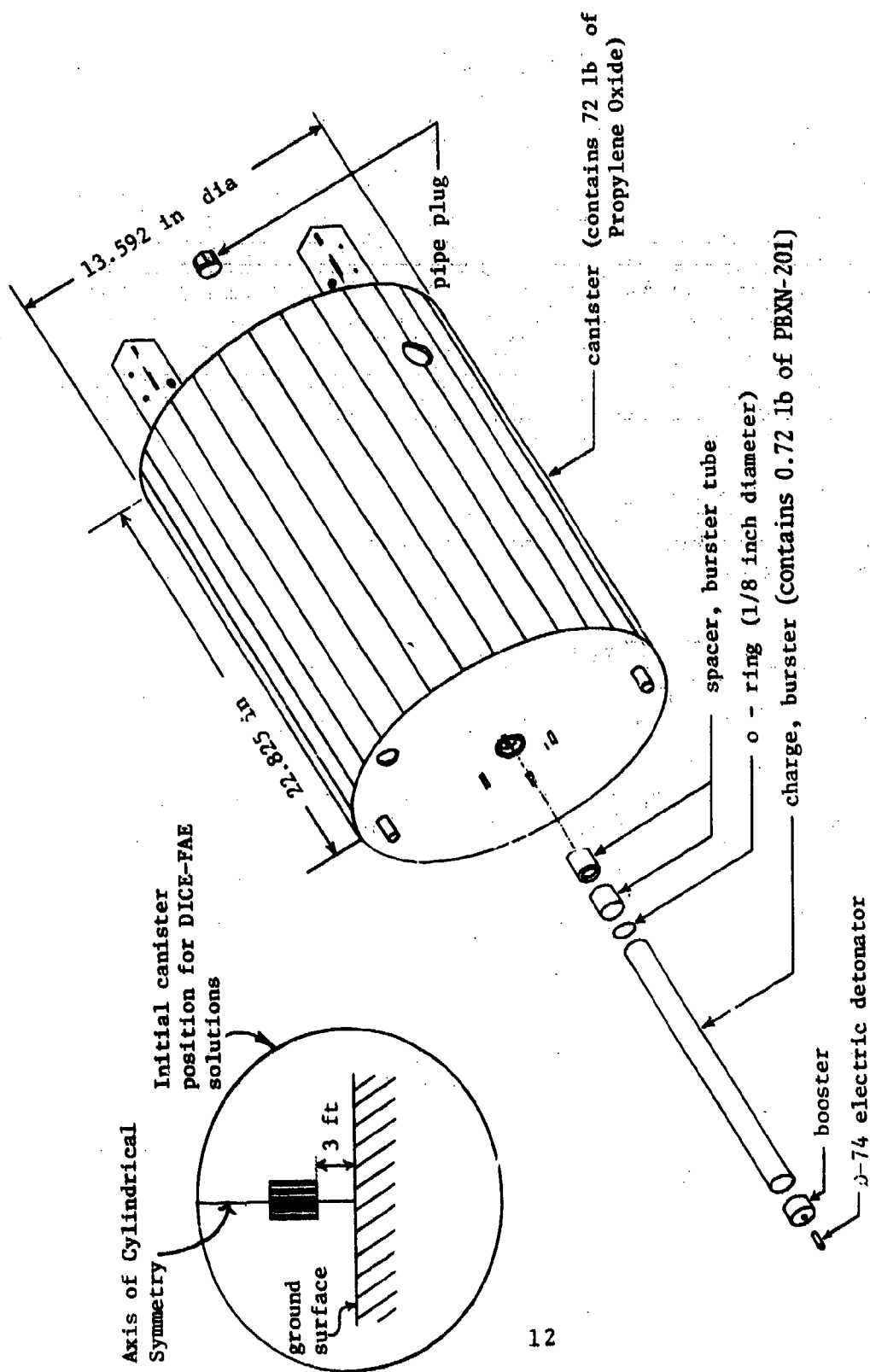


Figure 9. Schematic Diagram of the BLU-73 Canister Used in the DICE-FAE Solutions

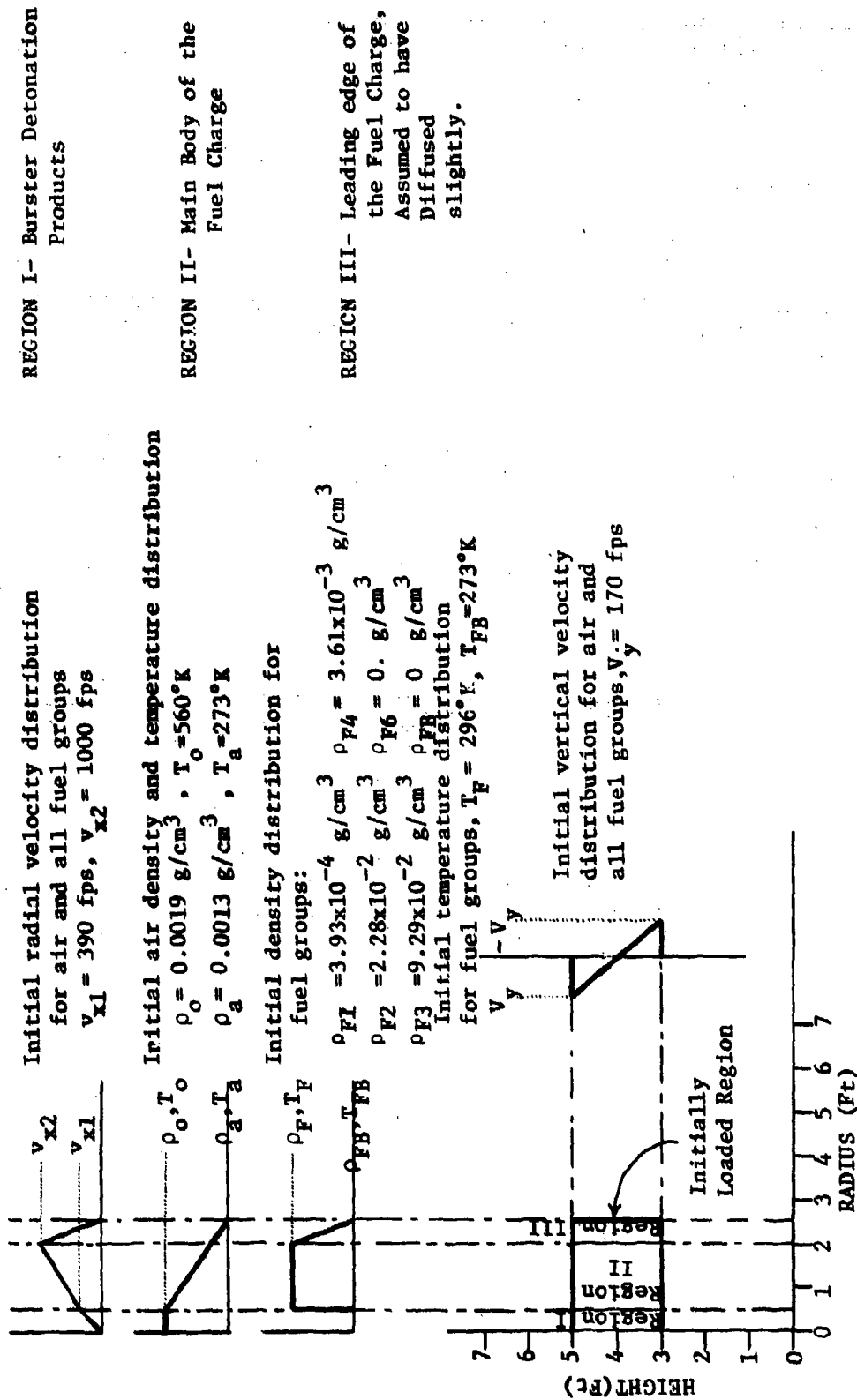


Figure 10. Initial Configuration for Problem FAE-5A

The total energy E_T available during the expansion phase of the FAE event was determined by assuming that the 0.72 lb of PBXN-201 explosive used as the burster yields 1000 calories per gram of explosive, or $E_T = 32.7 \times 10^4$ cal. This energy was initially distributed as shown in Table 1.

TABLE 1. INITIAL DISTRIBUTION OF ENERGY FOR THE DICE-FAE ANALYSIS

	Internal Energy (Percent)	Kinetic Energy (Percent)
Burster Detonation Products	15	3
Fuel Drops	12	70

This distribution was deduced from the following considerations:

- (a) Kot et al (Reference 2) provide 1-D code solutions which give the energy distribution in spherical burster devices as a function of time until the case ruptures. These solutions show that at the time of case rupture the kinetic energy of the liquid around the spherical burster is about 40 percent of the total energy. When the case ruptures and the pressure in the liquid is relieved, the KE of the liquid would be expected to increase at the expense of its internal energy; consequently the final kinetic energy of the fuel would be expected to be well above 40 percent of the total. (Kot ran one solution out to twice the time of case rupture, at which point the fuel kinetic energy accounted for 60 percent of the total energy.)
- (b) From flash x-rays of the expansion of liquids around spherical burster devices, Abrahamson (Reference 3) has generated data which suggest that the expanding annulus of fuel (after case breakup) does not increase in thickness until the annulus is relatively large. This implies (1) that the bulk density of the annulus is dropping as it expands, and (2) that at early times, all regions of the annulus are moving out at about the same speed. Zabelka (Reference 1) has published experimental results indicating that the outer edge of the expanding fuel from an 83-lb cylindrical FAE device is moving at something over 1000 fps at early times. If the entire fuel cloud for

the BLU-73 device were to be moving at 1000 fps, virtually all of the burster energy would reside in the fuel as kinetic energy.

As a consequence of these considerations, it was decided to put about 70 percent of the burster energy into fuel kinetic energy at the start of the DICE-FAE analysis, with the remainder divided approximately even between internal energy of the fuel and the burster detonation products.

Six fuel groups were used in the solutions. Four groups represented specified ranges of fuel drop diameters for liquid fuel; one represented fuel vapor; one represented combustion products from fuel/air burning. Table 2 lists the characteristics, and the fraction of the total initial fuel mass contained in each group. The total mass of fuel was 72 lbs.

TABLE 2. FUEL PARTICLE SIZE GROUPS

Group	Range of drop diameters (Cm)	Representative drop diameter ^a (Cm)	Percent of initial fuel mass in group
1	0 - 0.2	0.01 ^b	1
2	0.2 - 0.75	0.48	63
3	0.75 - 1.0	0.88	26
4	1.0 - 25.0	13.0	10
5	Combustion products from fuel/air burning		0
6	Fuel vapor		0

The large representative diameter assigned to the drops in Group 4 is not physically realistic; this group was included in an attempt to determine the effect very large drops might have on fuel cloud development.

^a "Representative drop diameter" refers to the specific drop size used to characterize all drops in a group for purposes of aerodynamic and thermodynamic interactions.

^b Within about 10 msec, Group 1 was populated primarily by the droplet "fragments" of larger drops which had broken up due to aerodynamic forces. These droplets are very small, consequently the 0.01 cm representative size was chosen.

The initial distribution of particles in the first four fuel groups was determined by assuming that the fuel drop diameters have a truncated normal distribution. The standard deviation of the distribution was specified by requiring that 10 percent of the total initial fuel mass resided in Group 4. The details of these calculations are presented in Appendix A.

The air in which the FAE event took place was at normal atmospheric pressure, temperature, and density. The lithostatic pressure variation with altitude was established, and the solutions were run with the effects of gravity included.

2. MATERIAL PROPERTIES

For each material treated in a DICE-FAE solution, it is generally necessary to define the following relationships:

- a pressure-volume-energy equation of state $P=P(\rho, e)$, where P is the pressure, ρ is the density, e is the specific internal energy,
- a caloric equation of state, $T=T(\rho, e)$, and
- a phase diagram in the P - T plane.

Additional material data may be required for any special models which are employed. For example, the liquid drop breakup model requires a critical Weber number, viscosity, and surface tension for the drop material.

In the solutions reported herein, the above properties were required for propylene oxide (the fuel) and air. Appendix B contains the specific properties used.

3. FUEL DROPLET BREAKUP MODEL

Fuel drops ejected at high speeds from the FAE canister are acted on by aerodynamic forces which cause stripping or breakup into smaller droplets. These breakup processes are important in the dispersion of an FAE cloud, (since the drag on particles, and hence the maximum extent of the cloud, depends on the particle sizes) and in the detonation of the cloud (since breakup will establish the particle size distribution at the time of the second event initiation).

The DICE-FAE code can accommodate any breakup model whose parameters are carried as cell variables in the solution. The specific breakup model chosen for the present DICE-FAE solution is described in Appendix C. This model is applied to each particle size group in each computational cell each time step.

Given the velocities of the particles relative to the air in the cell, the model determines whether drops in each size range are breaking up, and if so, the rate of their breakup and the size distribution of the resulting new droplets. As a fraction of the particles in a given size range break up, their "fragments" go into appropriate smaller size ranges.

4. DEVELOPMENT OF CLOUD

The first phase of DICE-FAE Solution 5A covered the expansion or fuel dispersion processes, and covered a 60-msec time interval. The dynamics of the development of the fuel cloud during this phase were strongly affected by (1) drop breakup due to aerodynamic interactions with the air, and (2) evaporation from fuel drops to form fuel vapor.

Figures 11, 12, and 1 are plots of the air velocity vectors throughout the developing cloud at 5, 10, and 30 msec. At early times, the expanding cloud of fuel drops drags air out of the region near the device, thereby locally reducing the pressure. As a consequence, a partially converging flow is seen at 5 msec (Figure 11) of air from above and below the FAE device towards the meridian plane (i.e., the horizontal plane at about 4-ft height which passes through the center of the canister). By 10 msec (Figure 12) this vertical flow convergence towards the meridian plane is beginning to produce outward flow in that plane. The outward flow is very pronounced at 30 msec (Figure 1). Two strong vortices form just above and below the meridian plane. These flow patterns cause large local variations in fuel concentrations; the vortices themselves are fuel-rich, while the regions immediately between the vortices are fuel-poor. A very fuel-rich region occurs near the meridian plane at ranges just beyond the vortices. Figures 2 and 3 which give the total fuel density along the vertical surface between the centers of the vortices (at $r=8.75$ ft) and along the horizontal plane at 3.8-ft height ($y=3.8$ ft) show the magnitude of the local variations in fuel concentration. The variations develop for the following reasons:

- The air vortices initially form in fuel-rich regions wherein the fuel exists primarily in the form of vapor and small drops. Since vapor and small drops essentially flow with the air, the fuel which gets caught in the vortices is "trapped" there, i.e., the circular flow field in the vortex region allows almost no material to flow out.

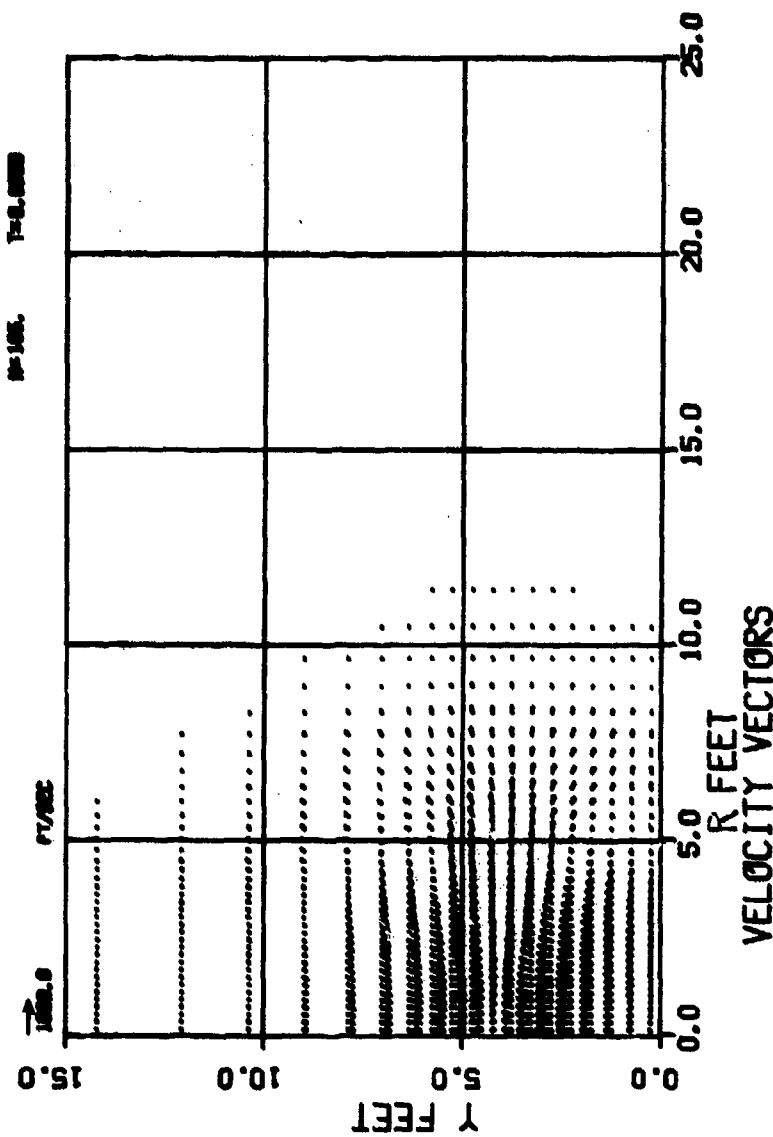


Figure 11. Air Velocity Vectors for DICE-PAE Case 5A at 5.0 Msec

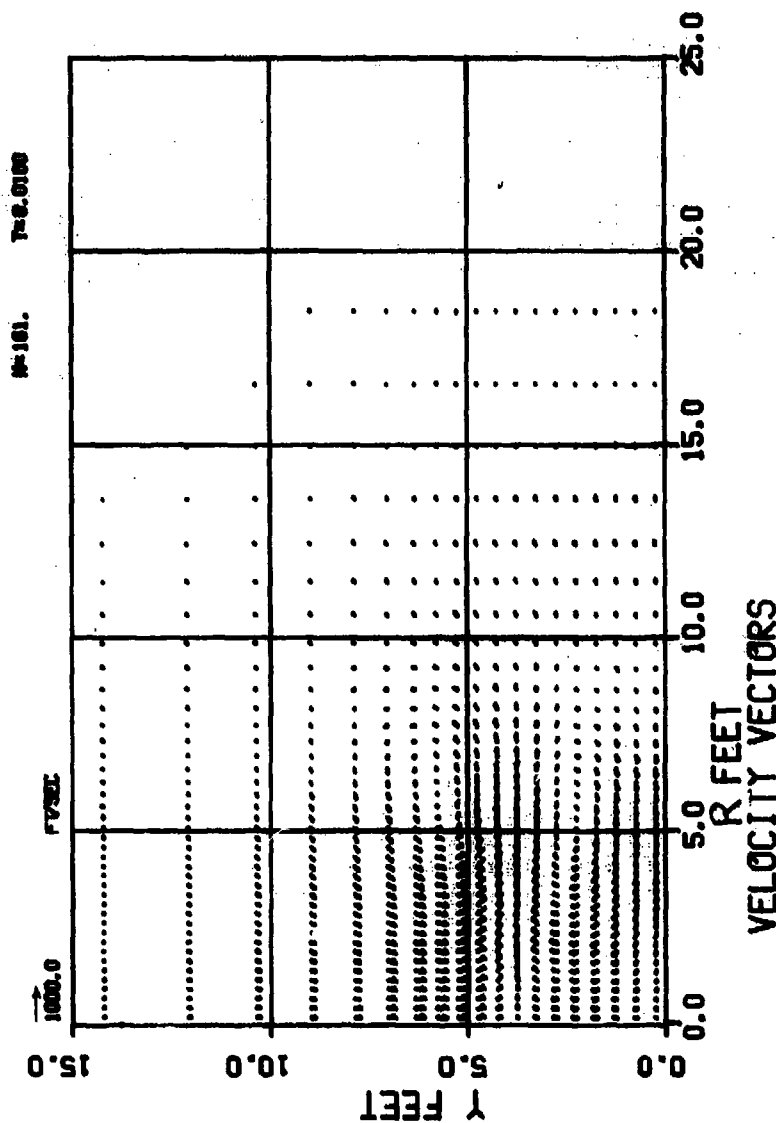


Figure 12. Air Velocity Vectors for DICE-FAE Case 5A at 10.0 Msec

- After the vortices form, the region between them is characterized by large horizontal velocities and small vertical velocities. Air/fuel in this region flows rapidly from small to large radii. The air/fuel, however, originates largely in fuel-poor regions above and below the meridian plane; consequently the fuel density in the inter-vortex region remains low. The fuel flowing out of the inter-vortex region slows down and begins to "pile up". The result at late times is a "hole" in the center of the fuel cloud, surrounded by 3 annular high concentration regions.

During the expansion of the cloud, fuel drop breakup by aerodynamic shattering quickly reduces all but the very largest drops to small droplets. This is clearly seen in Figure 13. By 10 msec, all of the particles in Group 2 (0.2 to 0.75 cm) and in Group 3 (0.75 to 1.0 cm) have broken up, and are in Group 1 (0 to 0.2 cm).

Appendix D contains fuel concentration contours for the droplet size ranges at different times during the cloud development. In addition, Appendix D contains plots of the air pressure versus time at several stations within or near the cloud. Pressures are generally low throughout the field during the fuel dispersions. At a point 5 ft away from the canister and level with it, the peak overpressure is only about 5 psi (Figure D-13). At 40 ft, the overpressure is less than 1 psi (Figure D-14).

Appendix D also contains plots of density histories of the fuel drop groups at stations in the meridian plane. The phenomena mentioned earlier, whereby large drops break up into small drops and all drops evaporate to form vapor, are apparent in these plots. In addition, the effects of the radial motion of the fuel cloud are superimposed upon these processes. At station 23 (Figure D-17), at a radius of 5 ft, the 100 micron particles reach the relatively high peak density of $3 \times 10^{-3} \text{ g/cm}^3$ at about 5 msec. By the time the second event is initiated, however, the radial flow of the cloud has reduced the density to $\sim 10^{-4} \text{ g/cm}^3$. Station 25 (Figure D-20) at 15 ft, is relatively devoid of fuel until 40 msec; after that time fuel vapor and 0.01 cm particles flow into the region at such a rate that by 60 msec, when the second event is initiated, the fuel density at 15 ft has reached the value of 10^{-3} g/cm^3 .

(See Figure 27 for the mass distribution after the initiation of the dispersed cloud at 60 msec)

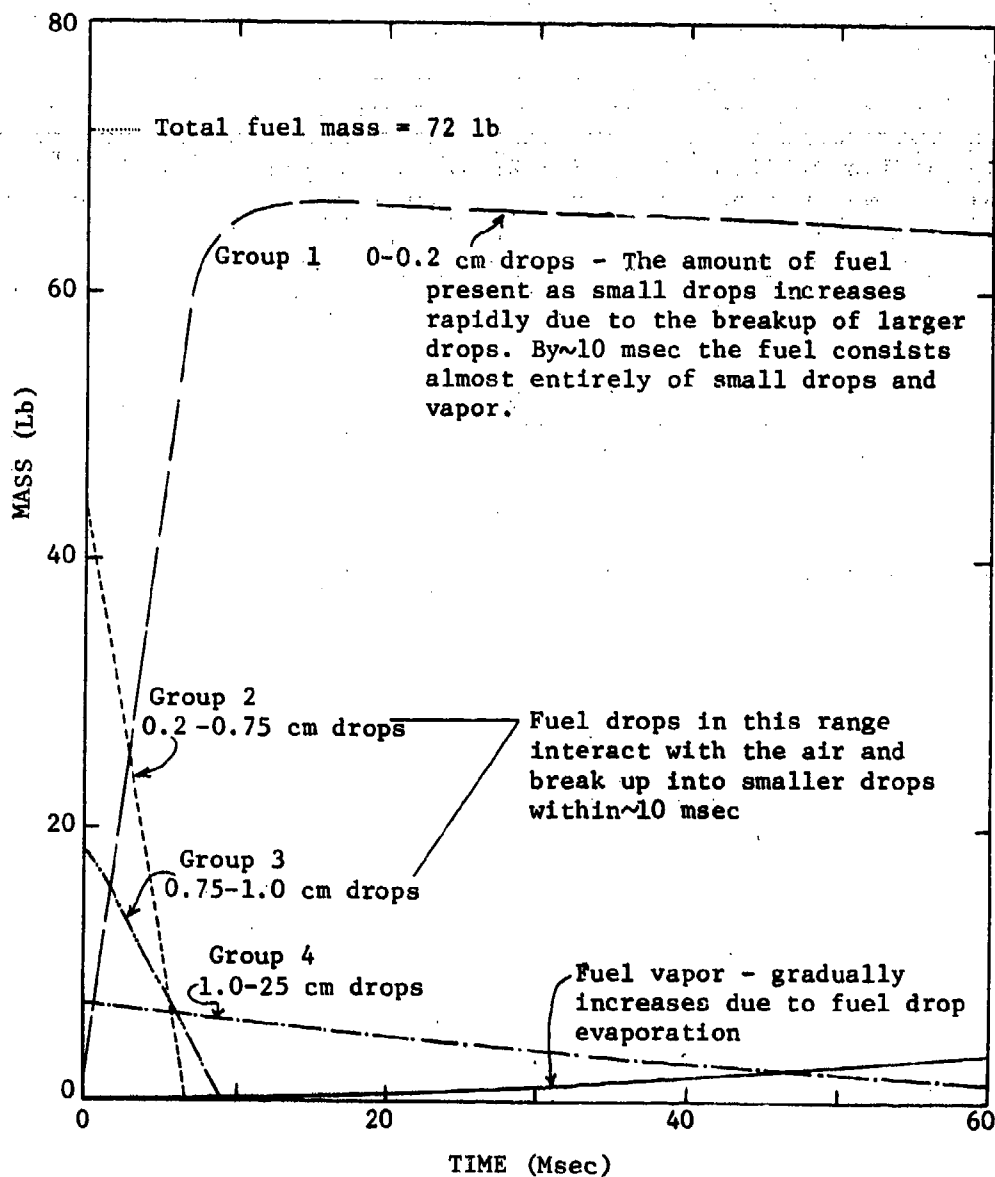
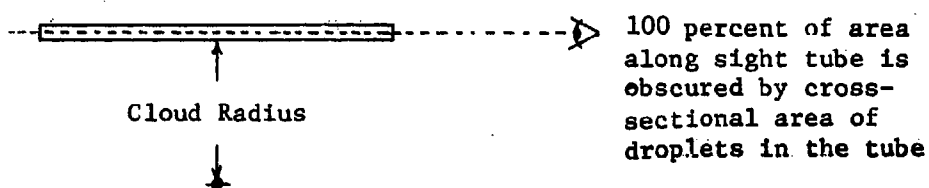


Figure 13. Distribution of Fuel Drop Diameters in the Expanding Fuel Cloud Prior to the Second Event Detonation at 60 msec

5. CLOUD CHARACTERISTICS AT END OF DISPERSAL PHASE (60 msec)

At the end of the fuel cloud dispersion analysis (60 msec), 90 percent of the fuel mass consists of particles in Group 1, the smallest size range (0-0.2cm). Figures 14 and 4 show the velocity vector field and concentration contours for Group 1 at this time.

Figure 5 shows time-histories of the fuel cloud dimensions (height and radius) that were obtained from DICE-FAE Solution 5A. Experimental results obtained by Zabelka (Reference 1) showing the visible cloud radius for an 83-lb FAE device are shown for comparison. In Figure 5, the periphery of the DICE-FAE cloud is defined by the maximum range (or height) where a line of sight is totally obscured by the cross-sectional area of the fuel drops along that line. i.e.,



The calculated and experimental radii at 60 msec in Figure 5 are in good agreement considering the difference in size of the devices.

Figure 15 shows the fuel-to-air mass ratio (F_a) in the cloud at 60 msec as a function of radius, at heights of 0.25, 2.75, 4.25, and 5.75 ft. Fuel vapor and Group 1 (0-0.2 cm) droplets are included in the fuel. Group 4 drops (>1 cm) are excluded, since it was felt fuel in such large drops would be unavailable for immediate burning or detonation.

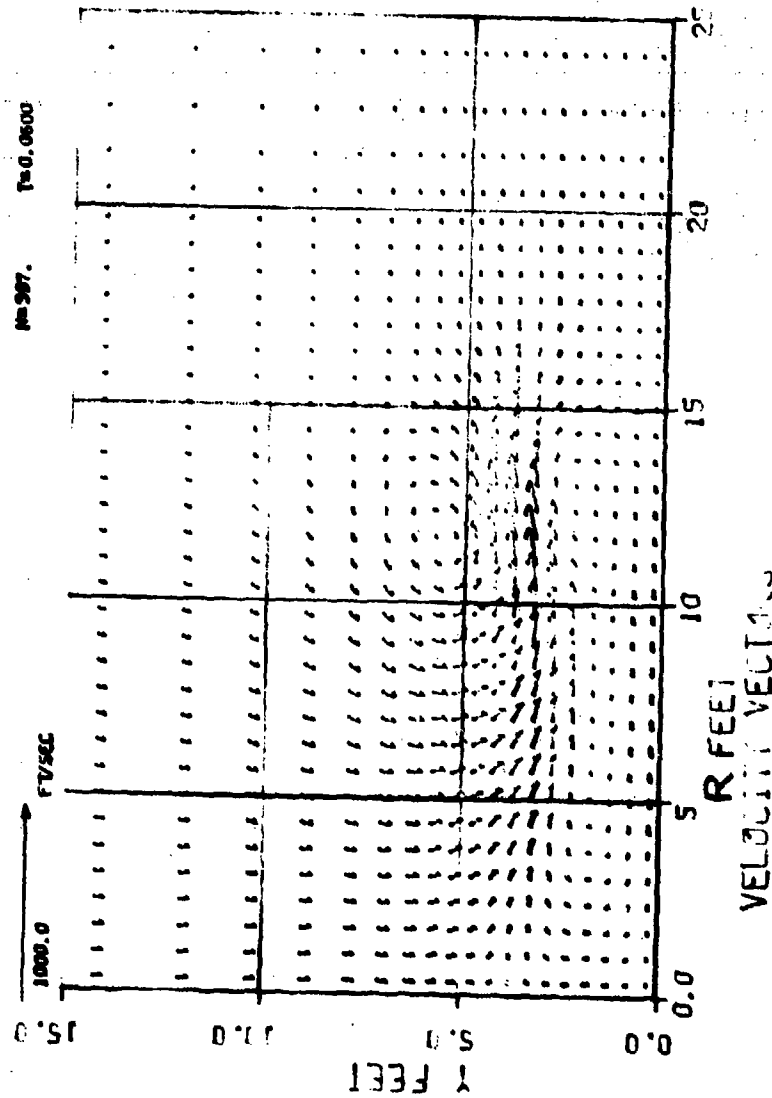


Figure 14. Air Velocity Vectors for DICE-FAE Case 5A at 60.0 msec

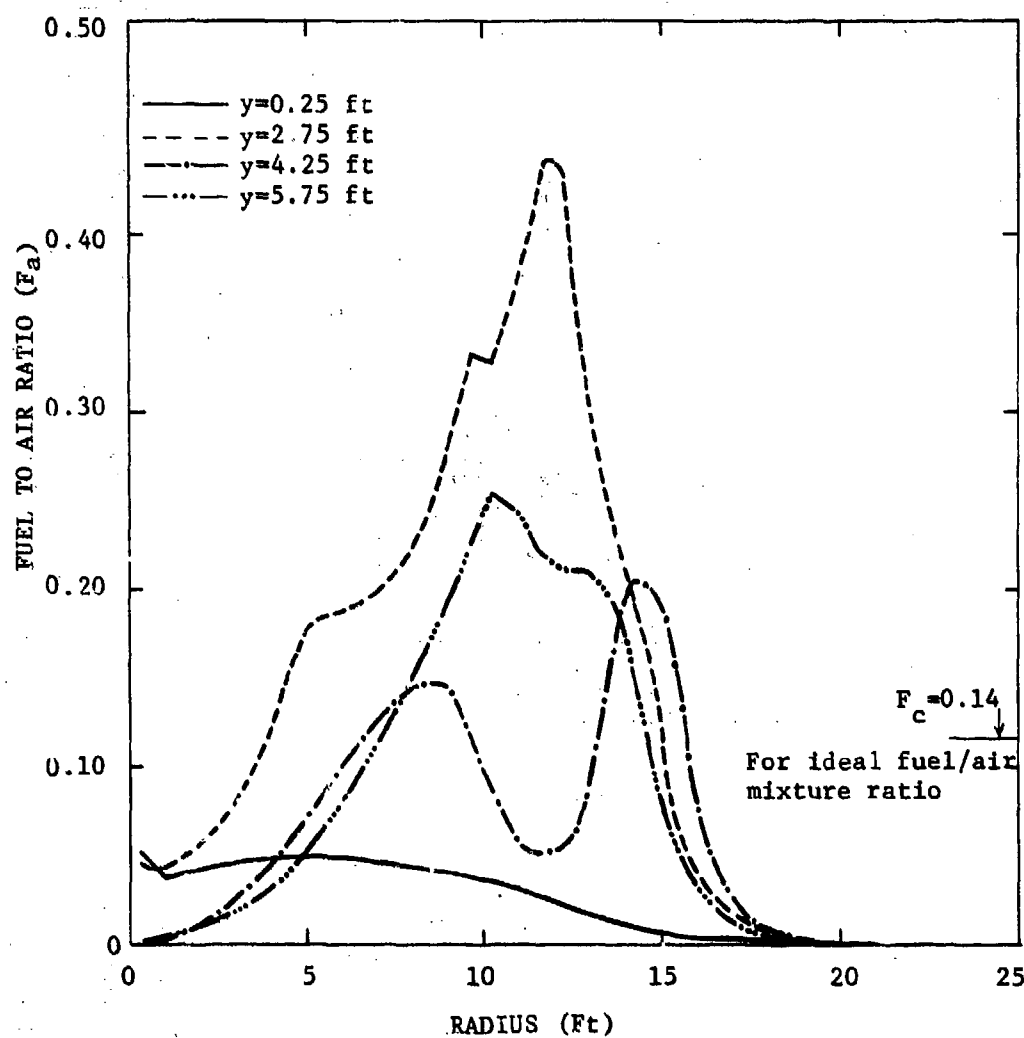


Figure 15. Fuel to Air Ratio versus Radius in the Fuel Cloud at 60 msec (just prior to SE initiation) for Heights of 0.25, 2.75, 4.25, and 5.75 ft

SECTION IV

ANALYSIS OF FUEL CLOUD DETONATION

The second, or detonation, phase of DICE-FAE Solution 5A lasted from 60 msec to about 77 msec.

1. MODEL FOR BURNING AND DETONATION

Simulation of the detonation of the FAE cloud required a burning^a model which quantitatively defines the rate and magnitude of energy release when given the temperature, fuel density, air density, and other relevant parameters in a computational cell.

As in the case of the particle breakup model described in Section III, paragraph 3, it is pointed out that DICE-FAE has great flexibility in the nature of models which can be used for detonation or burning. In formulating the specific model used in the present DICE-FAE analyses, output generated by the TIGER (Reference 4) code for the burning of propylene oxide in air was utilized. The TIGER code has the capability of treating a mixture of reacting gases and predicting the reaction products and energy generation subject to the constraint that a detonation wave propagates in the reacting mixture. Figure 16 shows TIGER output for shock pressure and temperature at the C-J point as a function of the percent propylene oxide (by weight) in the mixture. Figure 17 shows the TIGER output for energy released per gram of propylene oxide-air mixture as a function of the percent propylene oxide. Also shown in Figure 17 is the function obtained by assuming that propylene oxide and air always combine in the same proportions, and yield the same energy as at the peak of the TIGER curve (i.e., any air or propylene oxide left over is assumed to be unaffected by the reaction). This curve is sufficiently close to the TIGER curve to be adequate for the present application. This suggested the following burn model which was adopted for DICE-FAE Solution 5A.

- ^a Burning, as used here, refers to the chemical reaction of the fuel and the air. Detonative burning occurs when the reaction rate is high enough to propagate a shock wave. Deflagrative burning occurs when the reaction rate is insufficient to maintain a shock wave.

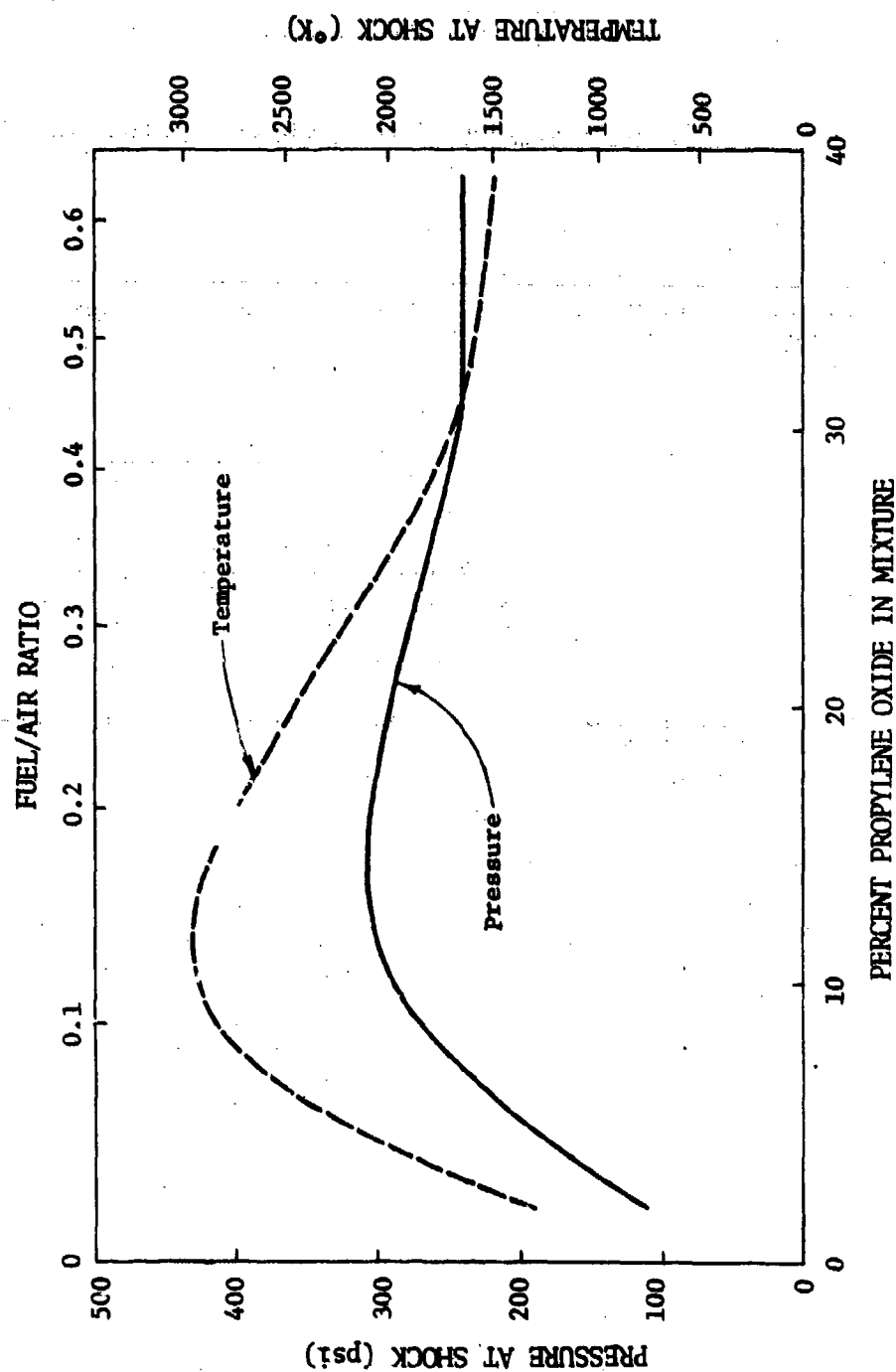


Figure 16. Pressure and Temperature of the Detonation Shock in a Propylene Oxide-Air Mixture, as a Function of the Percent Propylene Oxide (TIGER code data)

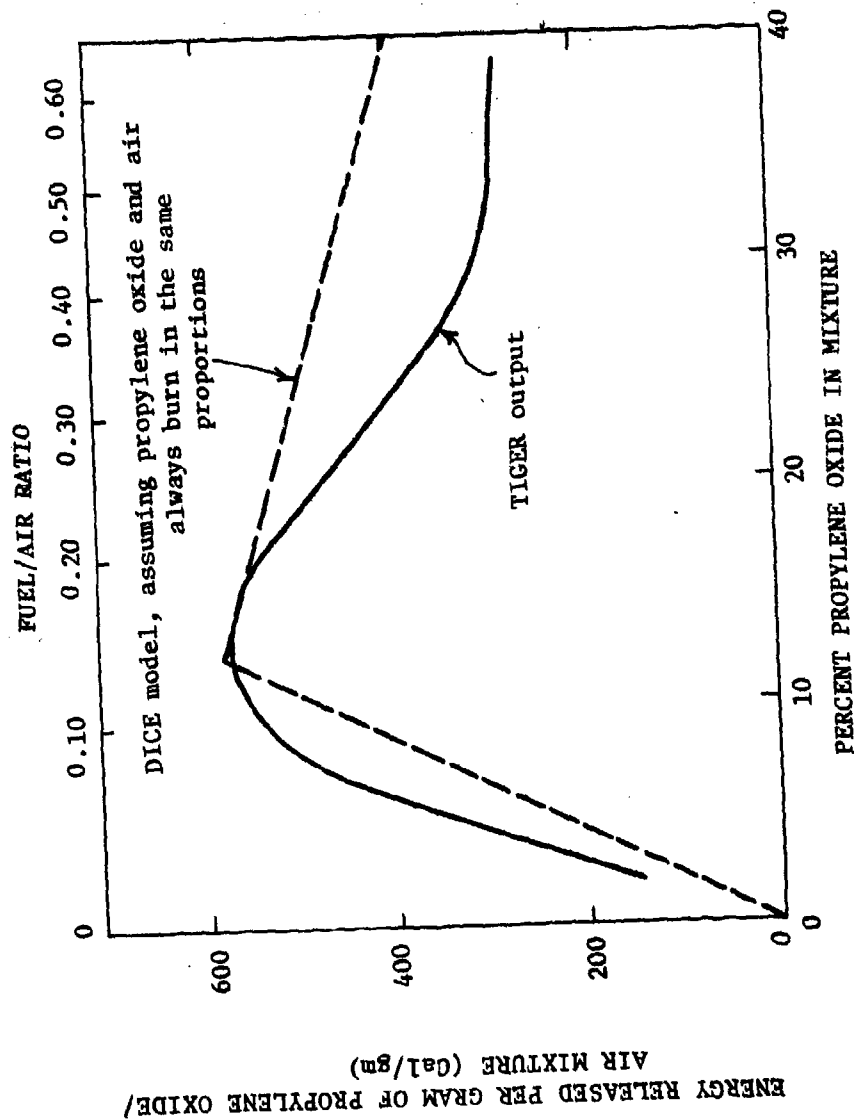


Figure 17. Energy Released in Burning per Gram of Propylene Oxide Mixture versus the Fuel Air Ratio from TIGER Output and as Assumed in the DICE Model

- o It is assumed that (1) fuel vapor and air always combine in the same critical proportion, F_C , (2) always produce the same reaction products, and (3) the amount of energy produced per gram of fuel vapor consumed is constant. Fuel drops must become vapor (by boiling or evaporation) before they can burn.
- o If the actual ratio of fuel vapor to air F_a , in a computational cell, exceeds F_C , then burning proceeds until the oxygen in the air is exhausted. Burning then stops.
- o If $F_a < F_C$, burning proceeds until the fuel vapor is consumed.
- o Burning is possible only when the temperature is greater than some constant temperature T_B .
- o Burning is not instantaneous, but is controlled by a rate parameter τ . If an amount M_F of *fuel vapor* is available to be burned in some volume element, then an amount $m = \frac{\Delta t}{\tau} M_F$ will be consumed in a time increment, Δt .

This model is simple and physically reasonable. It releases the appropriate amount of chemical energy, and it depends on the laws of continuum mechanics to determine, for each computational cell, whether this energy is sufficient to cause detonation or whether just burning occurs. The ability to make this distinction is important for evaluating FAE devices.

The four material-dependent parameters required by the burning model are:

- o F_C , the critical fuel vapor-to-air ratio at which burning takes place. This number is determined from Figure 17 to be that fuel-to-air ratio at which the rate of energy release is greatest. ($F_C = 0.14$).
- o Q , the energy released per gram of mixture burned. The value corresponding to the critical fuel-air ratio, F_C , is chosen. ($Q = 580$ cal/g)

- o τ , the characteristic time for burning. τ is assumed to be given by the time it takes a detonation wave to cross a typical computational cell in the DICE-FAE computational grid. This definition is necessary for numerical stability. In general, τ is so small compared to the time required for hydrodynamic processes to occur that the numerical solution does not depend strongly on its value. ($\tau = 80 \mu\text{sec}$)
- o T_B , the minimum temperature for burning. Pierce (Reference 5) et al have indicated that as a general rule a Mach 3 shock wave is required to produce explosive ignition. In the DICE-FAE model T_B is therefore chosen to correspond to the temperature of a Mach 3 shock wave in air. ($T_B = 740^\circ\text{K}$)

The specific constants used in the burning model as well as the break-up model for propylene oxide are given in Table B-1. It is emphasized that since the FAE detonation model used here in DICE-FAE specifies only the energy release rate as a function of fuel-air ratio in the cloud, *the detonation wave is in no way pre-specified*. Its velocity, strength, and other characteristics (including whether a detonation wave propagates at all) are determined by the basic laws of continuum mechanics. The detonation wave characteristics which are generated by DICE-FAE offer an independent check of the physical model uses. (An example of one independent check is presented at the end of this section.)

As stated above, only fuel vapor can burn or detonate. DICE-FAE has a physically realistic model governing the evaporation, condensation, and boiling of the fuel; however in the present application no data were available to accurately determine the material-dependent rate constants required by the model (τ_b for boiling, τ_c for condensation/ evaporation). Even though the DICE-FAE detonation model uses the amount of fuel vapor as a fundamental quantity, this lack of certainty in determining τ_b and τ_c does not have a significant effect on the cloud dynamics during the detonation for the following reasons:

- (a) As seen earlier in Figure 13, the fuel exists primarily in the form of very small drops and fuel vapor after about 10 msec. Both small drops and vapor flow with the same velocity as the air; the spatial distribution of *total fuel density* (drops plus vapor) at the time of SE initiation is therefore only weakly dependent on the evaporation and boiling rate parameters.

- (b) When the detonation wave arrives at a computational cell, the temperature rises abruptly to values well above the boiling point of the propylene oxide fuel. Thus, for any reasonable value of τ_b (boiling parameters), the fuel drops boil very rapidly. The important pre-detonation parameter is therefore not the amount of fuel vapor in the cell, but the total amount of fuel present as vapor and small drops. Thus even though the relative amounts of fuel drops and fuel vapor present at the time of the cloud detonation may be subject to some uncertainty, this should not affect the validity of the solution.

2. INITIAL CONDITIONS FOR DETONATION PHASE

The starting conditions for the detonation phase were taken directly from the final conditions (at 60 msec) of the dispersal phase, as summarized in Section III, paragraph 5 and in Figures 14, 4, 5, and 15. In Figure 15, it is seen that the fuel mixture is lean at all heights, but extremely lean above 4 ft. This implies that if the second event is to be initiated on the symmetry axis:

- o Initiation will be attained more easily if the initiator is as low as possible, and
- o The SE initiator will have to be reasonably powerful, in order to generate a shock wave with sufficient strength to propagate into regions with more favorable values of F_a .

For DICE-FAE Solution 5A, the second event was initiated by detonating a 350 gm explosive charge (1000 cal/gm) on the axis 3.25 ft above the ground.

3. CLOUD DETONATION PROCESSES

At early times the flow field in the detonation event, as shown by the velocity vector plots, is characterized by a shock front which surrounds the detonating region, and an interior wherein flow is dominated by divergent velocities near the region of most rapid energy release. The velocity plots at 61.5 msec (Figure 18) and 64 msec (Figure 19) show this behavior. When the detonation wave has reached the edge of the fuel cloud and detonative burning has stopped, the flow becomes radially divergent from approximately the problem origin ($r=0$, $y=0$), as illustrated by the velocity plot at 68 msec (Figure 20). At a still later time, as shown by the velocity vectors at 77 msec (Figure 21), the velocity field becomes much less violent and is influenced by the deflagrative burning of the fuel vapor which was not previously consumed in the detonation wave. The deflagration is controlled by the rate of oxygen flow into the oxygen-depleted portion of the cloud.

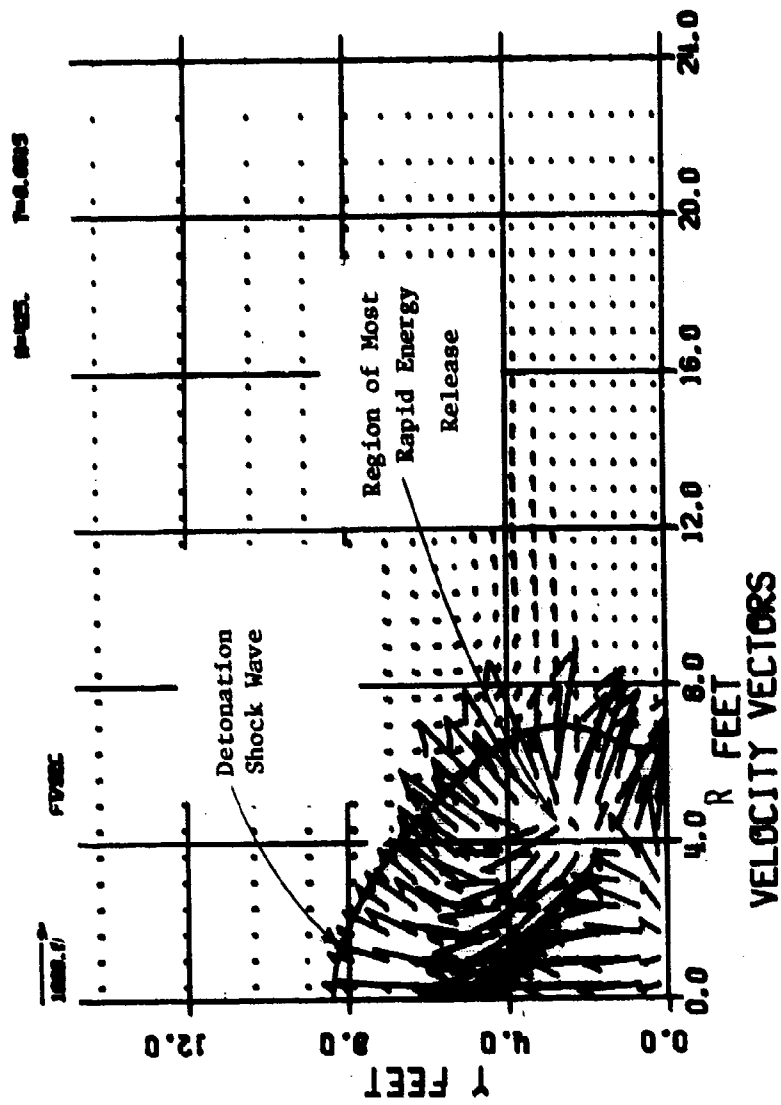


Figure 18. Air Velocity Vectors for DICE-FAE
Case 5A at 61.5 msec

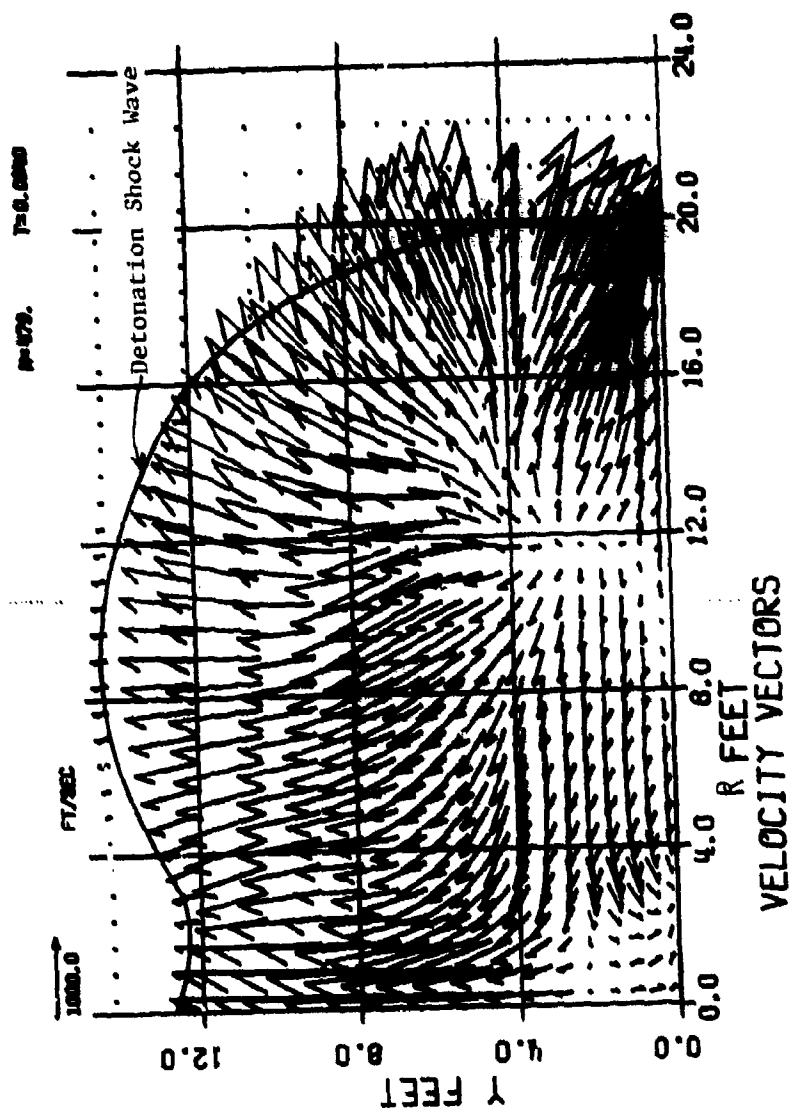


Figure 19. Air Velocity Vectors for DICE-FAE
Case 5A at 64.0 msec

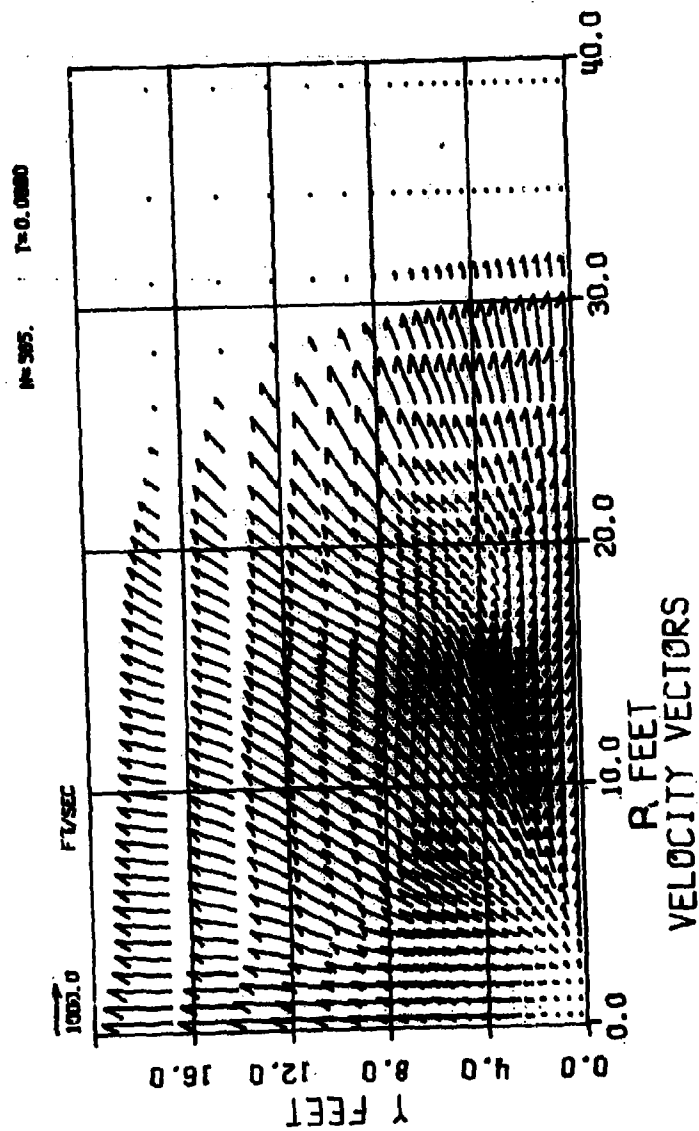


Figure 20. Air Velocity Vectors for DICE-FAE Case 5A at 68.0 msec

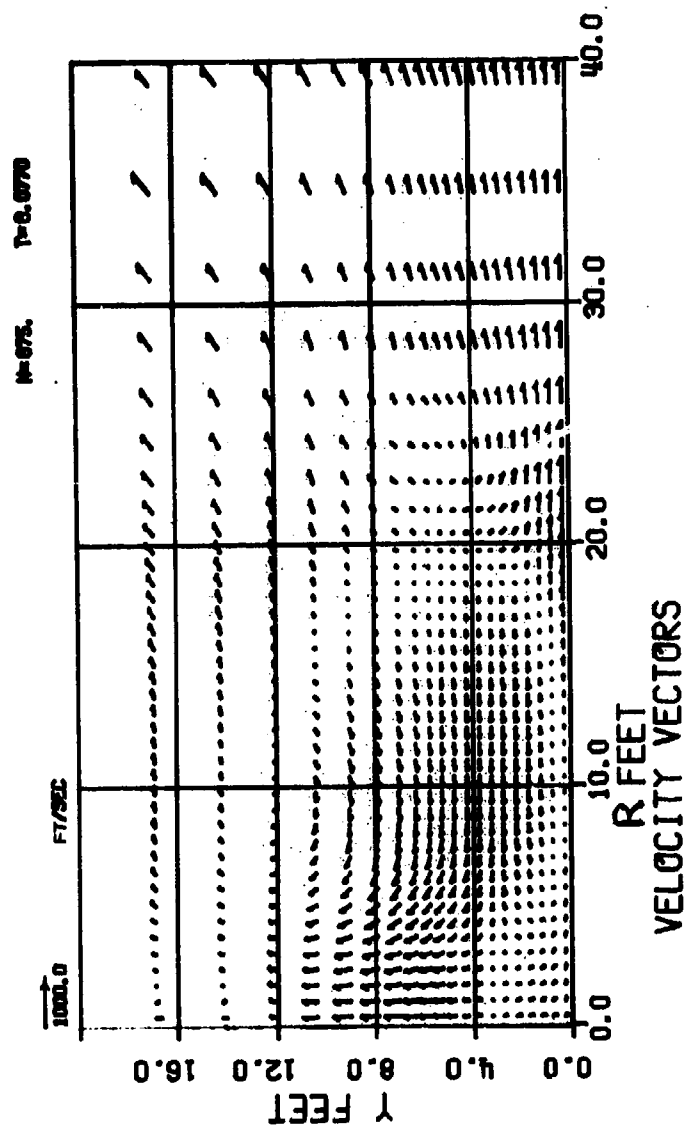


Figure 21. Air Velocity Vectors for DICE-FAE Case 5A at 77.0 msec

The sequence of physical events which occur as the detonation wave passes a point within the fuel cloud can be described with reference to Figure 22.

- (1) The detonation shock wave arrives (Region B). The fuel drops begin to break up (because the relative velocity between drops and air increases) and to boil (because the temperature has increased). The density of fuel vapor therefore increases.
- (2) After a characteristic time, during which fuel vapor increases at the expense of fuel drops, detonative burning occurs (Region C).
- (3) Either the fuel is consumed, and burning stops; or the oxygen is consumed. Deflagrative burning commences as oxygen flows in from adjacent regions.

The plots of the fuel density and air temperature contours in Figures 23, 24, and 25 further illustrate these processes. In general, fuel drops exist only in front of the detonation shock wave. Immediately behind this shock, they have been converted entirely to fuel vapor. Figure 23, which shows contours of fuel drop density at 61.5 msec, shows an indentation caused by this effect. The vapor density is generally high between the detonation shock front and the point where burning is initiated, because the boiling of the fuel drops has caused additional vapor to form in the region. Behind the region where burning is taking place, the fuel vapor density drops as fuel vapor is consumed. Figure 23, which shows the fuel vapor contours at 61.5 msec, illustrates this characteristic of the fuel vapor density field. Behind the region of intense burning, the fuel vapor in Figure 20 is entirely consumed, while between the detonation shock front and the burning front the density of the fuel vapor exhibits a local maximum.

The incomplete burning due to the fuel-rich regions in the fuel cloud is illustrated in Figure 26, which shows the fuel vapor contours at 77 msec (well after the detonation wave has left the fuel cloud region) and Figure 22, which shows the distribution of fuel mass during the detonation event. *About 12 percent of the original fuel mass remains as vapor at 77 msec.* This vapor is slowly being consumed by deflagrative burning as oxygen flows into the region containing the vapor.

In Figure 27, the 0-0.2 cm drops (Group 1) are seen to be rapidly consumed by boiling as they are encompassed by the detonation shock wave. The mass of fuel vapor initially increases as the 0-0.2 cm drops boil, then begins to decline

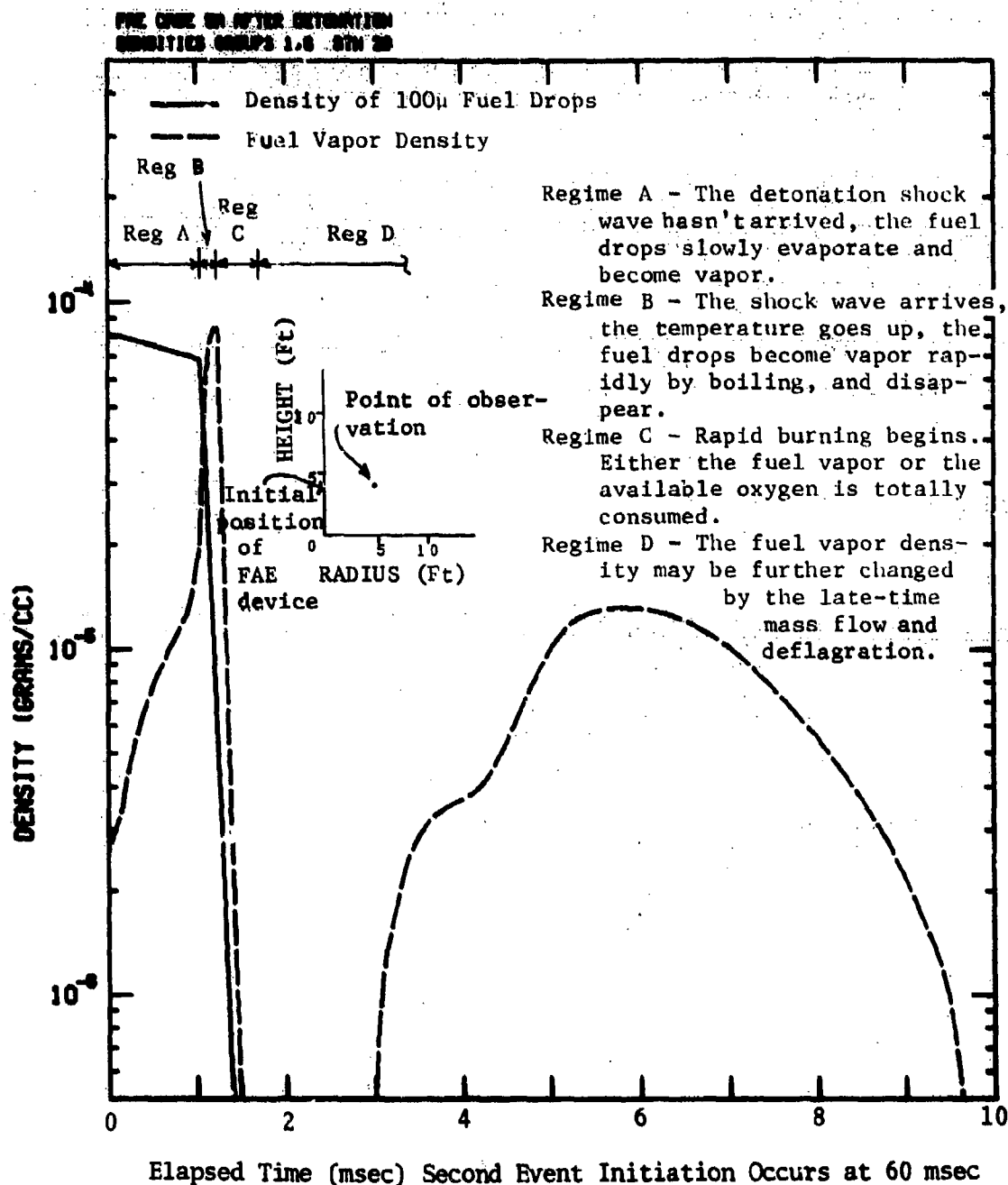
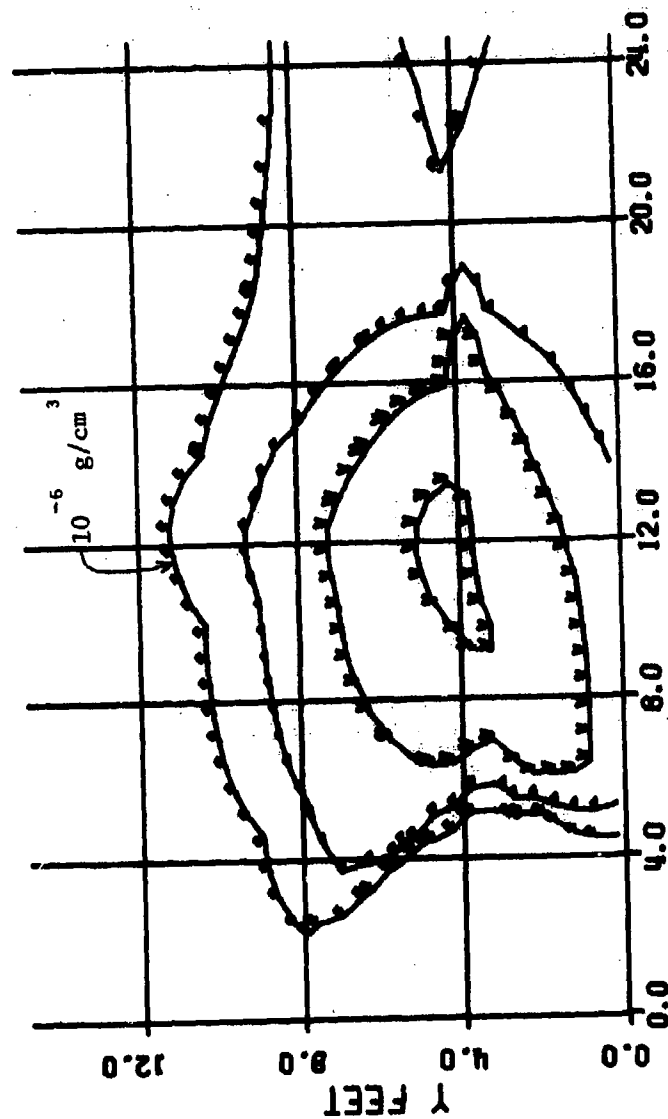


Figure 22. Density History During the Second Event Detonation of the 100 μ Fuel Drops and the Fuel Vapor, Taken at a Height of 4 ft and a Radius of 5 ft

10-0000E-05



DENSITY COUNTERS, GROUPS 1-4

CONTOUR SYMBOLS AS FOLLOWS (units are gm/cm³):

V = 10.0000E-05 , ~ = 10.0000E-06 , * = 10.0000E-07

Figure 23. Fuel Drop Density Contours for DICE-FAE Case 5A at 61.5 msec

10-005. 1-0.0035

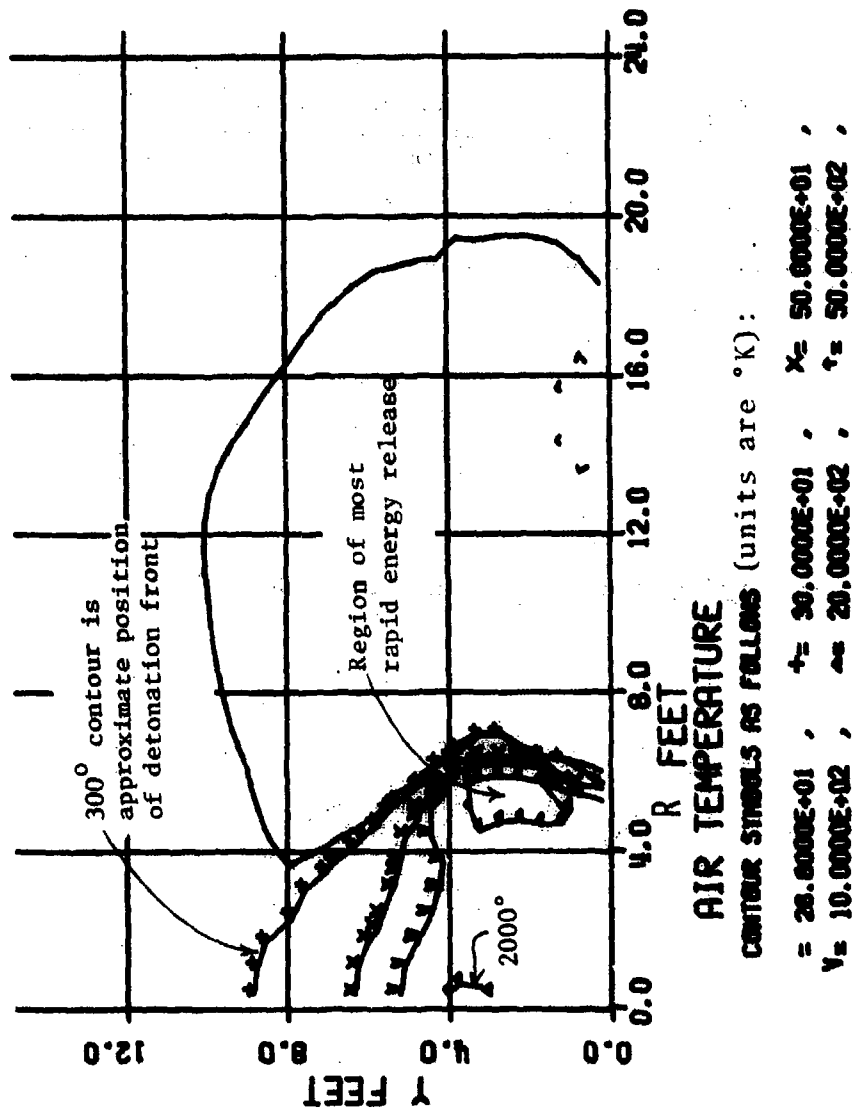
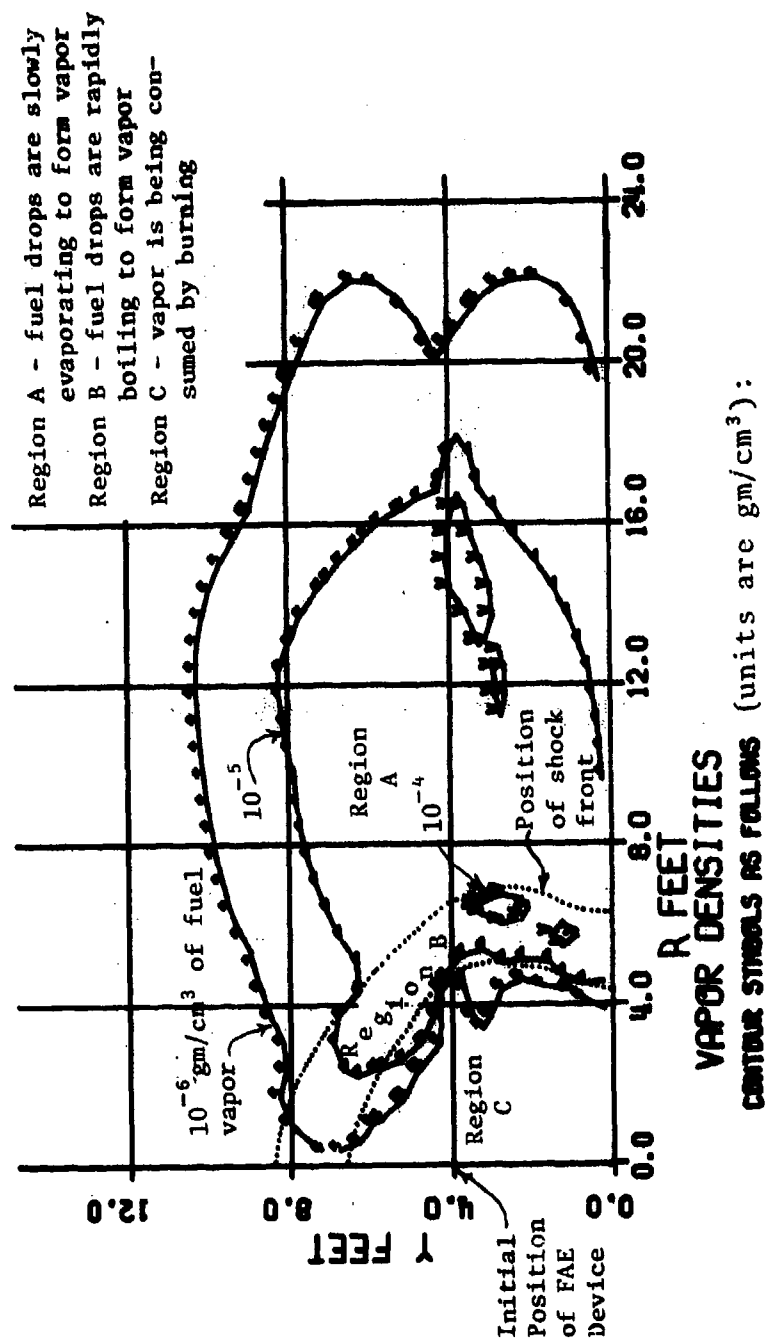


Figure 24. Air Temperature Contours for DICE-FAE
Case 5A at 61.5 msec

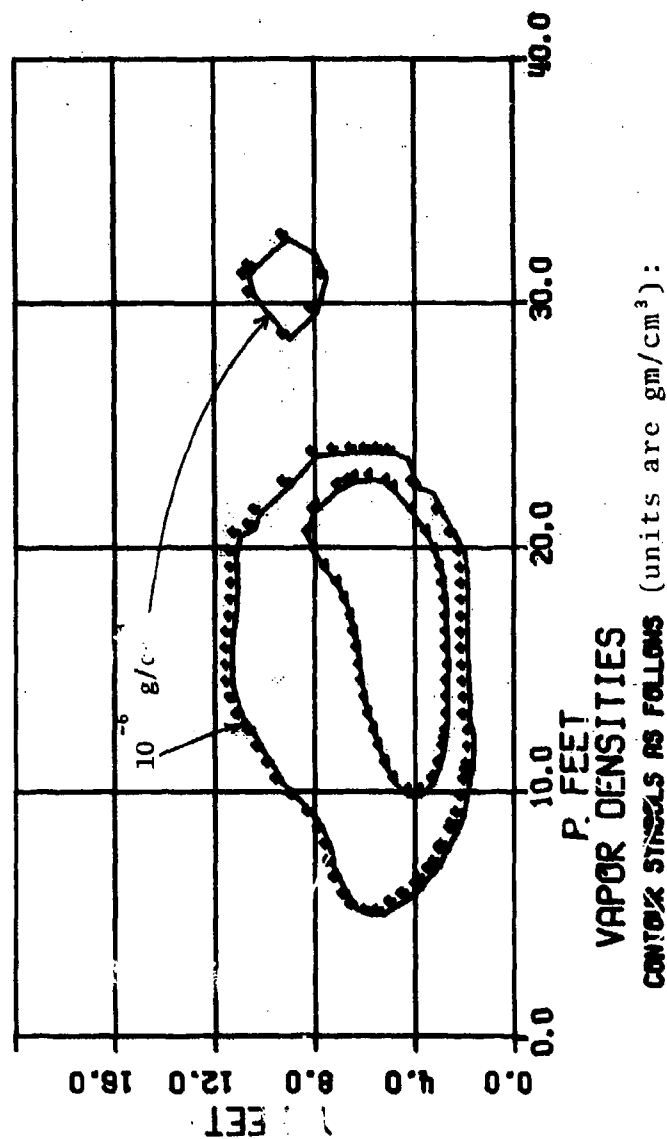
10-125. 7-9.0005



$V = 10.0000E-05$, $A = 10.0000E-06$, $\gamma = 10.0000E-07$,

Figure 25. Fuel Vapor Density Contours for DICE-FAE Case 5A at 61.5 msec, Showing the Regions of Activity Associated with the Detonation Front

W-075. P=0.0770



$V = 10.0000E-05$, $A = 10.0000E-06$, $T = 10.0000E-07$,

Figure 26. Fuel Vapor Density Contours for DICE-FAE
Case 5A at 77.0 msec

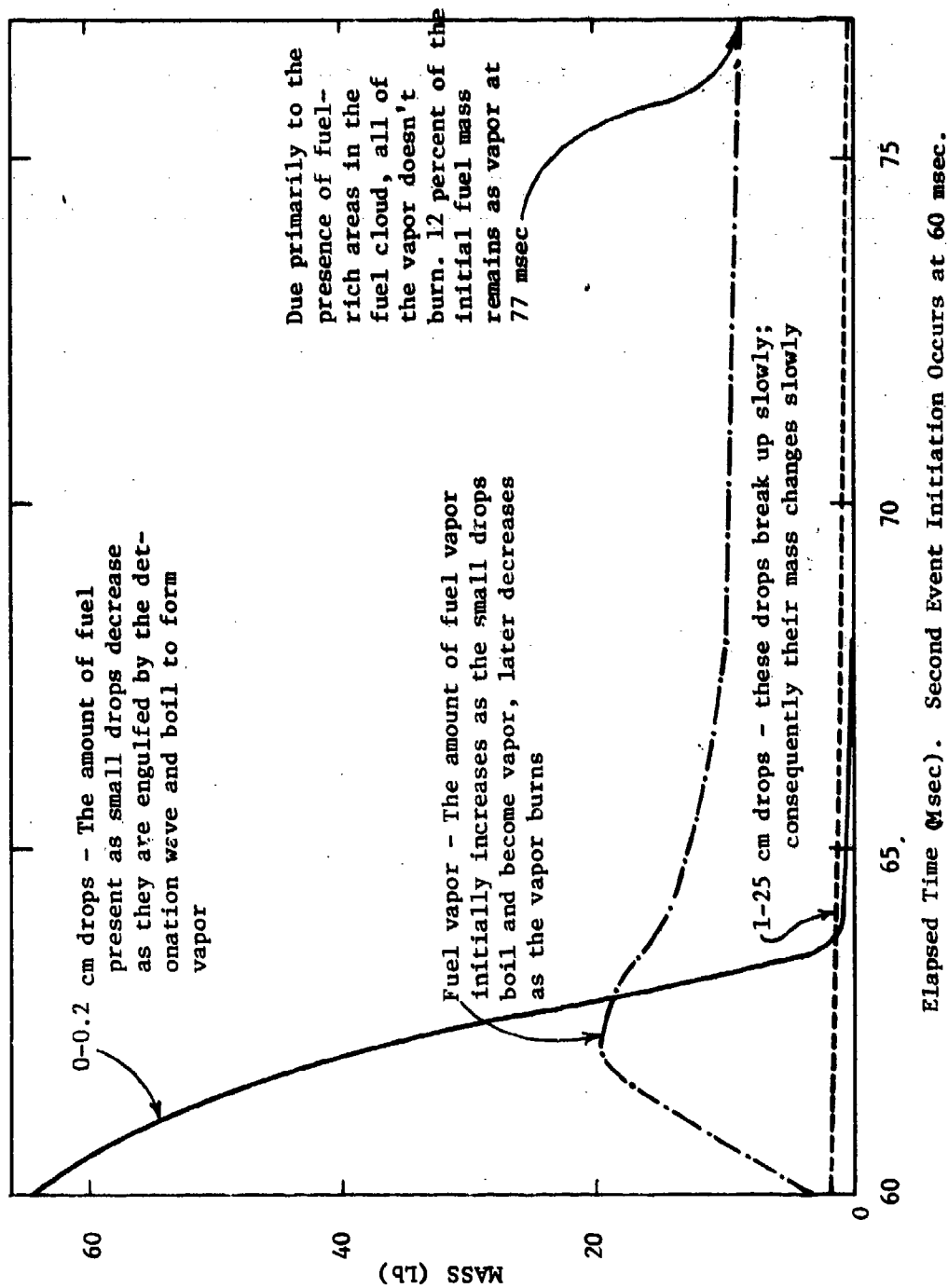


Figure 27. Distribution of fuel Drop Diameters in the Fuel Cloud Subsequent to the Second Event Initiation at 60 msec

as the vapor is burned. The 1-25 cm drops (Group 4) are relatively unaffected by breakup or boiling/evaporation, and are located well away from the cloud center; consequently their total mass remains almost unaffected by the detonation.

Air pressure versus time at fixed stations along the ground are plotted in Figures 28, 29, and 30. The curves generally show a steep rise from ambient pressure to peak values, followed by a gradual decay back to normal pressure. Figure 7 shows peak pressure versus range on the ground. The maximum pressure experienced was about 14 atmospheres (200 psi), attained at a radius of about 10 ft. The maximum pressure experienced anywhere during the FAE detonation was about 16 atmospheres (240 psi), attained at a height of 4 ft and a radius of 15 ft.

Figure 8 shows the impulse-density ($\int (P - P_a) dt$) delivered by the detonation to the ground surface as a function of radius after 77 msec (17 msec after the detonation was initiated). The impulse/density peaks at $r=0$, which demonstrates that the long duration of the pressure versus time curves near the axis of cylindrical symmetry more than compensates for the fact that the peak pressure is relatively low near the axis, as compared to several ft away.

Experimental data directly applicable to the detonation of the fuel cloud were not available. However, the TIGER code output provides a reasonable verification of the peak shock pressures obtained during the DICE-FAE second event detonation. For example, the TIGER code output in Figure 16 can be used to convert the fuel-to-air ratios versus radius obtained from the DICE-FAE fuel dispersion analysis at 60 msec to shock pressures; the result will be a pressure versus radius curve which should be reasonably close to the peak shock wave pressure versus radius curve calculated by DICE-FAE for the detonated fuel cloud. Figure 31 shows a plot of the pressure function generated in this way, along with the peak shock pressure versus radius curve obtained from the DICE-FAE solution. The two functions compare favorably.

Additional plots in Appendix E give the density histories at various data stations for the 0.01 cm fuel drops (Group 1) and the fuel vapor (Group 6). The behavior of these fuel groups is qualitatively the same for each station, and can be divided into the four regimes defined in Figure 22, i.e.,

- (1) Ambient regime (A) - This period precedes the arrival of the SE detonation shock wave, and is characterized by the slow evaporation of the 0.01 cm drops to form fuel vapor.

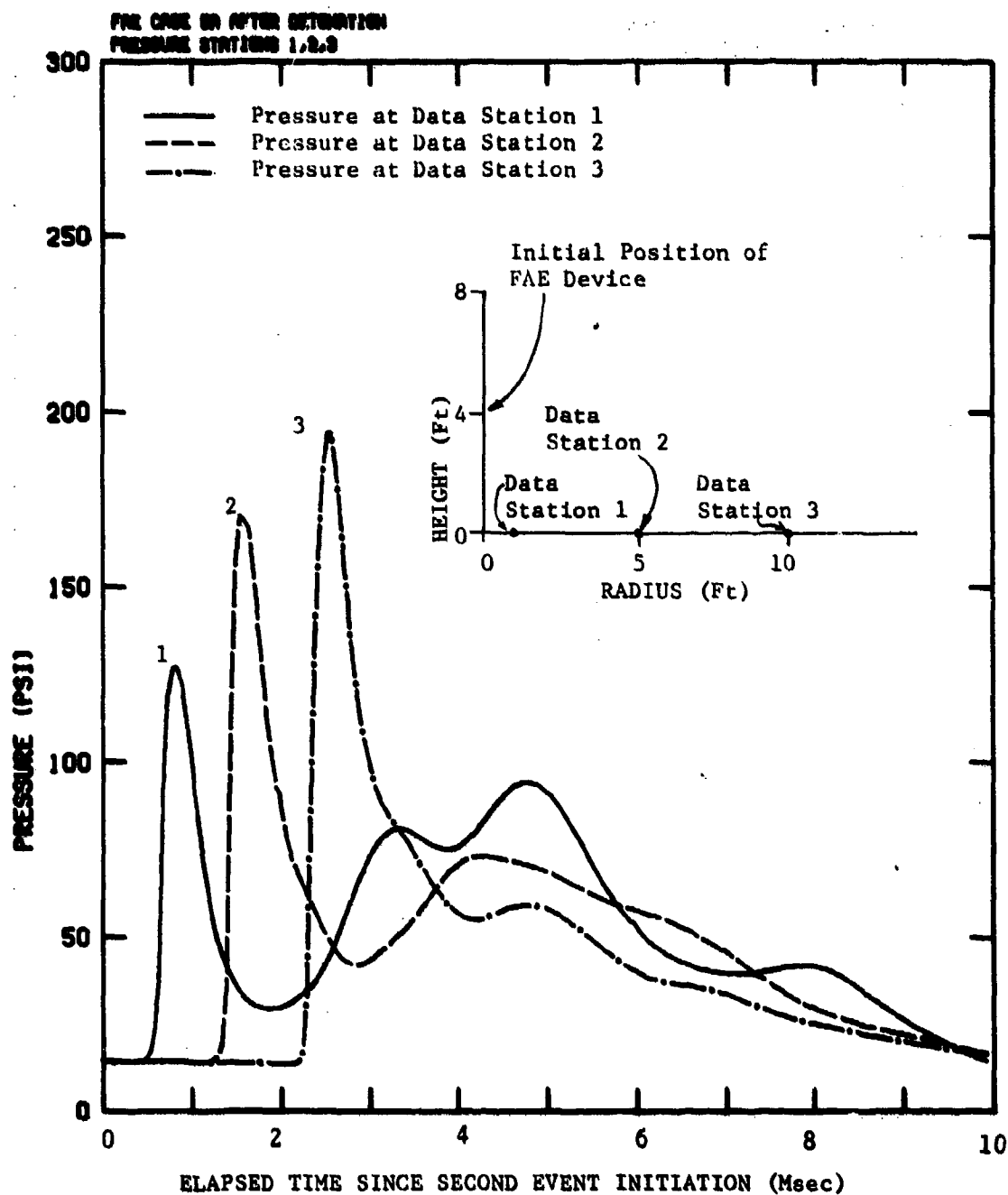


Figure 28. Ground Level Pressures at 1, 5, and 10 Ft Radius versus Time Following the Second Event Initiation at 60 msec

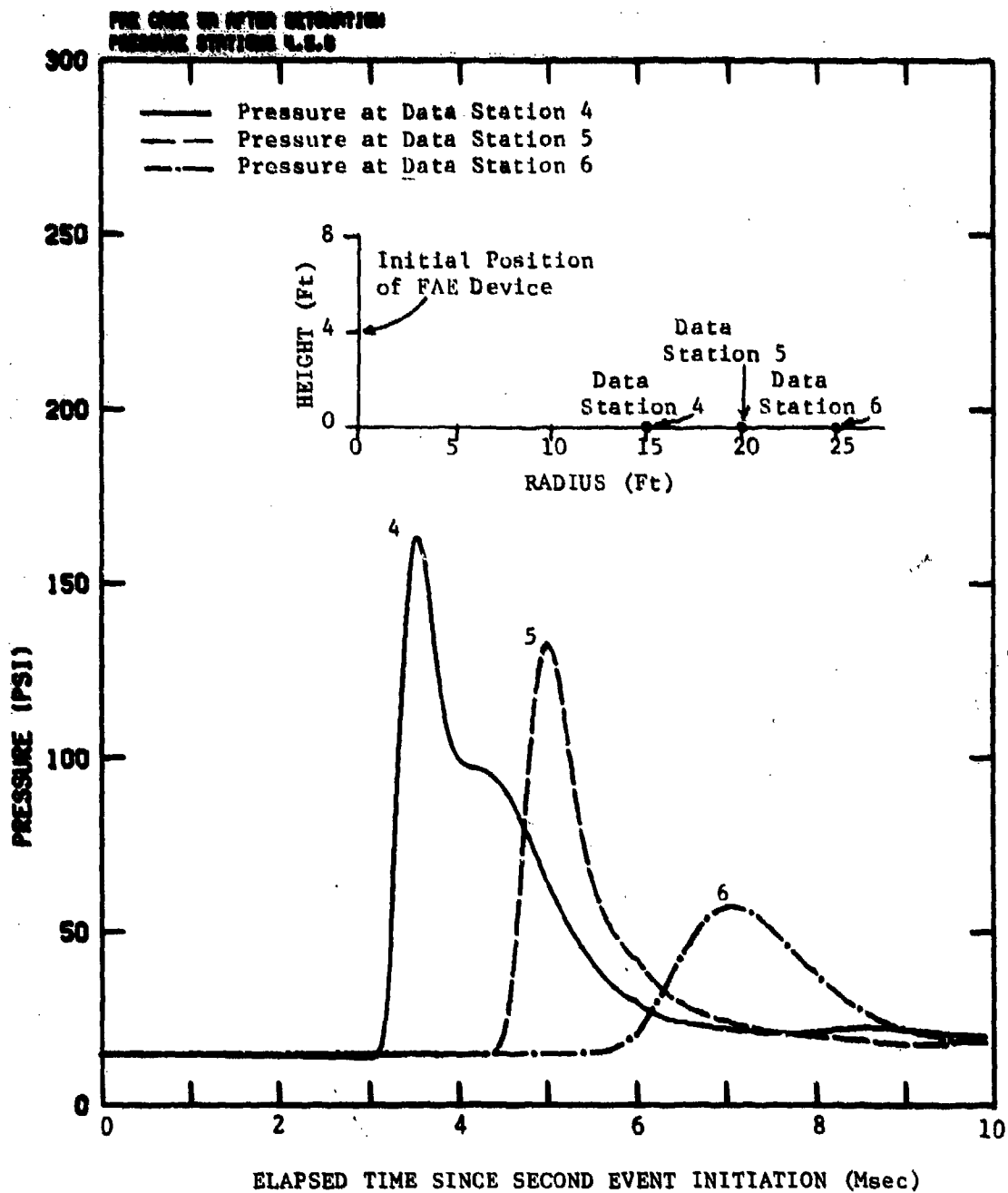


Figure 29. Ground Level Pressures at 15, 20, and 25 Ft Radius versus Time Following the Second Event Initiation at 60 msec

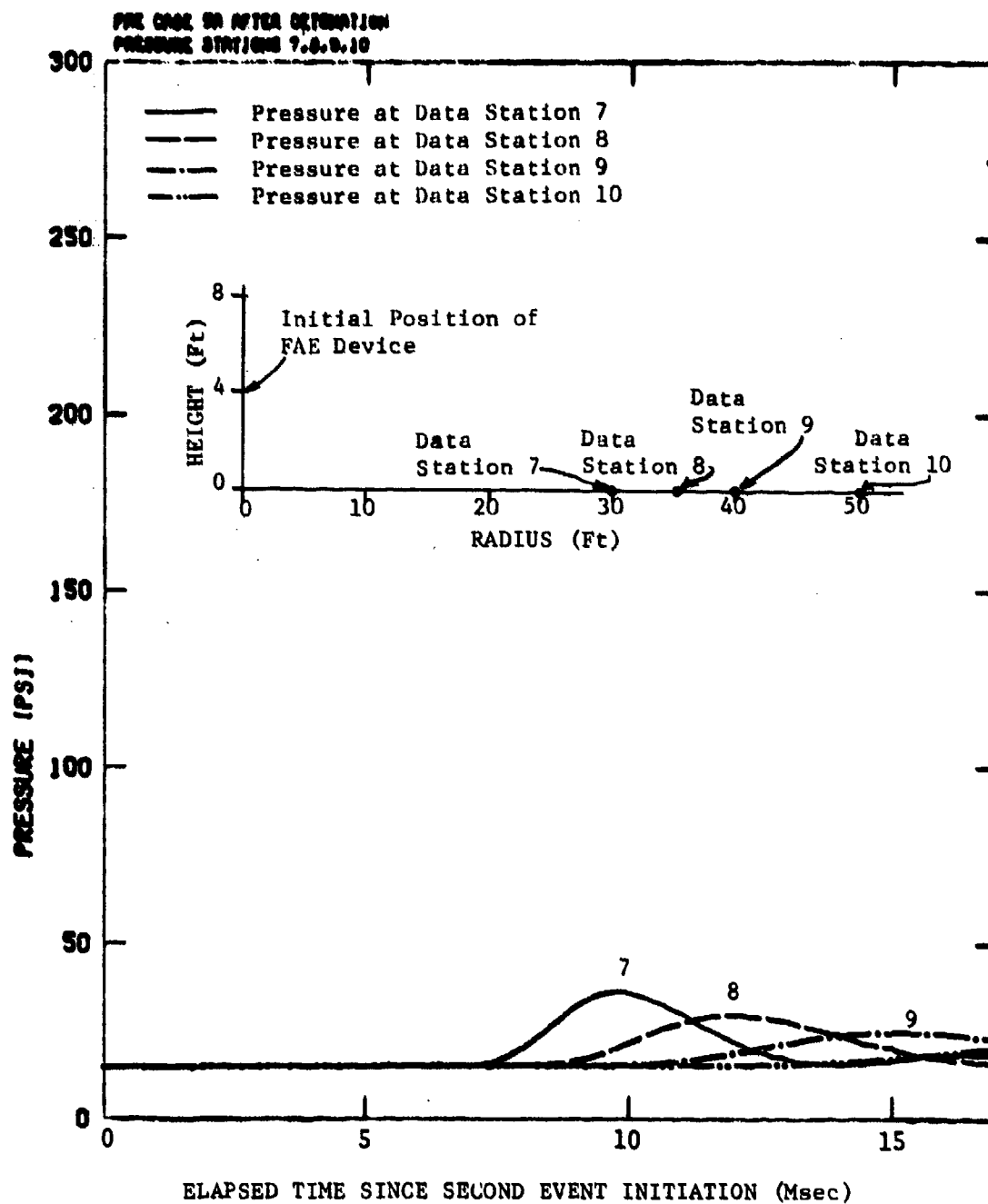


Figure 30. Ground Level Pressure at 30,35,40, and 50 Ft Radius versus Time Following the Second Event Initiation at 60 msec

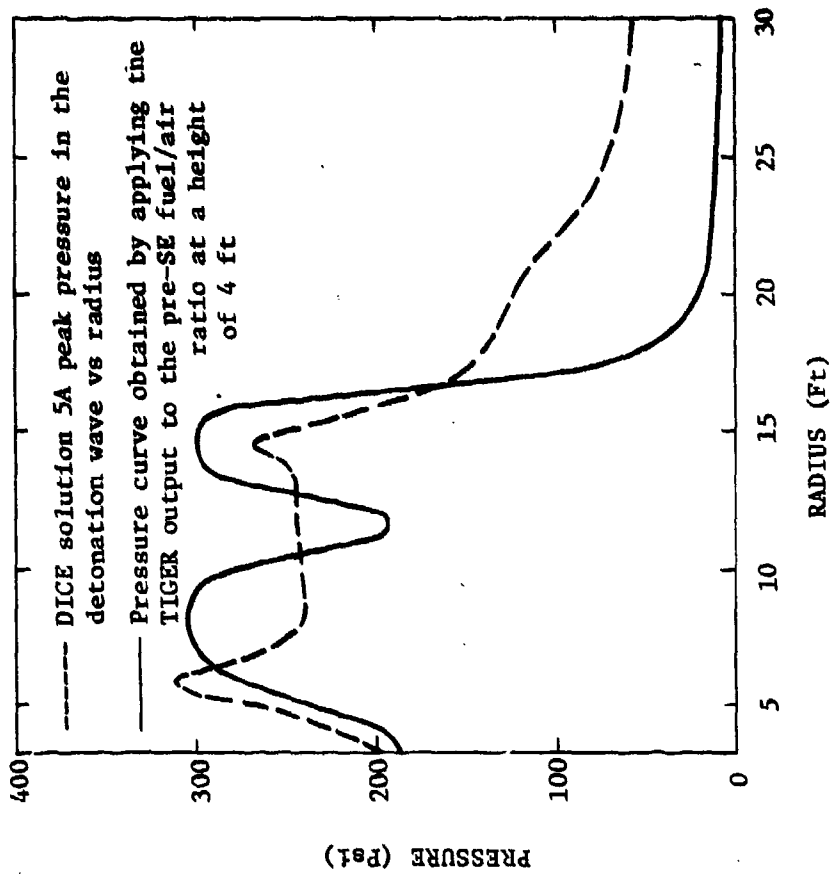


Figure 31. Peak Pressure in the Detonation Front versus Radius for DICE Solution 5A Compared to an Estimate of These Pressures Based on Output from the TIGER Code

- (2) Shocked regime (B) - This period follows the arrival of the detonation shock wave, but precedes any significant burning. It is characterized by rapid boiling (to extinction) of the 0.01 cm drops.
- (3) Burning regime (C) - This period is characterized by burning of the fuel vapor. It burns until either the fuel or the oxygen is exhausted.
- (4) Flow regime (D) - After the fuel or oxygen in a cell is consumed through burning, the flow of the air/fuel/reaction products may cause the fuel density to change and deflagration may occur.

SECTION V

CONCLUSIONS AND RECOMMENDATIONS

1. The DICE-FAE code has been used to predict the time-and spatial-resolved processes which occur in fuel cloud dispersion and detonation by FAE devices. Experimental data for direct comparison are sparse, but the numerical results appear physically credible. These results demonstrate that DICE-FAE solutions can be used to obtain understanding of the dynamic mechanisms involved in an FAE event which would be difficult or impractical to observe experimentally. The technique can therefore be useful in developing and evaluating improved FAE devices or concepts.

2. More definitive experimental verification of the accuracy of DICE-FAE and its major constituent models is desirable. Jointly-planned efforts involving coordinated experiments and DICE-FAE solutions should be undertaken, with the following specific objectives:

- (a) Experimental validation of the technique and models,
- (b) Evaluation and refinement of models used for particle breakup and detonation,
- (c) Improvement of initial conditions to be used in DICE-FAE

3. In DICE-FAE solutions, parameters can be varied *independently*. This allows the effects of these parameters upon the efficiency of an FAE device to be systematically examined. (It is often difficult and sometimes impractical to independently control and vary important parameters in FAE experiments.) The following are specific questions or areas where parametric studies would be of value in helping to develop improved FAE concepts and/or devices:

- (a) *Fuel-to-burster ratio*. This affects the initial velocity, energetics, and breakup characteristics. How do these factors affect the fuel dispersion processes and cloud characteristics?
- (b) *Initial fuel droplet size distribution*. Understanding the effects of changing this distribution would lead to criteria for improving the fuel and/or canister breakup characteristics. In particular, attention should be given to the behavior and influence of larger drops (greater than 1 cm).

- (c) *Initial altitude and velocity of the device.* What are the effects of these factors upon the fuel dispersion, and what are the optimum values?
- (d) *Properties of the fuel.* How do changes in the surface tension, viscosity, etc., affect fuel drop-let shattering and vaporization during the cloud dispersion phase, the ultimate characteristics of the cloud, and the subsequent detonation?
- (e) *Location of SE initiator.* Where are the most (and least) reliable positions at which to initiate the SE detonation?
- (f) *Explosive energy of the SE initiator.* Given the characteristics of the disseminated fuel cloud, how can the SE initiator be modified to improve the FAE detonation reliability? What are the minimum SE initiator energy requirements for initiators at various locations in a cloud?
- (g) *Time of SE initiation.* Given the flow characteristics of the fuel cloud, what is the best time for SE initiation?

4. New FAE concepts should be simulated, wherever possible, using DICE-FAE numerical calculations, so as to understand new mechanisms and to suggest improvements. Such numerical simulations may be particularly useful, for example, in evaluating concepts involving simultaneous cloud detonations.

5. In this limited, exploratory study, almost all of the effort was devoted to modifying the code, to obtaining the DICE-FAE numerical solutions, and to graphically displaying the results. Solutions of this type, however, can have a much greater impact on FAE development and improvement if an equal effort can be directed towards detailed examination, interpretation, and correlation of the quantitative results. This will lead to a more thorough understanding of the various competing mechanisms, and should suggest approaches for overcoming major problems or deficiencies in FAE fuel dispersal and detonation.

APPENDIX A

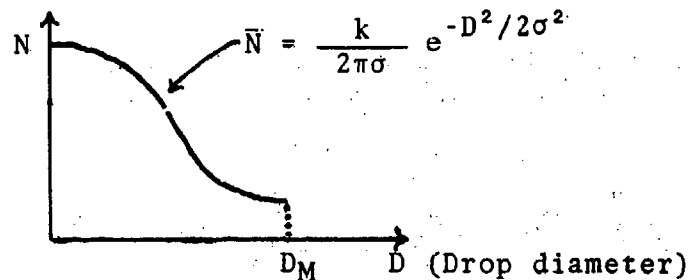
DETERMINATION OF THE INITIAL
RELATIVE DENSITIES OF THE FUEL DROP
GROUPS IN THE DICE-FAE SOLUTION

APPENDIX A

DETERMINATION OF THE INITIAL RELATIVE DENSITIES OF THE FUEL DROP GROUPS IN THE DICE-FAE SOLUTIONS

In the DICE code the fuel drops are categorized into several discrete groups, each of which contains all of the drops within a certain range of diameters, and is characterized by a minimum diameter L_i and a maximum diameter R_i . In the DICE-FAE solutions the initial mass in each group was chosen according to the following criteria:

- (a) It was assumed that at all points within the initial fuel cloud, the *number density* of the fuel drops was distributed according to a truncated normal distribution, with maximum diameter, D_M , as shown in the sketch below:



- (b) It was assumed that a certain group, say group I, is to contain a fraction f_I of the initial fuel mass.

If we consider a volume element containing N_T fuel drops, each with density ρ , then criterion (a) implies that the total mass (M) with diameters between L_i and R_i is:

$$M = \int_{L_i}^{R_i} N_T \frac{4}{3} \pi \left(\frac{D}{2}\right)^3 \rho \bar{N} dD = \frac{\sqrt{\pi} N_T \rho \sigma k}{6 \sqrt{2}} \left[\bar{N}(R_i) - \bar{N}(L_i) \right] \quad (A-1)$$

$$\text{where } \bar{N}(D) = \frac{\sqrt{2\pi}}{\sigma k} \int_0^D D^3 \bar{N} dD = \left[e^{-D^2/2\sigma^2} (D^2 + 2\sigma^2) \right] - 2\sigma^2$$

The fraction of the total mass in group i , f_i , is therefore given by:

$$f_i = \frac{\bar{N}(R_i) - \bar{N}(L_i)}{\bar{N}(D_M) - \bar{N}(0)} \quad (A-2)$$

and criterion (b) becomes:

$$f_i = \frac{\bar{N}(R_L) - \bar{N}(L_i)}{\bar{N}(D_M) - \bar{N}(0)} \quad (A-3)$$

The required f_i 's can be determined from Equation (A-2), after solving Equation (A-3) for σ . (The value of k is not required for this procedure, but could be obtained by requiring that \bar{N} be normalized). For the DICE-FAE solutions there are 4 groups, and f_4 was specified as 0.1. Table A-1 summarizes the results obtained from the above procedure using these values:

TABLE A-1. INITIAL PARAMETER VALUES FOR THE FUEL DROP GROUPS OF THE DICE-FAE SOLUTIONS

Group	L_i (cm)	R_i (cm)	f_i
1	0	0.2	0.01
2	0.2	0.75	0.63
3	0.75	1.0	0.26
4	1.0	25.0	0.10

APPENDIX B
PROPERTIES OF AIR AND
PROPYLENE OXIDE

APPENDIX B

PROPERTIES OF AIR AND PROPYLENE OXIDE

1. AIR

Air was assumed to have an ideal gas pressure equation of state:

$$P = (\gamma - 1)pe \quad (B-1)$$

with $\gamma = 1.404$

The caloric equation of state was derived from the AFWL equation of state of air (Reference 6). It is assumed to be a function of specific internal energy only:

$$T = \frac{C_a e}{C_b(e - C_c)^{.53908}} \quad \begin{array}{l} e \leq 5.63 \times 10^9 \text{ ergs/g} \\ e \geq 5.63 \times 10^9 \text{ ergs/g} \end{array} \quad (B-2)$$

where

$$\begin{aligned} C_a &= 1.41 \times 10^{-7} \text{ }^\circ\text{K/erg/g} \\ C_b &= 6.133 \times 10^{-3} \text{ }^\circ\text{K(erg/g)}^{.53908} \\ C_c &= 2.596 \times 10^9 \text{ erg/g} \end{aligned}$$

Air is assumed to always remain gaseous; it is therefore not necessary to define an air phase diagram.

2. PROPYLENE OXIDE

The pressure equation of state for propylene oxide is required *only for the vapor state*. An ideal gas equation of state (Equation B-1) was therefore assumed. For any gas, γ is approximately given by

$$\gamma = 1 + \frac{R}{C_v} \quad (B-3)$$

where R is the universal gas constant and C_v is the specific heat of the gas. For propylene oxide, $C_v = 1.118 \times 10^9$ ergs/mole/ $^\circ\text{K}$, which gives $\gamma = 1.074$.

The caloric equation of state of propylene oxide, based on data obtained from Reference 7, is given by the relations:

$$T = C_1 e + C_2, \text{ where}$$

$$C_1 = 5.196 \times 10^{-8} \text{ K/erg/g}$$

$$C_2 = -51.96^\circ\text{K, liquid state} \quad (\text{B-4})$$

$$C_2 = -399.78^\circ\text{K, vapor state}$$

The phase diagram for propylene oxide, obtained from Reference 7, is plotted in Figure B-1. Since the conditions of the FAE event considered here were such that no freezing would occur, only the liquid vapor phase line was determined. For the DICE-FAE solutions, this phase curve was fit by the following analytical approximation:

$$P = E \exp A (T - T_0) / (T - T_B) \quad (\text{B-5})$$

where $E = 26.00 \text{ dynes/cm}^2$

$$A = 20.0$$

$$T_0 = 168^\circ\text{K}$$

$$T_B = 44^\circ\text{K}$$

Figure B-1 contains this equation, which is seen to be a very good fit of the experimental data. At atmospheric pressure, note that propylene oxide boils at a temperature of 34°C , just 14°C above room temperature.

In addition to equation of state and phase transition data, the DICE-FAE solutions require several additional material property constants for use in the propylene oxide drop breakup model (see Appendix C) and the detonation model (see Section IV, paragraph 1). These constants are summarized in Table B-1.

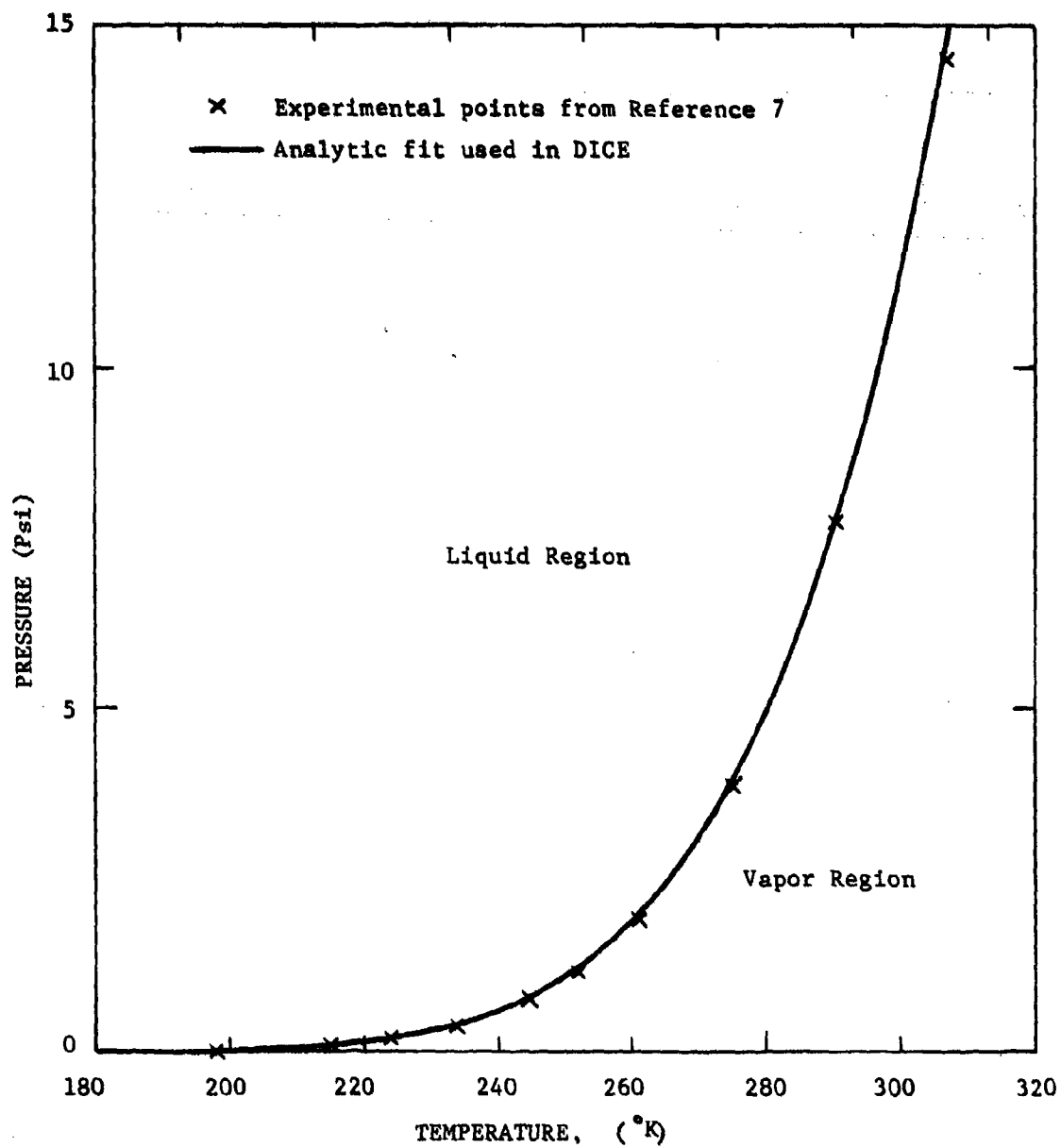


Figure B-1. P-T Phase Diagram for Propylene Oxide, Showing the Liquid-Vapor Phase Transition

TABLE B-1. MATERIAL CONSTANTS FOR PROPYLENE OXIDE

Constant	Description	Value	Source
W_B	Critical Weber number for drop breakup	6	Ref 3
σ	Surface tension	25 dynes/cm	Ref 7 Ref 8
ρ	Density	0.83g/cm ³	Ref 7
\bar{T}	Constant in drop breakup model	3.75	Ref 9
η	Viscosity	0.004 poise	Ref 7
F_C	Critical fuel to air ratio for burning	0.14	Determined from TIGER (Reference 4) code
Q	Energy released in burning per mass of fuel-air mixture (when $F_a = F_c$)	580 cal/g	Determined from TIGER code output
τ	Characteristic time for burning	80 μ sec	Based on Detonation Wave Velocity from TIGER output
T_B	Minimum temperature for burning	740°K	Approximate temperature of a Mach 3 shock wave in air
L	Latent heat of vaporization	160 cal/g	Ref 7

APPENDIX C
DROP BREAKUP MODEL

APPENDIX C

DROP BREAKUP MODEL

When a liquid drop is in motion with respect to the air surrounding it, the stresses acting on it may be sufficient to cause it to break up into a number of smaller drops. This breakup process has an important role in FAE technology, since the liquid fuel is subject to breakup after being accelerated by the burster charge, and also when exposed to the shock wave associated with the second event (SE) detonation. The physical extent of the fuel cloud and its detonability are both affected by the degree of fuel drop breakup.

When discussing drop breakup, a fundamental parameter is the Weber number, which is a measure of the ratio of the aerodynamic force on the drop to the surface tension pressure within it

$$W = \frac{\rho_a U^2 d}{2\sigma} \quad (C-1)$$

where

ρ_a	is the air density
U	is the drop-air relative velocity
d	is the drop diameter
σ	is the drop surface tension

Current theoretical and experimental results indicate that there are three regimes of breakup activity, each associated with a range of Weber numbers, as follows:

- (1) $W < W_B$. If the Weber number is less than some constant $W_B \approx 5$, drop breakup does not occur at all. The forces tending to hold the drop together dominate over the aerodynamic forces acting on the drop.
- (2) $W_B < W < W_S$. In this range drops break up by the "bag" mechanism, whereby the drop develops the appearance of a paper bag, concave end toward the flow; and eventually bursts. The value of W_S is usually $\approx 10 W_B$.
- (3) $W > W_S$. For large Weber numbers drops break up in the "stripping" mode, in which boundary layer processes at the drop periphery are important. This is the dominant mode in the FAE devices.

An acceptable breakup model for DICE-FAE solutions must be able to distinguish whether the drops in a specified computational cell are breaking up, and if so, the rate of their breakup and the size distribution of the resulting new droplets. Input available to the model consists of the drop density and temperature, the air density and temperature, the drop-air relative velocity, and any required material dependent parameters.

Reinecke (Reference 10) has obtained empirical data which indicate that the rate of mass loss from a drop which is breaking up is given by:

$$\begin{aligned} \frac{dm}{dt} &= -\frac{m_o \pi}{2t_B} \sin(\pi t/t_B) & \text{if } t < t_B \\ \frac{dm}{dt} &= 0 & \text{if } t > t_B \end{aligned} \quad (C-2)$$

where m_o is the original mass of the drop
 t_B is the breakup time of the drop

If we make the approximation that the mass loss rate is constant, then the relation (C-2)

$$\begin{aligned} \frac{dm}{dt} &= -\frac{m_o}{t_B} & t < t_B \\ \frac{dm}{dt} &= 0 & t > t_B \end{aligned} \quad (C-3)$$

Note that Equations C-2 and C-3 each conserve mass, since

$\int_0^{t_B} \frac{dm}{dt} dt = m_o$ in both cases. Equations (C-2) and (C-3) are compared in Figure C-1, and are seen to be similar enough that the constant mass loss rate assumption is adequate for the present effort. The DICE-FAE model for drop breakup consequently makes this assumption, and uses the mass loss rate defined by Equation (C-3), which requires that t_B be available.

A number of investigations have been performed which attempt to determine the functional dependence of the drop breakup time, t_B , on appropriate physical parameters. The breakup time in both regimes (2) and (3) has been found experimentally by several investigators (References 9, 11) to fit the relation

$$\frac{t_B U}{d} \sqrt{\frac{\rho_a}{\rho}} = \bar{T} \quad (C-4)$$

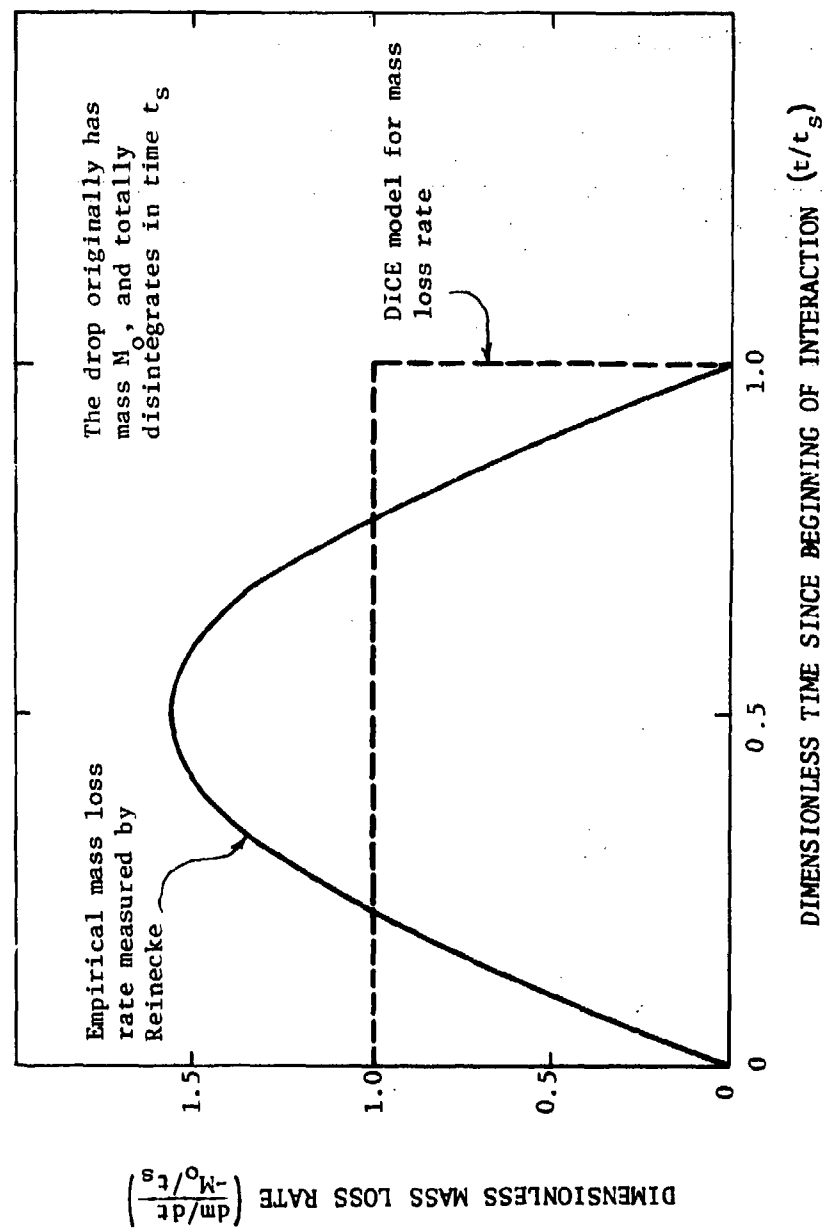


Figure C-1. Mass Loss Rate for a Disintegrating Drop versus Time as Measured by Reinecke¹⁰, and as Modeled in the DICE Solutions

where ρ is the density of the drop
 T is the dimensionless constant which depends on the drop material

Figure C-2 shows the results when Nicholson and Figler (Reference 11) applied Equation (C-4) to the experimental results of several investigators. The agreement is good, and Equations (C-3) and (C-4) are used in determining the mass loss rate in the DICE breakup model.

Having determined the rate at which breakup occurs, there remains the question of determining the size distribution of the newly formed drops. Wolfe and Andersen (Reference 12) have derived an equation which gives the average drop size δ when a drop of radius d breaks up:

$$\delta = \left[\frac{136 \nu \sigma^{3/2} d^{1/2}}{\rho_a^2 \rho^{1/2} u^4} \right]^{1/3} \quad (C-5)$$

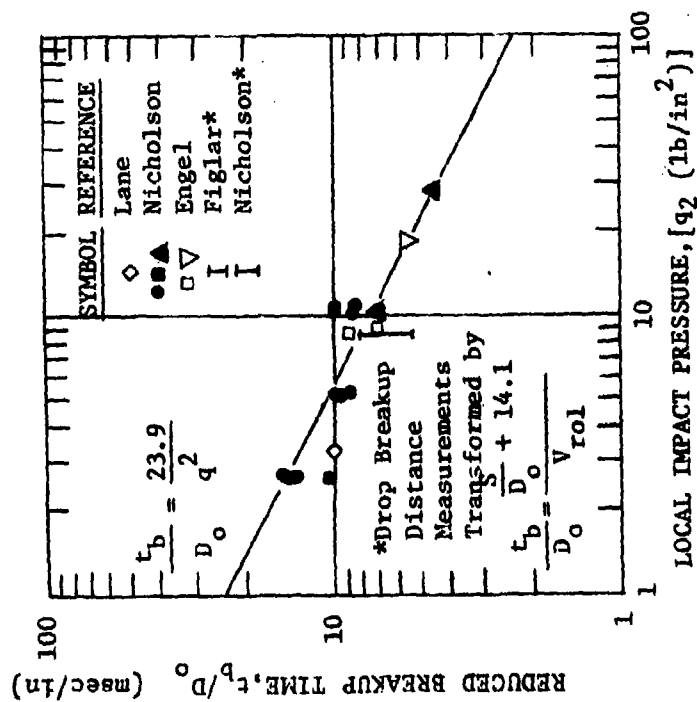
where ν is the drop viscosity

Figure C-2 shows a comparison of the predictions of Equation (C-5) with available experimental evidence, and the agreement is seen to be good. The major disagreement is in the velocity range characteristic of bag breakup, and it is probable that the disagreement here stems from the fact that bag breakup results in a bimodal distribution of drop sizes. In the DICE solutions the drops produced during breakup are assumed to all be of diameter δ , which is equivalent to making the assumption that their average diameter is δ , and the standard deviation of their diameters is small.

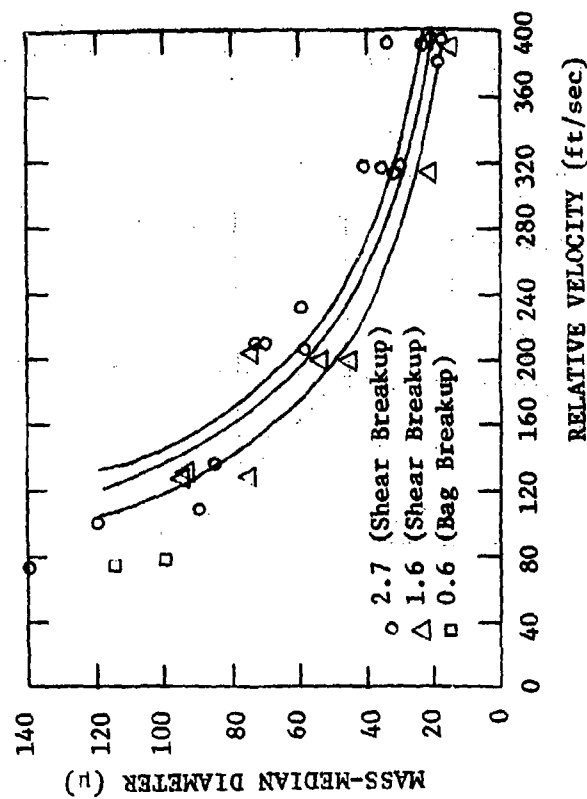
The preceding discussion states the essential features of the DICE-FAE breakup model. To summarize, the breakup model assumes the following:

- (a) A drop does not break up if its Weber number is less than some pre-specified value W_B .
- (b) If the drops of a certain size group in some computational cell are breaking up, the rate of mass loss is determined by Equation (C-3) and the breakup time t_B is determined by Equation (C-4). T is a pre-specified constant.
- (c) When a drop breaks up, the diameter of the resulting droplets is determined by Equation (C-5).

Figure C-3 shows the breakup time for water drops of various diameters as a function of relative velocity using the DICE-FAE model.



CORRELATION OF EXPERIMENTAL BREAKUP TIMES WITH THE FORMULA OF NICHOLSON AND FIGLER (Ref. 11)



COMPARISON OF PREDICTED DROPLET SIZE WITH EXPERIMENTAL OBSERVATIONS (Ref. 12)

Figure C-2. Experimental Verification of the DICE-II Model for Drop Breakup Times, and for the Mean Size of the Resulting Droplets.

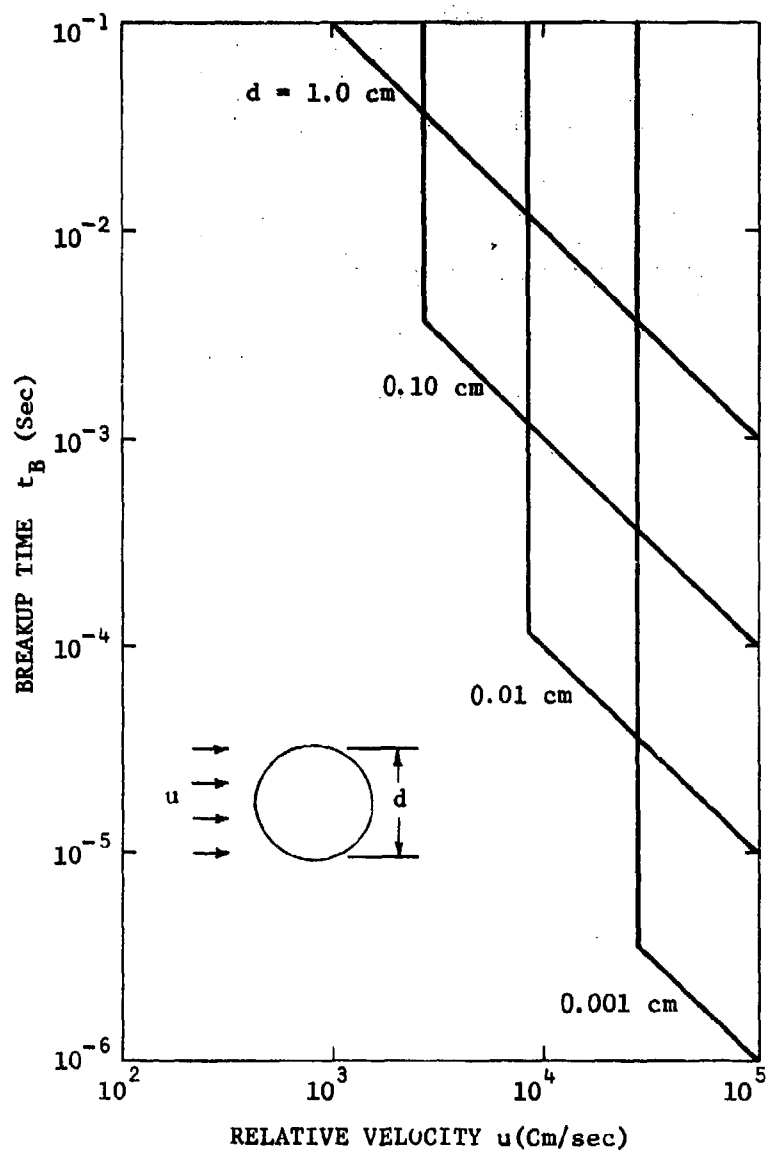


Figure C-3. Breakup Time versus Relative Velocity for a Water Drop, as Computed by the DICE-FAE Breakup Model

APPENDIX D

DENSITY CONTOUR PLOTS AND PARAMETER VERSUS TIME
PLOTS FOR SOLUTION 5A PRIOR TO THE SECOND EVENT DETONATION

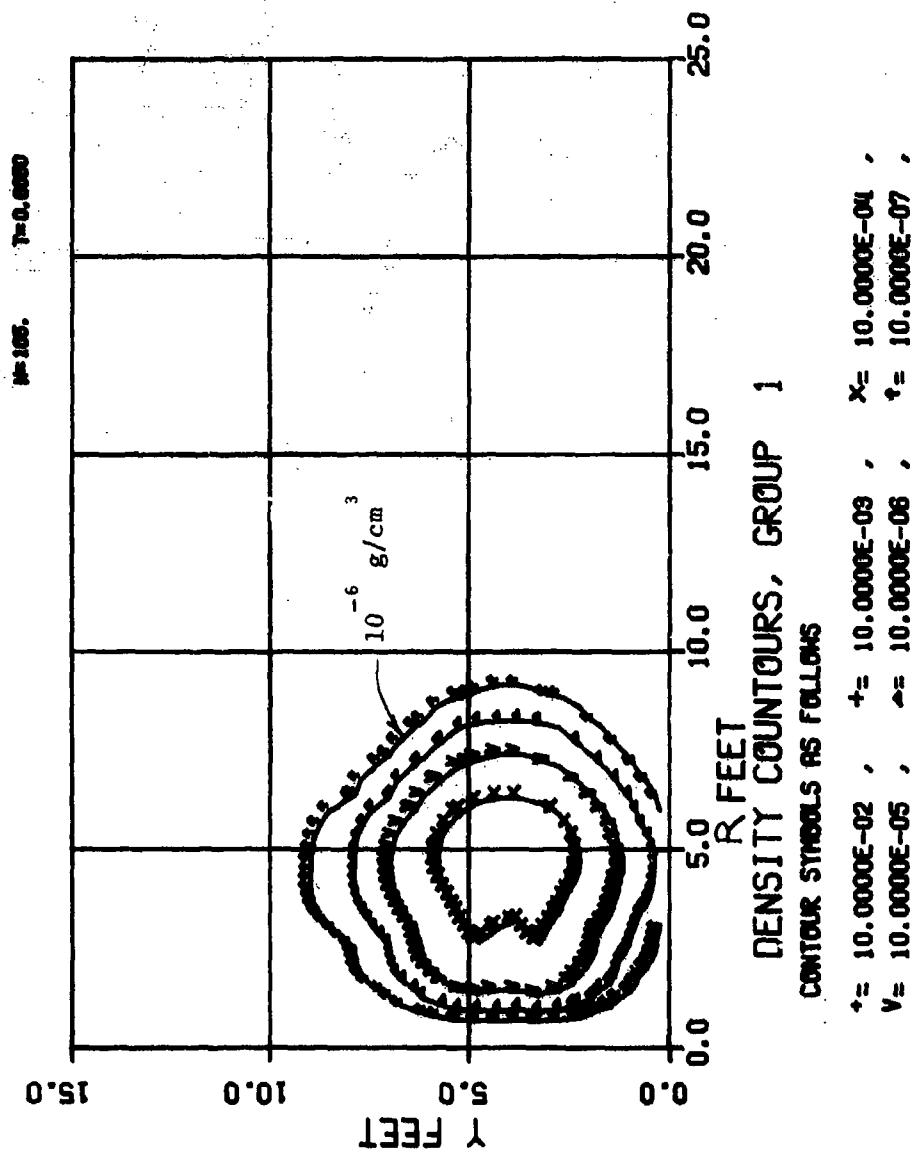


Figure D-1. Fuel Group 1 (0.01-cm Diameter Drops) Density
Contours for DICE-FAE CASE 5A at 5.0 msec

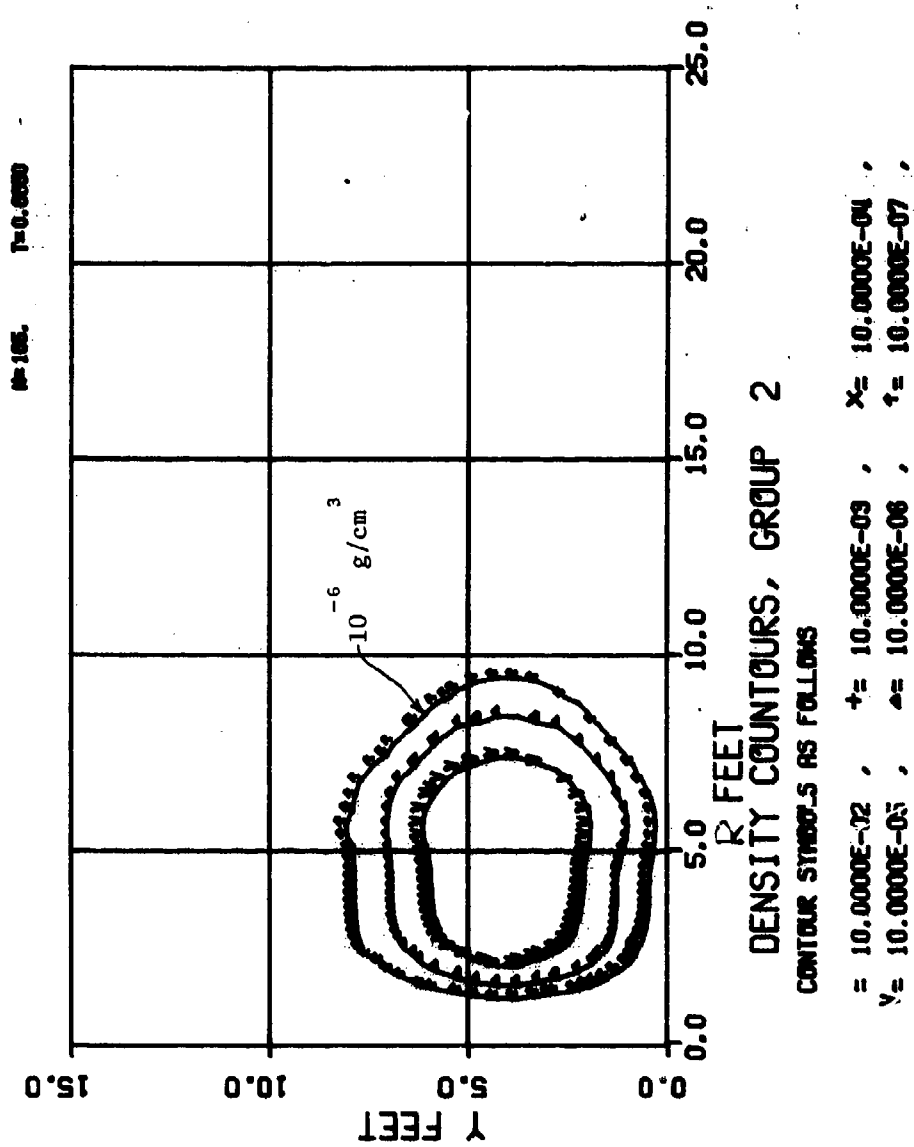


Figure D-2. Fuel Group 2 (0.48-cm Diameter Drops) Density
Contours for DICE-FAE Case 5A at 5.0 msec

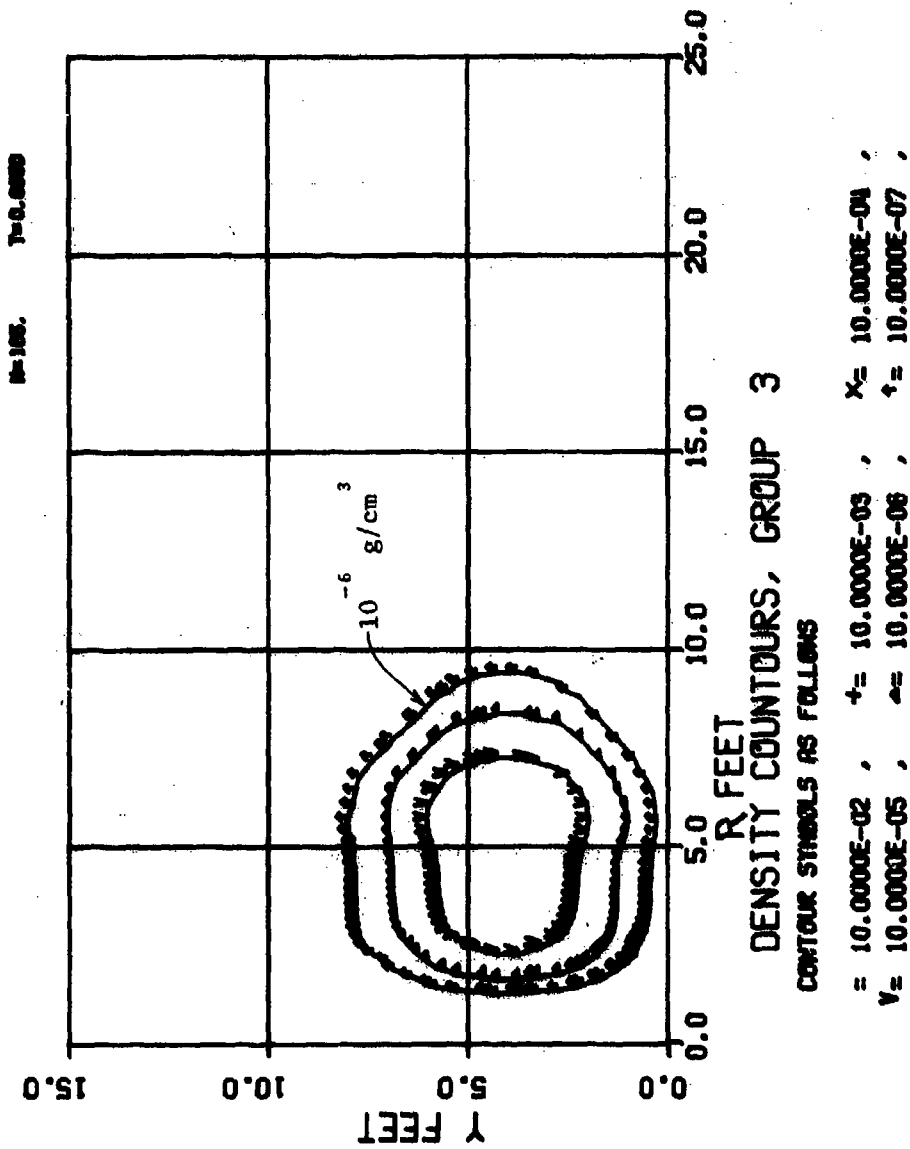


Figure D-3. Fuel Group 3 (0.88-cm Diameter Drops) Density
 Contours for DICE-FAE Case 5A at 5.0 msec

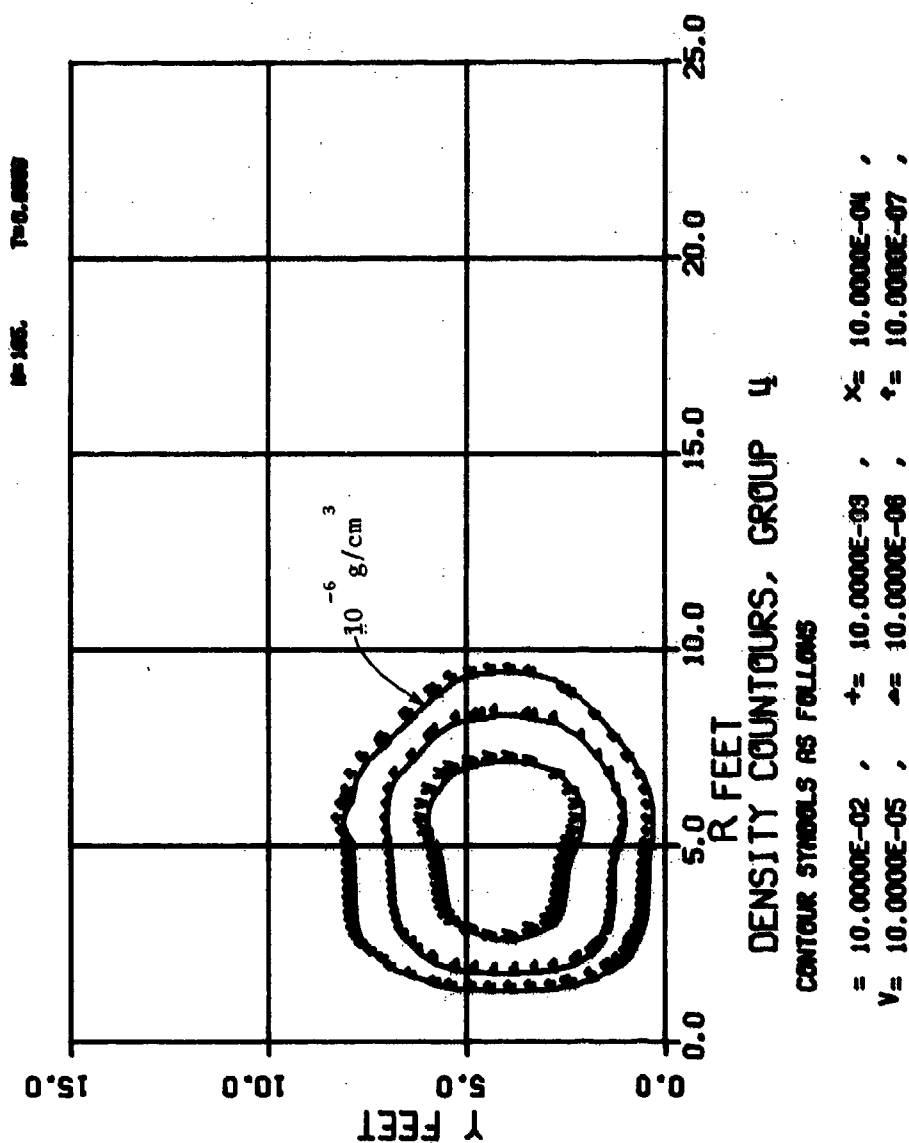


Figure D-4. Fuel Group 4 (13.0-cm Diameter Drops) Density Contours for DICE-FAE Case 5A at 5.0 msec

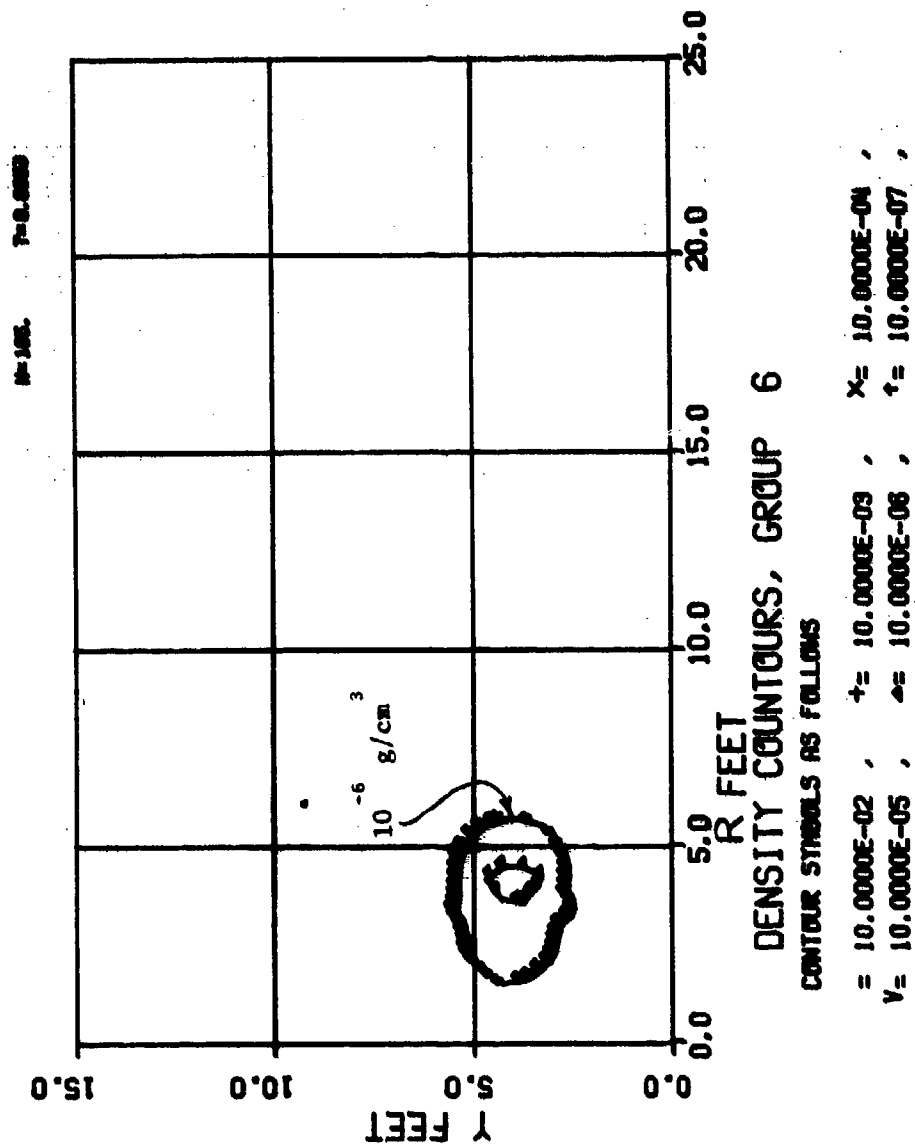


Figure D-5. Fuel Vapor Density Contours for DICE-FAE Case 5A at 5.0 msec

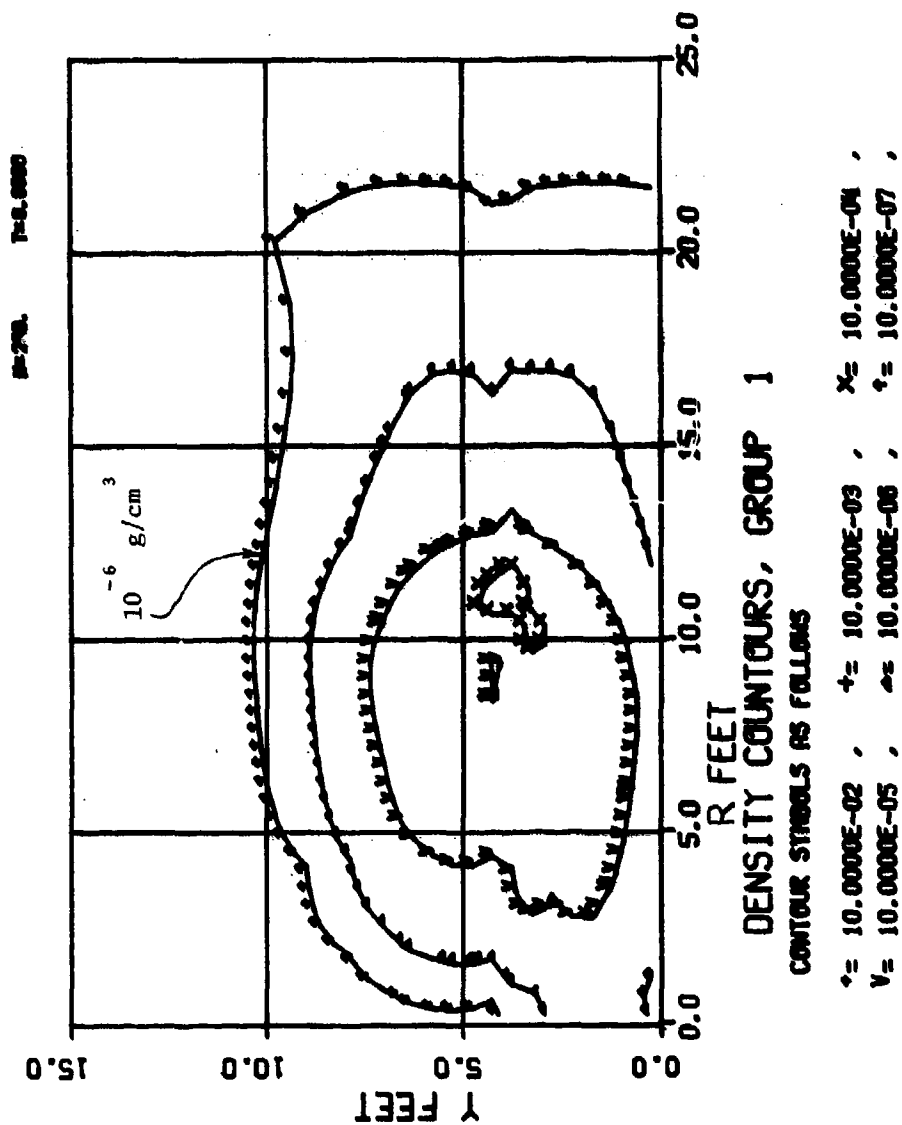


Figure D-6. Fuel Group 1 (0.01-cm Diameter Drops) Density Contours for DICE-FAE Case 5A at 30.0 msec

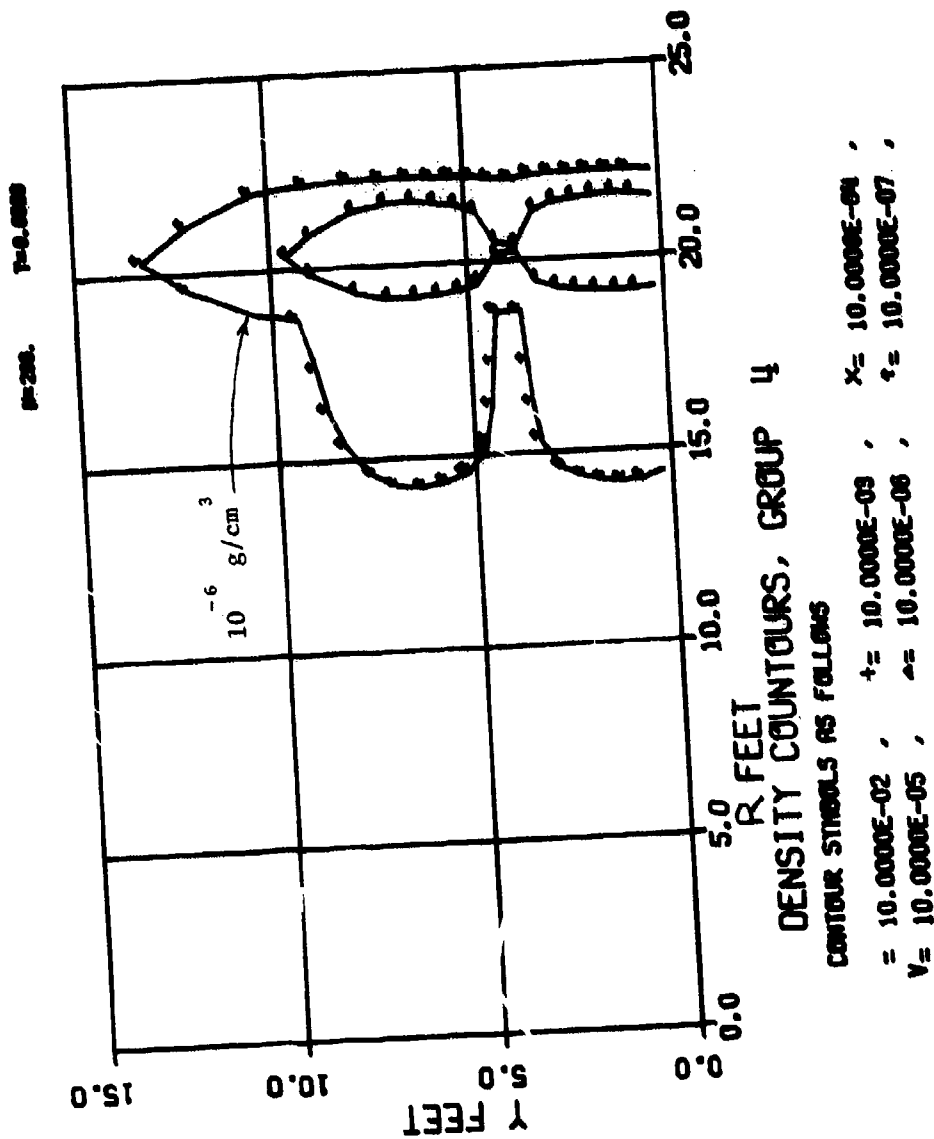


Figure D-7. Fuel Group 4 (13.0-cm Diameter Drops) Density
 Contours for DICE-FAE Case 5A at 30.0 msec

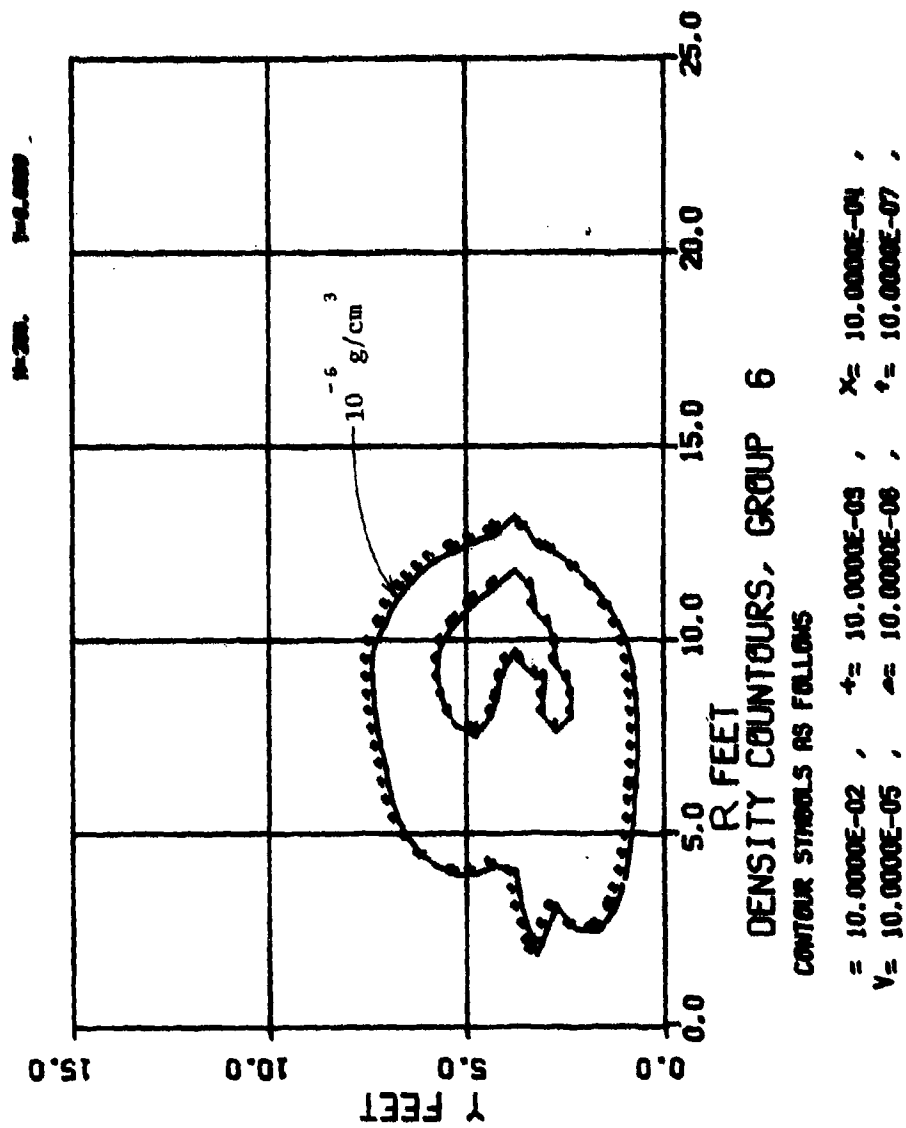


Figure D-8. Fuel Vapor Density Contours for DICE-FAE Case 5A
at 30.0 msec

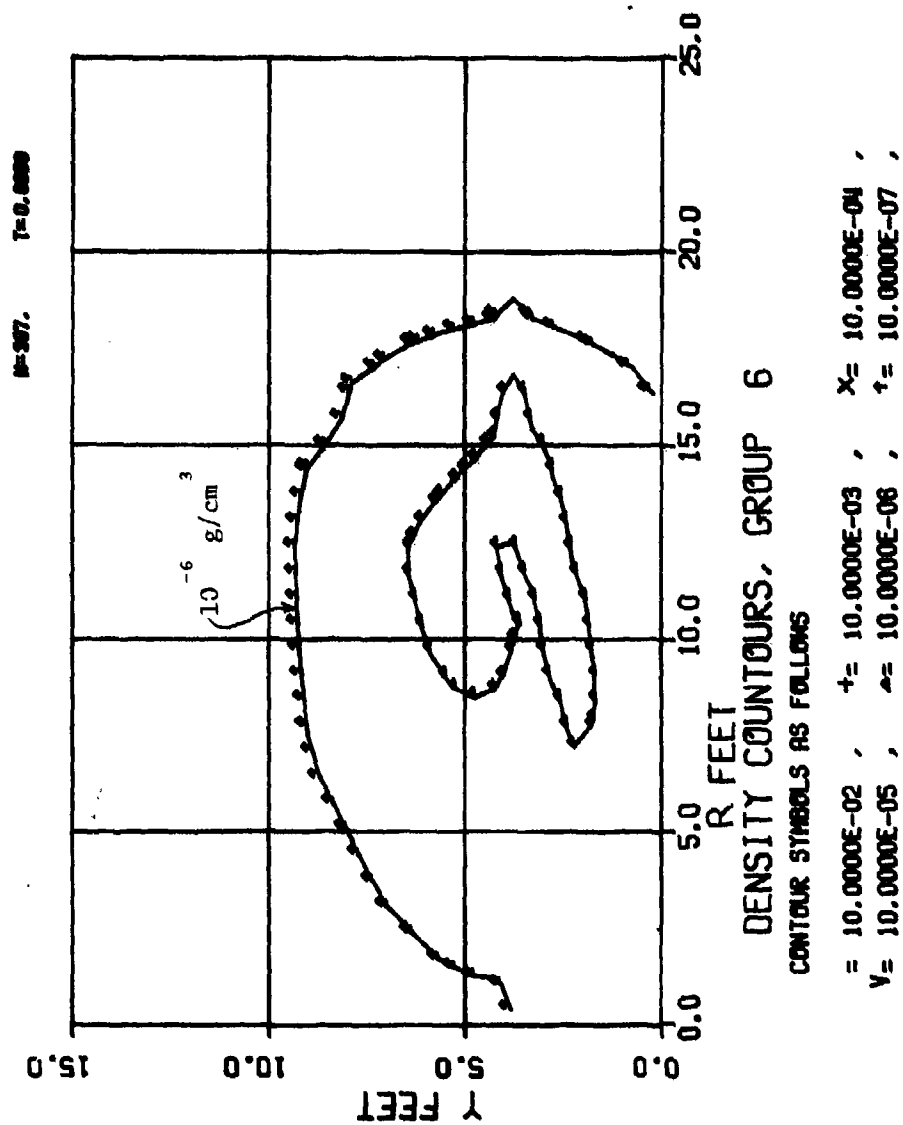


Figure D-9. Fuel Vapor Density Contours for DICE-FAE Case 5A
at 60.0 msec

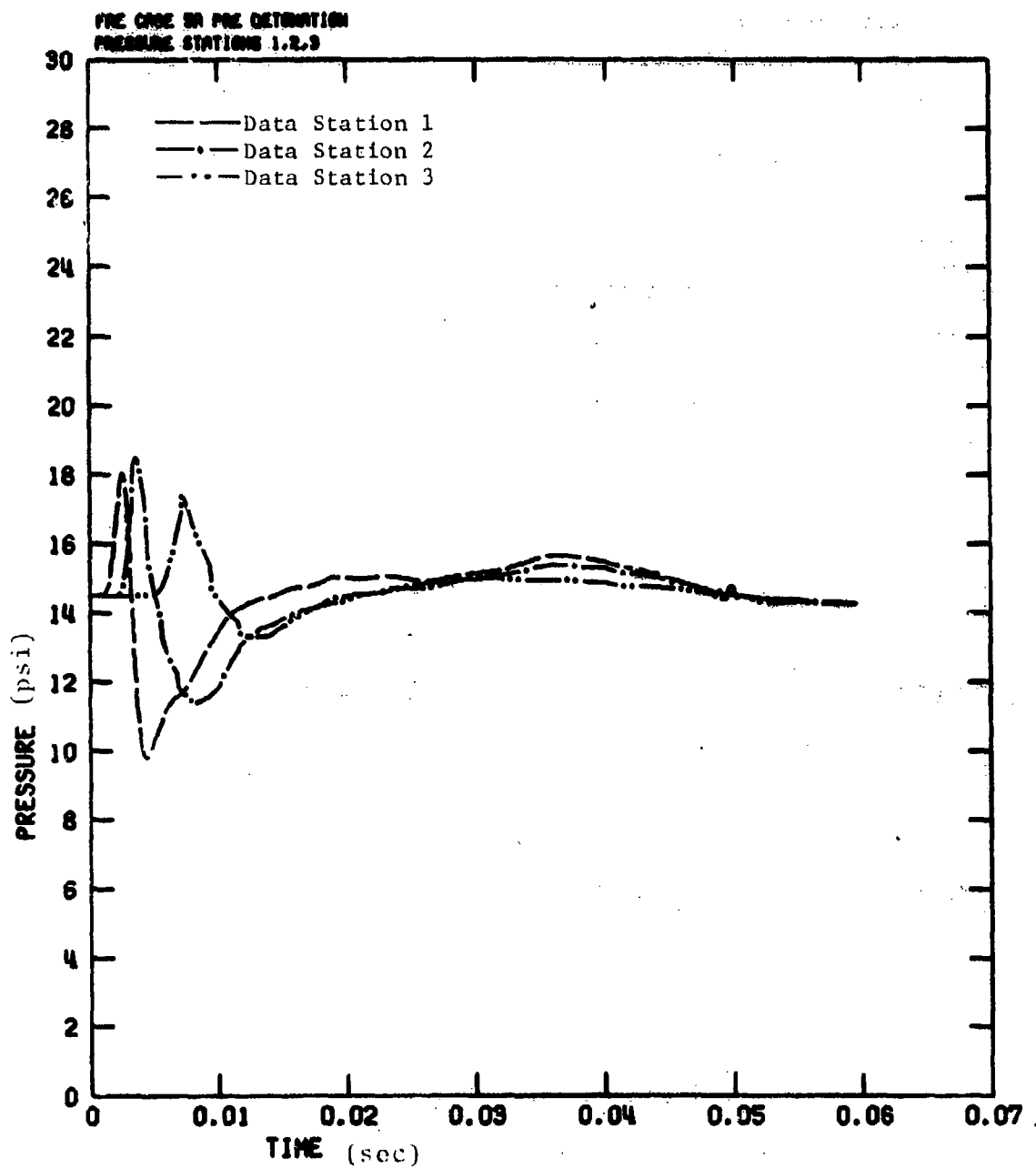


Figure D-10. Pressure versus Time at Data Stations 1, 2, and 3 Prior to the Second Event Initiation

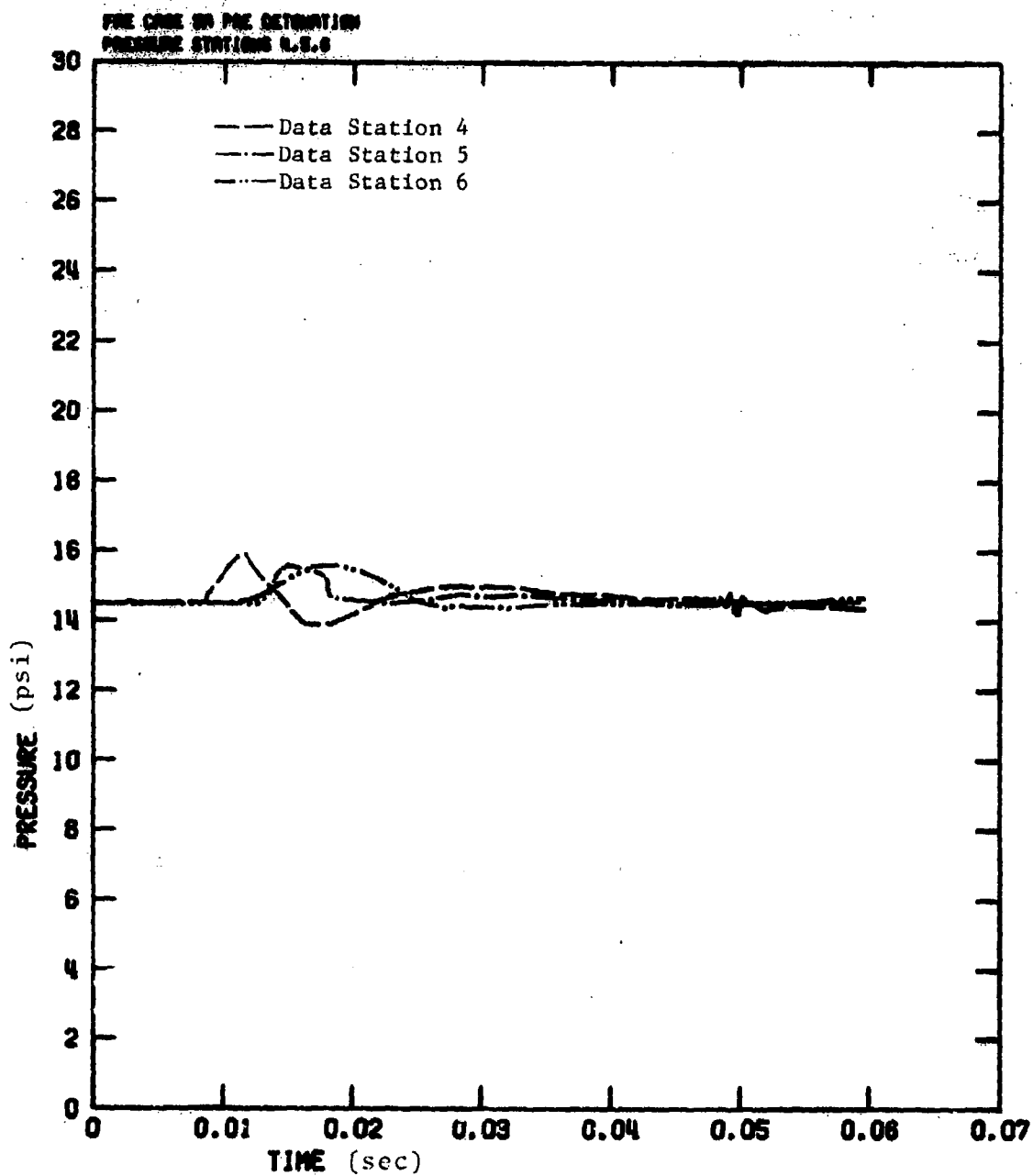


Figure D-11. Pressure versus Time at Data Stations 4, 5, and 6 Prior to the Second Event Initiation

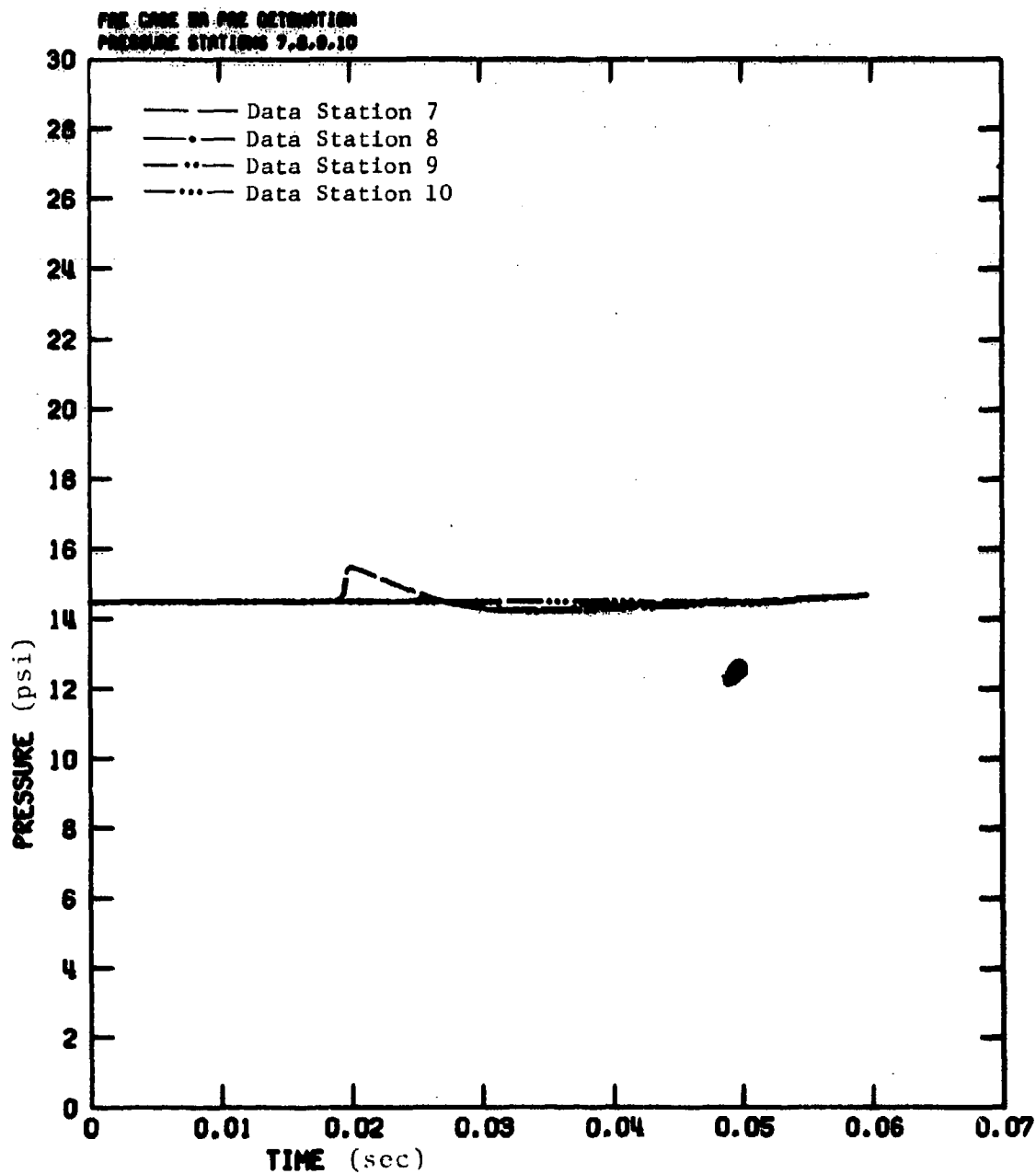


Figure D-12. Pressure versus Time at Data Stations 7, 8, 9, and 10 Prior to the Second Event Initiation

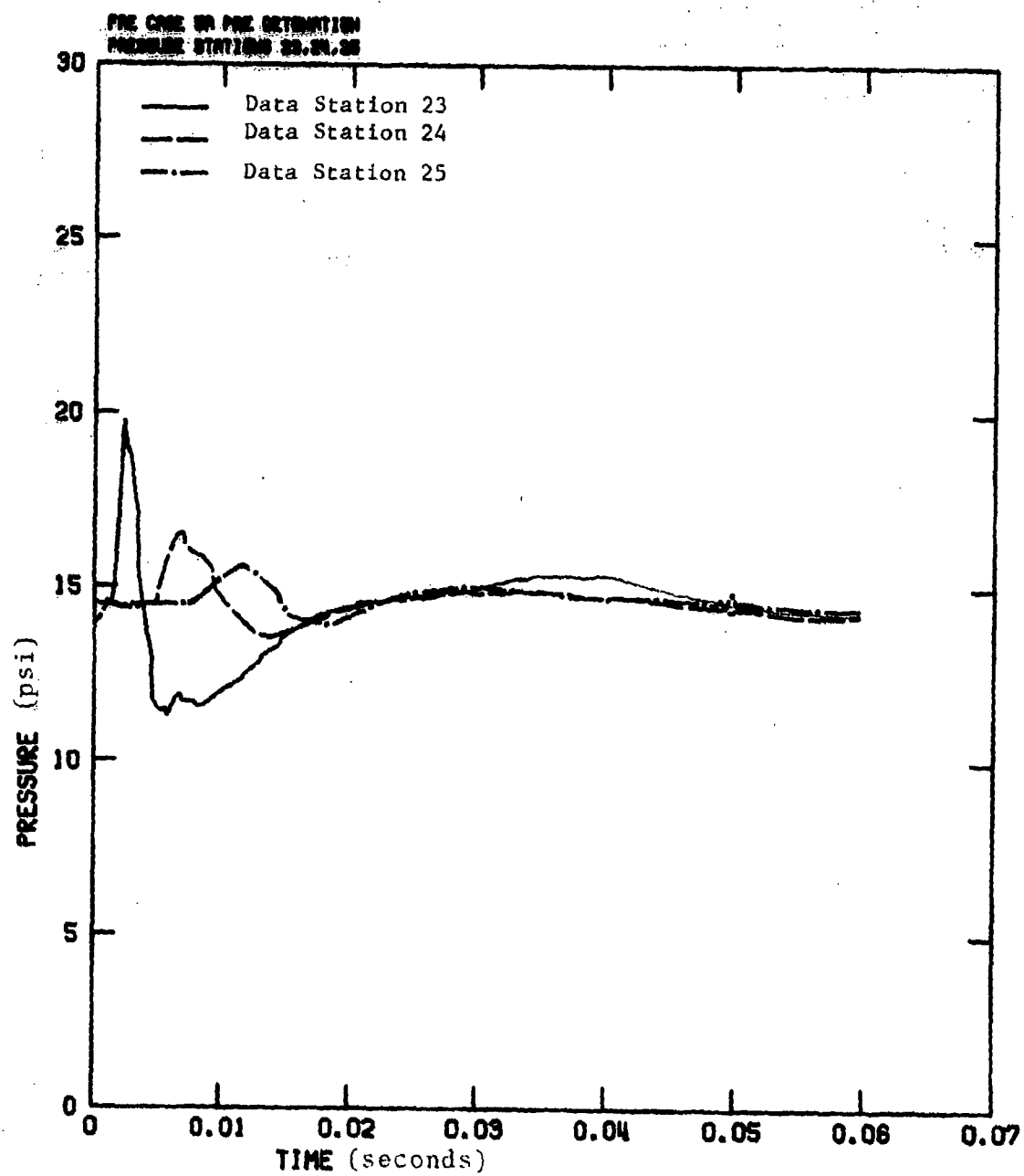


Figure D-13. Pressure versus Time at Data Stations, 23, 24, and 25 Prior to the Second Event Initiation

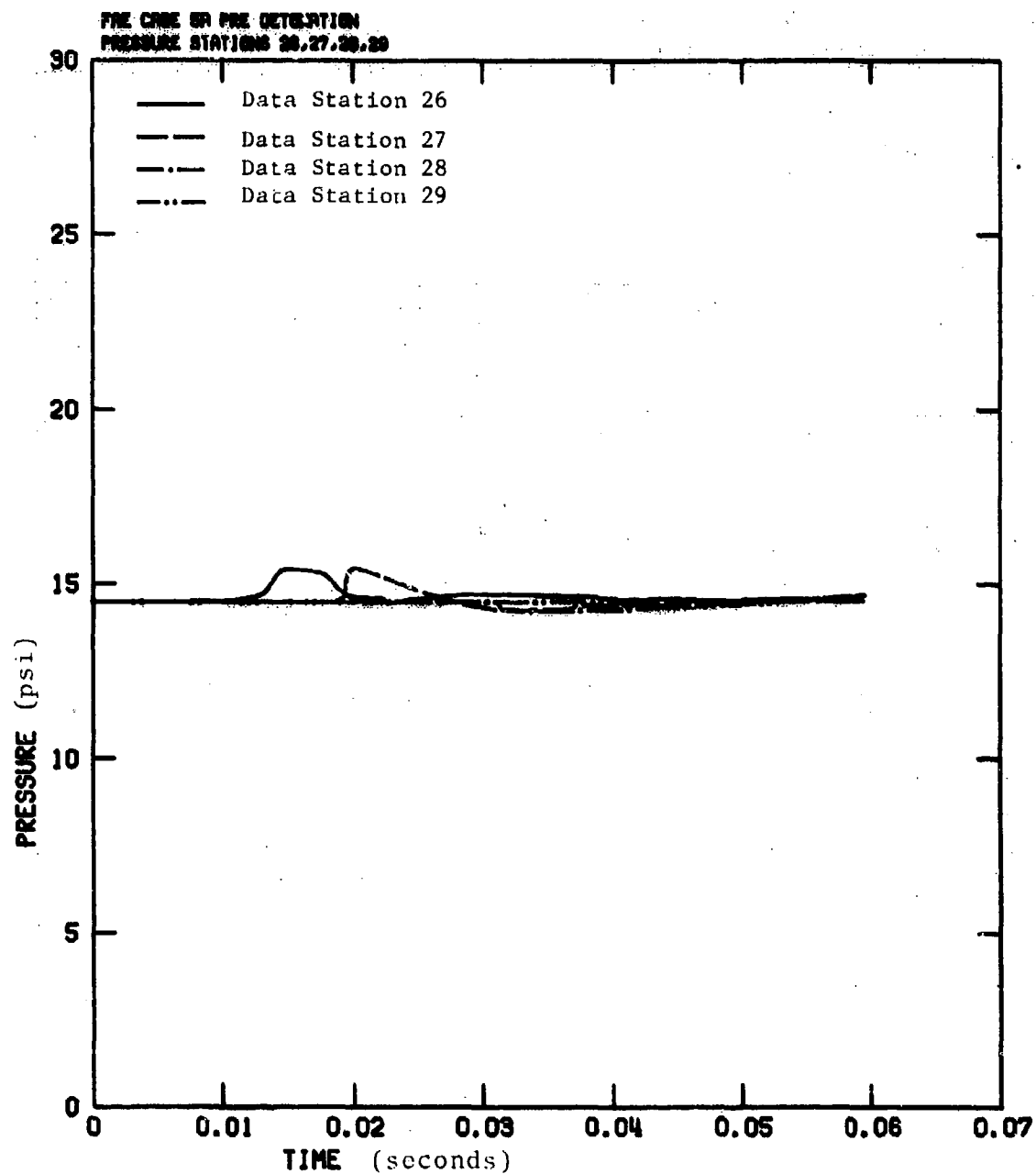


Figure D-14. Pressure versus Time at Data Stations 26, 27, 28, and 29 Prior to the Second Event Initiation

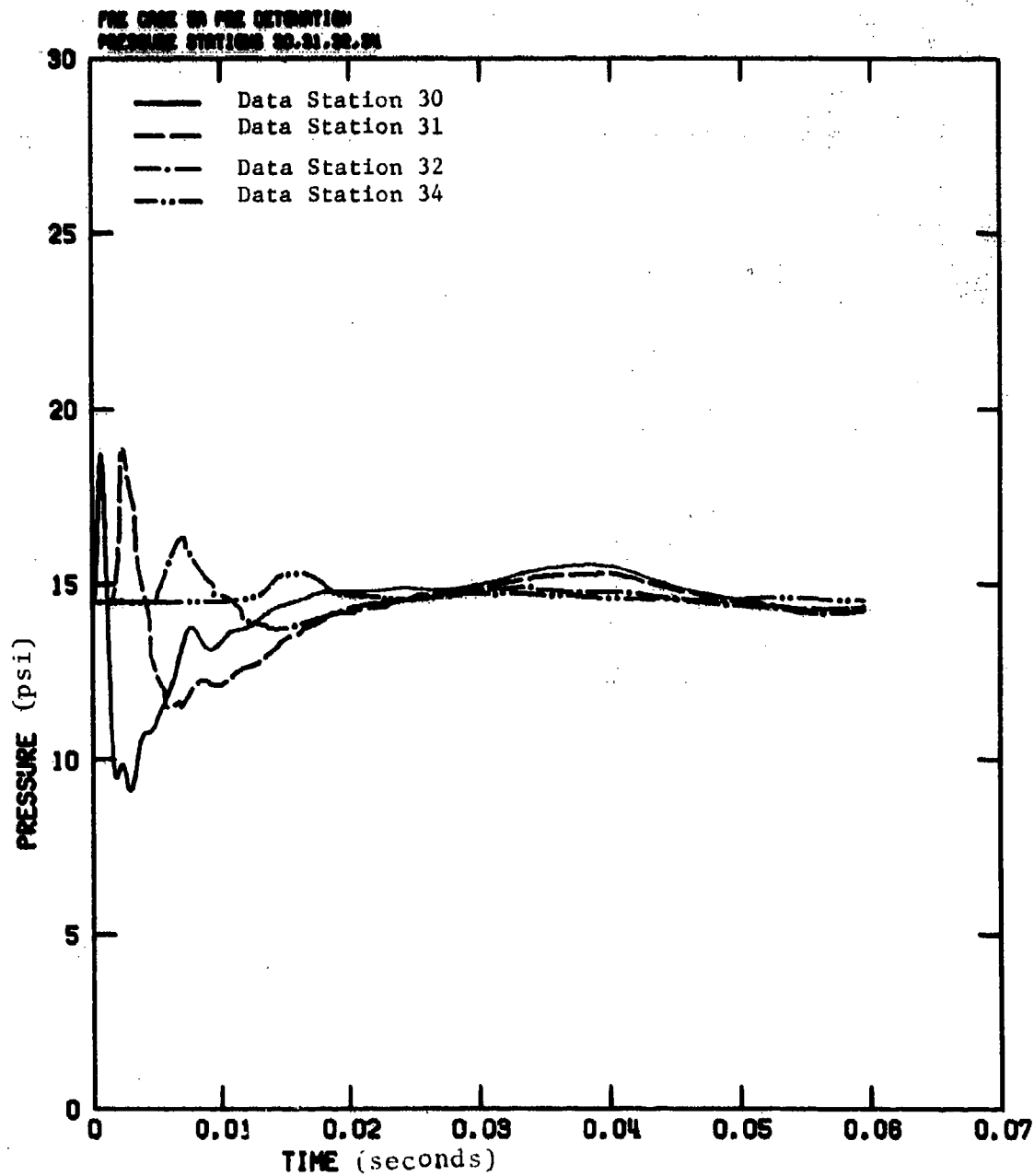


Figure D- 15. Pressure versus Time at Data Stations 30, 31
32, and 34 Prior to the Second Event Initiation

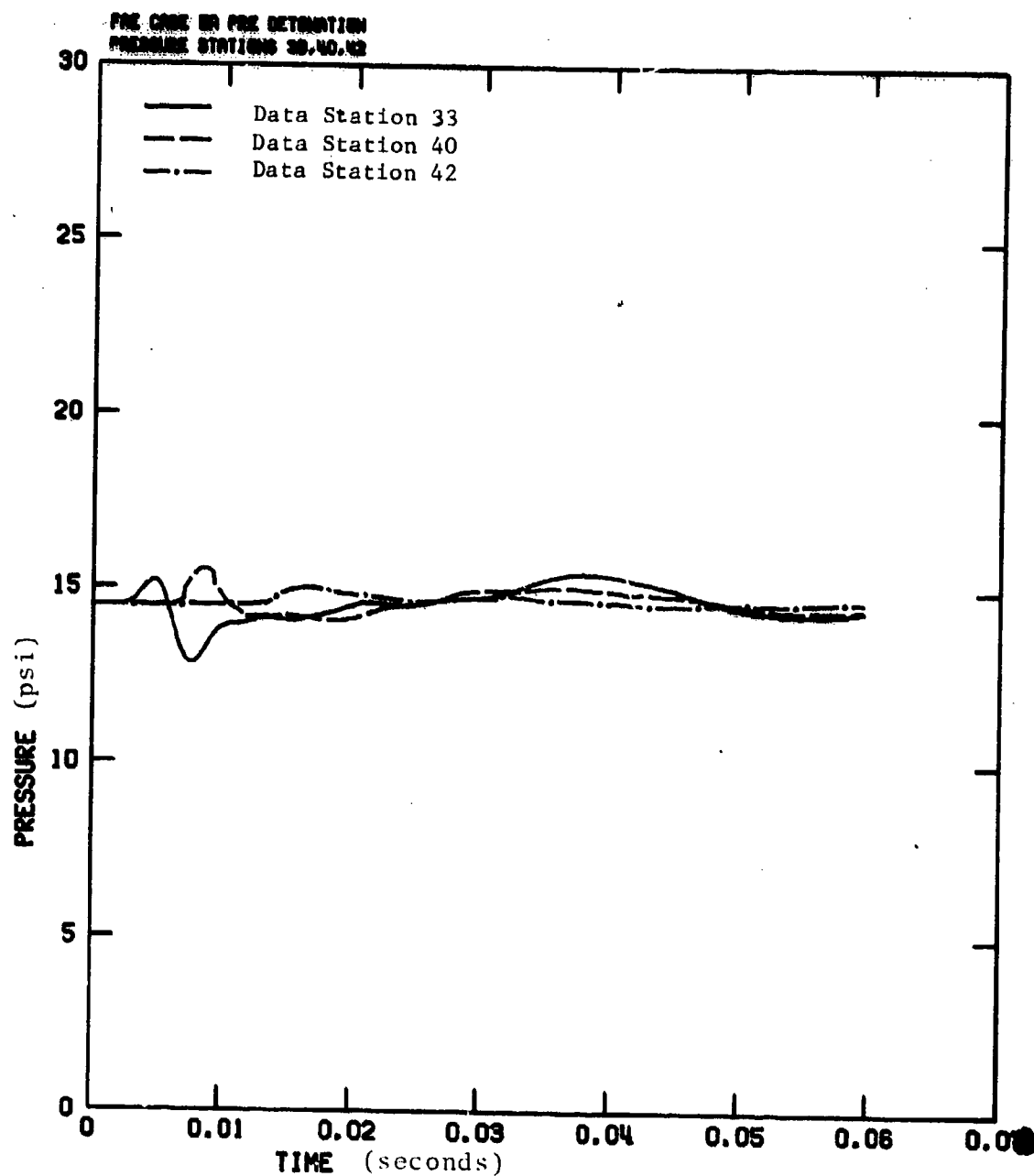


Figure D-16. Pressure versus Time at Data Stations 38, 40, and 42 Prior to the Second Event Initiation

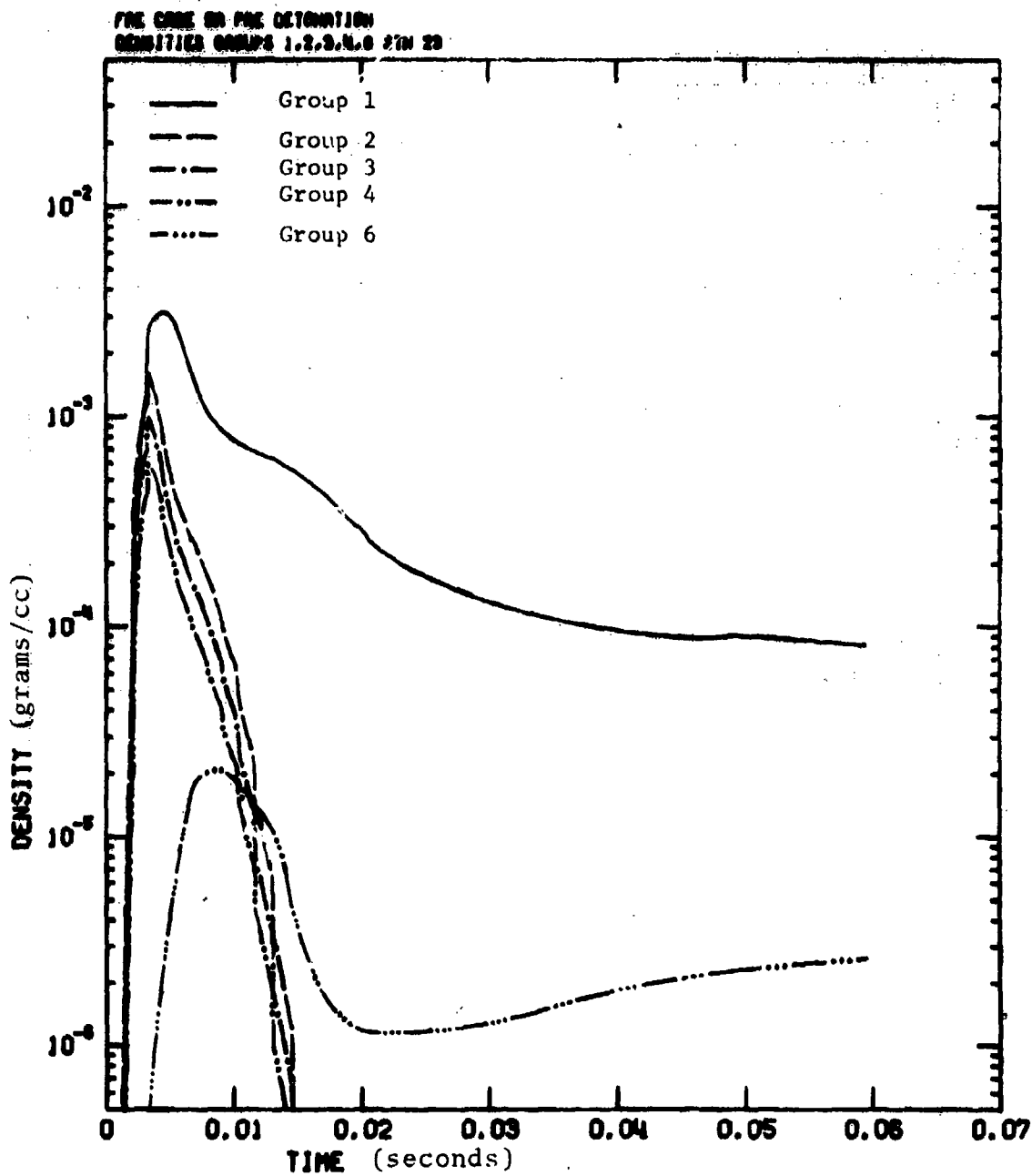


Figure D-17. Densities for the Various Fuel Groups at Data Station 23 Prior to the Second Event Initiation

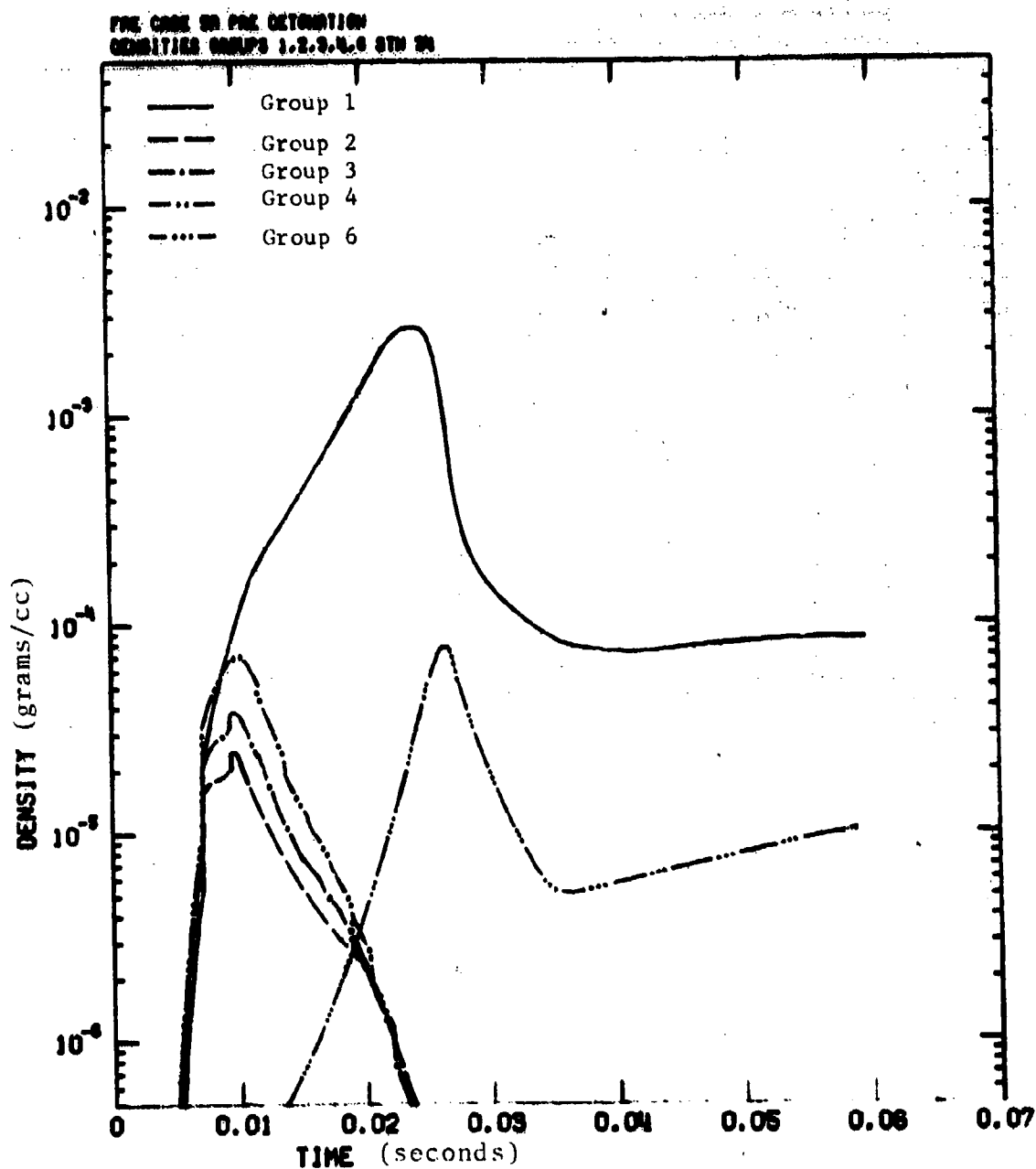


Figure D-18. Densities for the Various Fuel Groups at
Data Station 24 Prior to the Second Event
Initiation

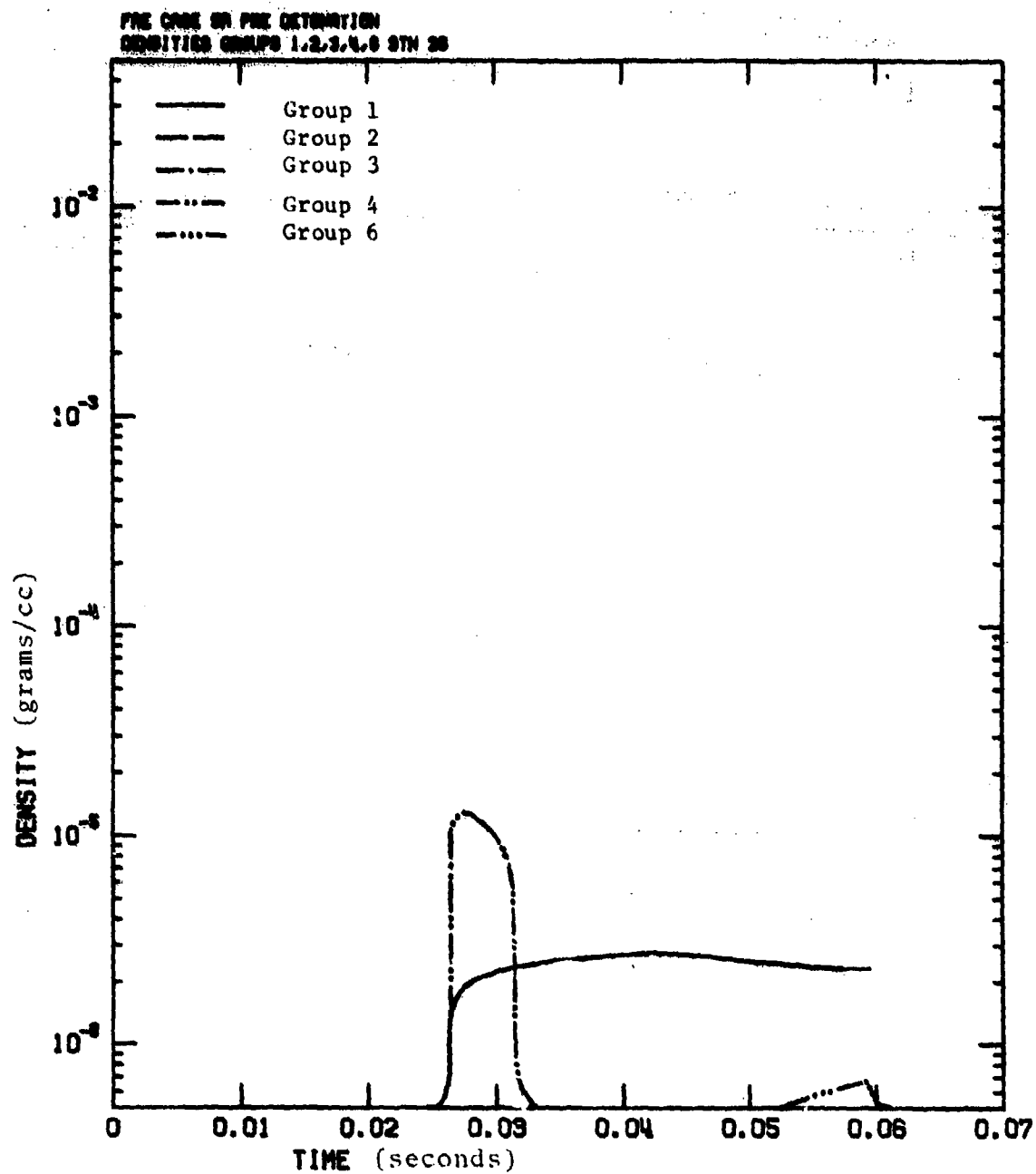


Figure D-19. Densities for the Various Fuel Groups at
Data Station 26 Prior to the Second Event
Initiation

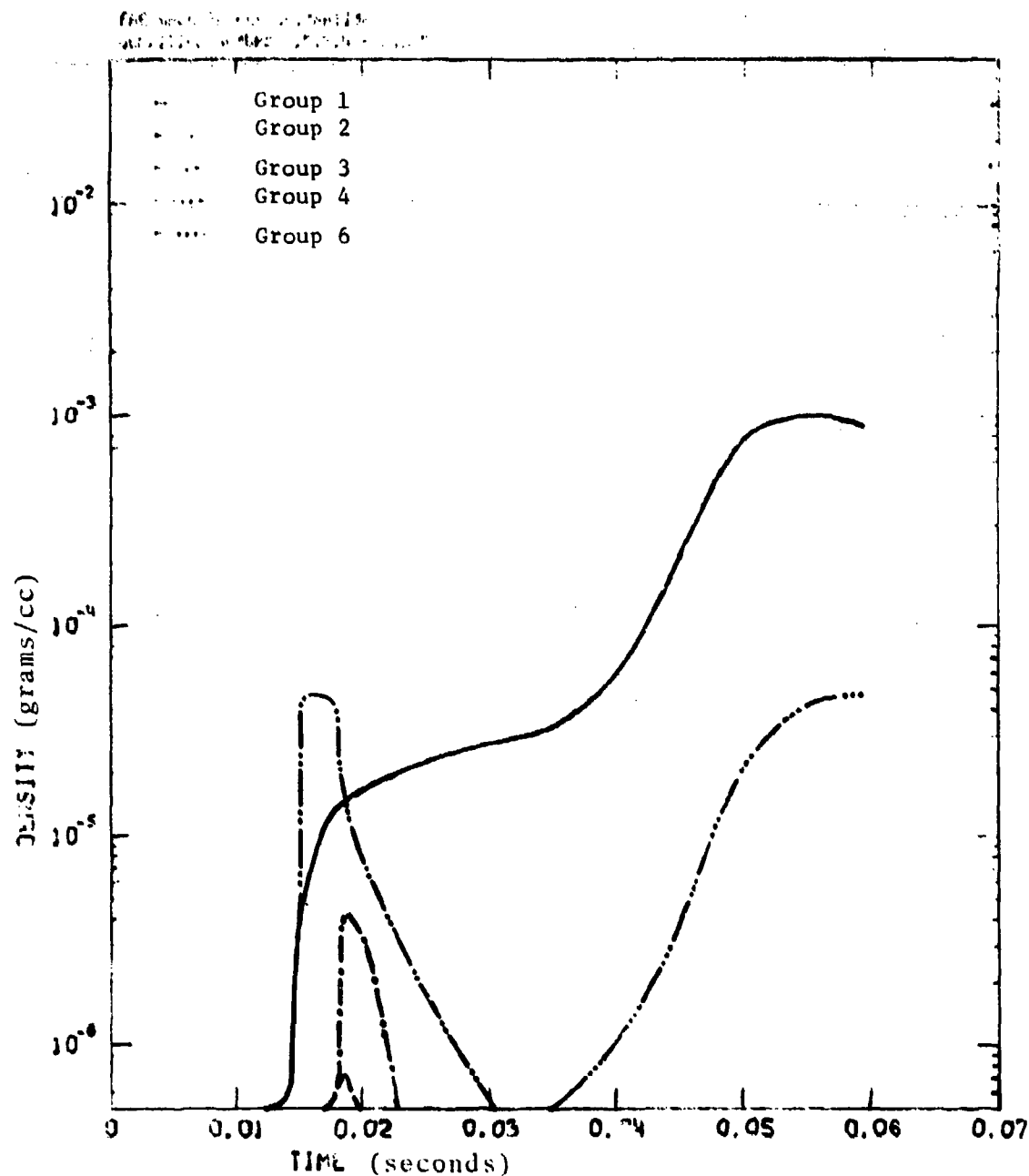


Figure D-20. Densities for the Various Fuel Groups at Data Station 25 Prior to the Second Event Initiation

PAE CASE OR PAE DETONATION
 DENSITY GROUPS 1,2,3,4,5 STN 22

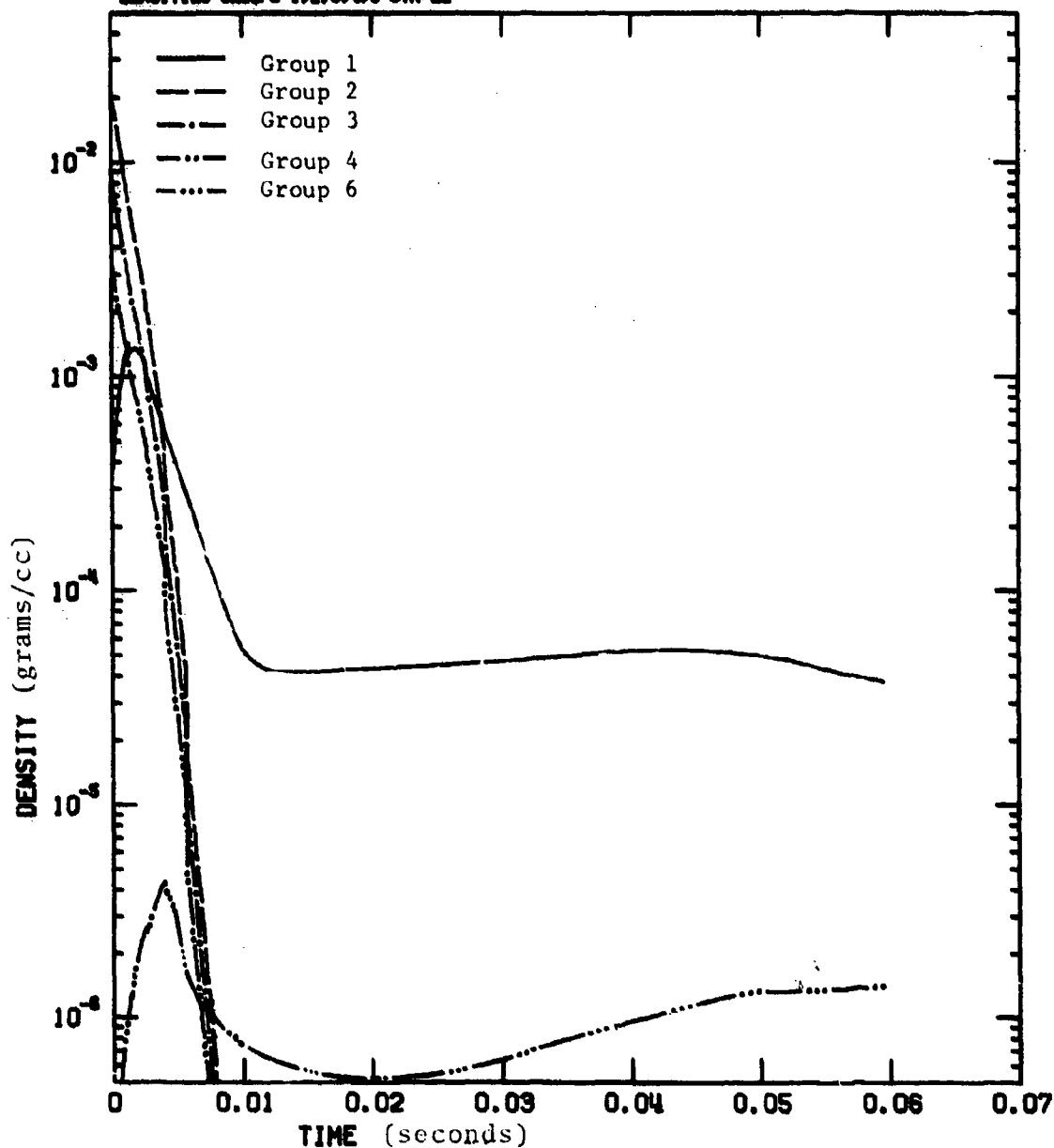
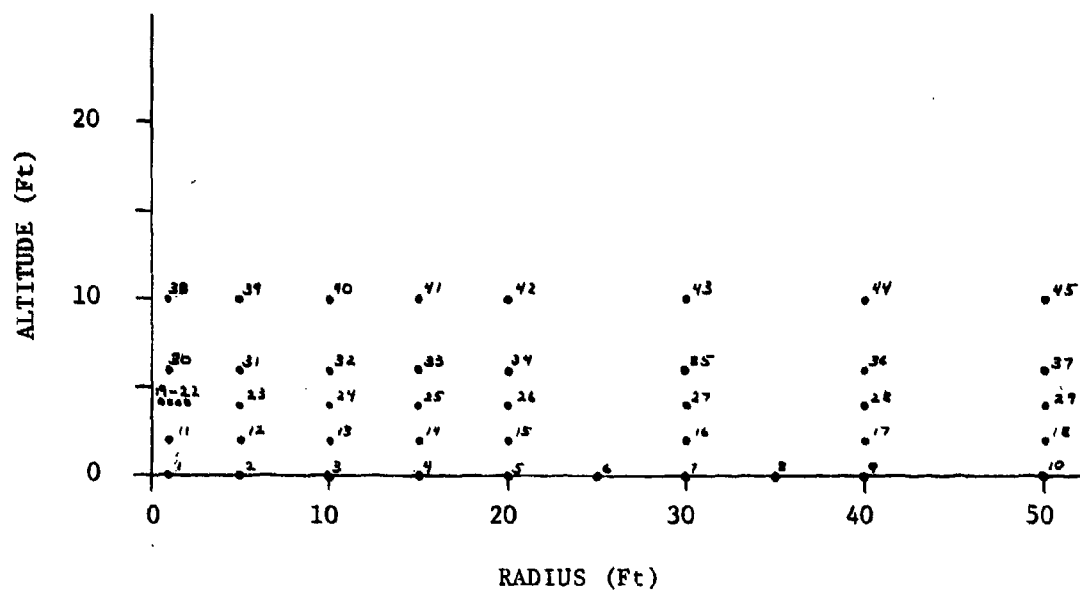


Figure D-21. Densities for the Various Fuel Groups at
 Data Station 22 Prior to the Second Event
 Initiation

APPENDIX E

DENSITY CONTOUR PLOTS AND PARAMETER VERSUS
TIME PLOTS FOR SOLUTION 5A SUBSEQUENT TO THE
SECOND EVENT DETONATION



Force Stations

Station	Radius (ft)	Alt (ft)	Station	Radius (ft)	Alt (ft)
1	1	0	24	10	4
2	5		25	15	
3	10		26	20	
4	15		27	30	
5	20		28	40	
6	25		29	50	
7	30		30	1	
8	35		31	5	
9	40		32	10	
10	50	2	33	15	6
11	1		34	20	
12	5		35	30	
13	10		36	40	
14	15		37	50	
15	20		38	1	
16	30		39	5	
17	40		40	10	
18	50	4	41	15	10
19	0.5		42	20	
20	1.		43	30	
21	1.5		44	40	
22	2.		45	50	
23	5				

Figure E-1. Points Within the Solution Region at which Parameter versus Time Histories were Generated in the DICE-FAE Solutions

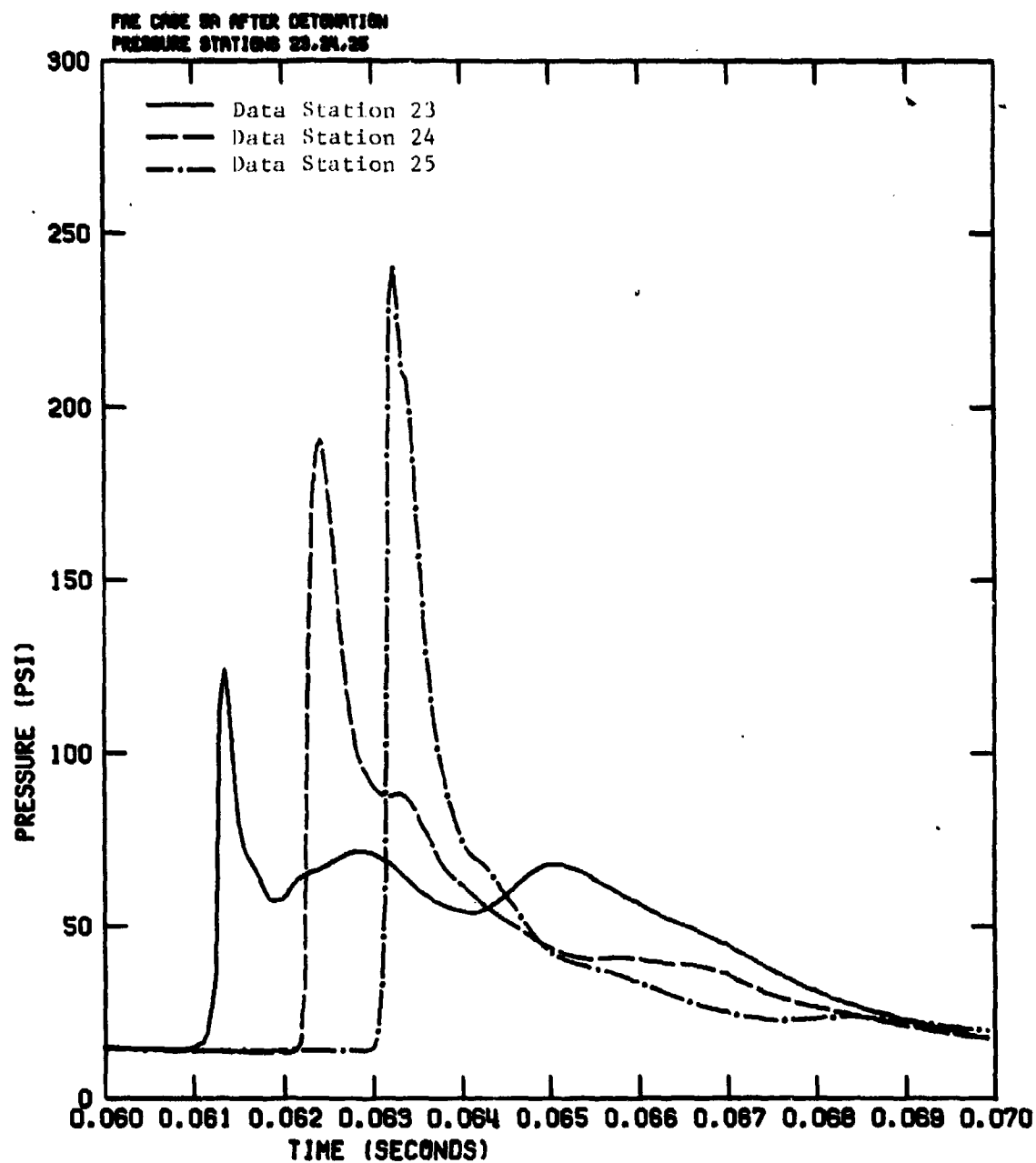


Figure E-2. Pressure versus Time at Data Stations 23, 24, and 25

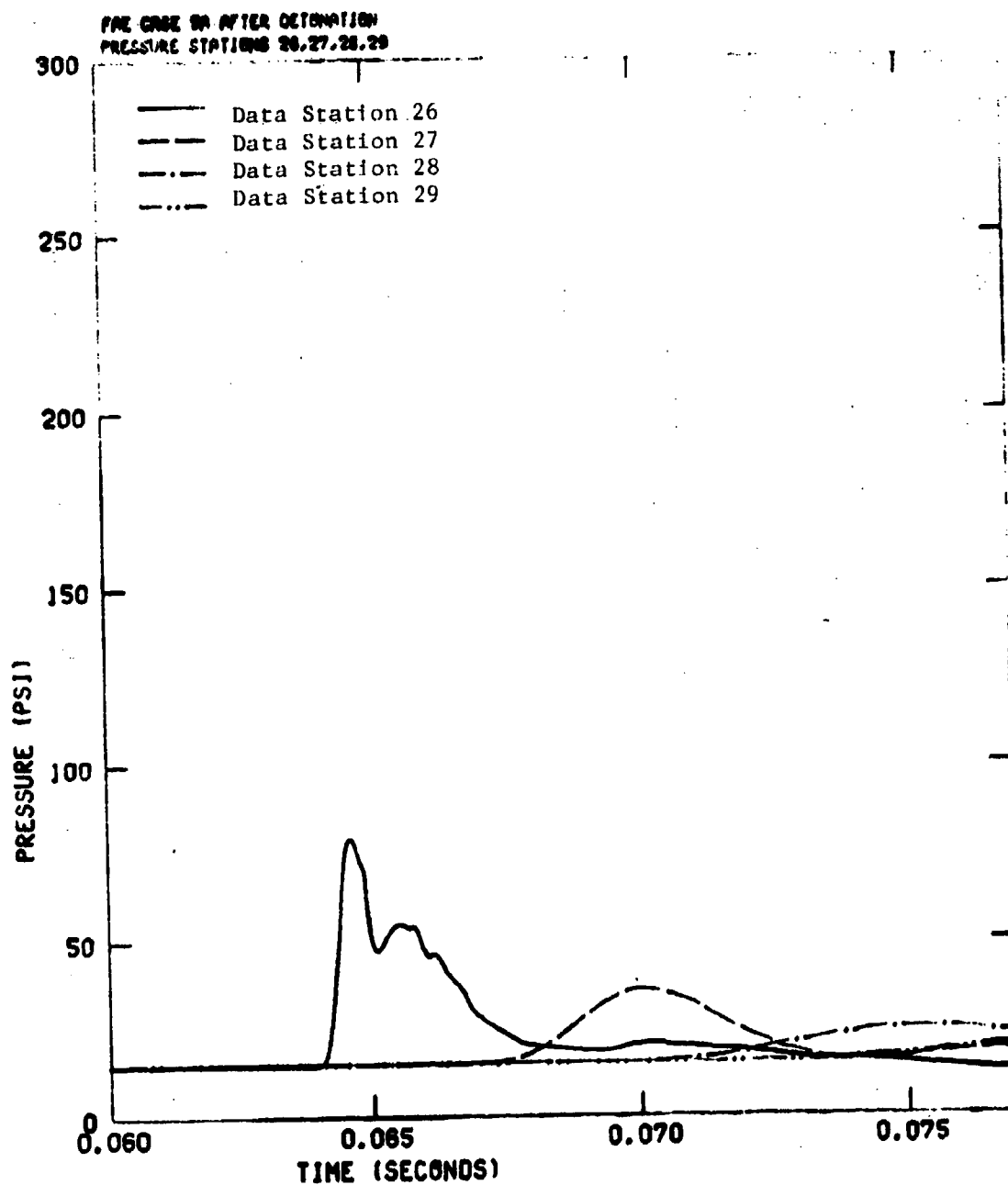


Figure E-3. Pressure versus Time at Data Stations 26, 27, 28, and 29

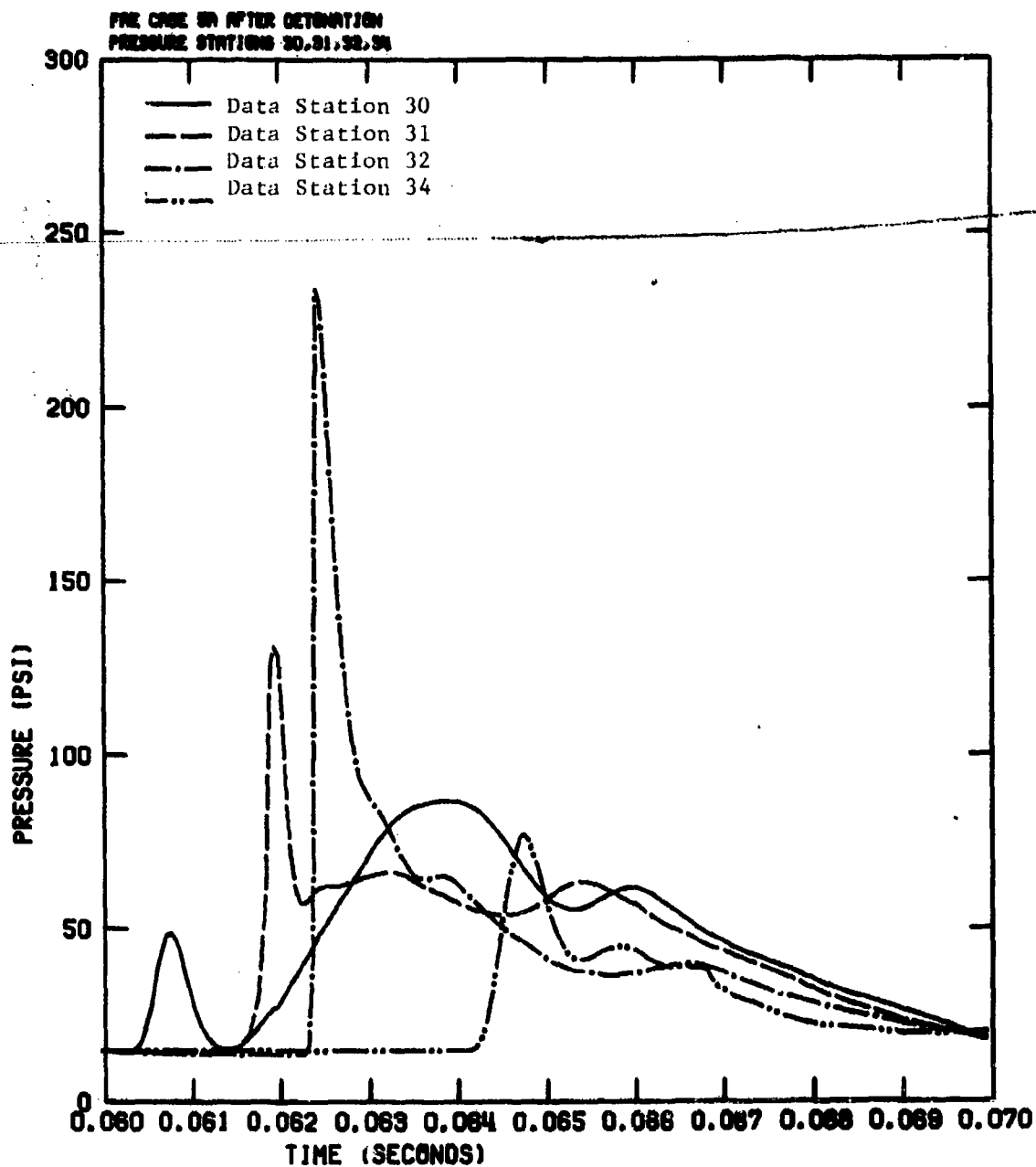


Figure E-4. Pressure versus Time at Data Stations 30, 31, 32, and 34

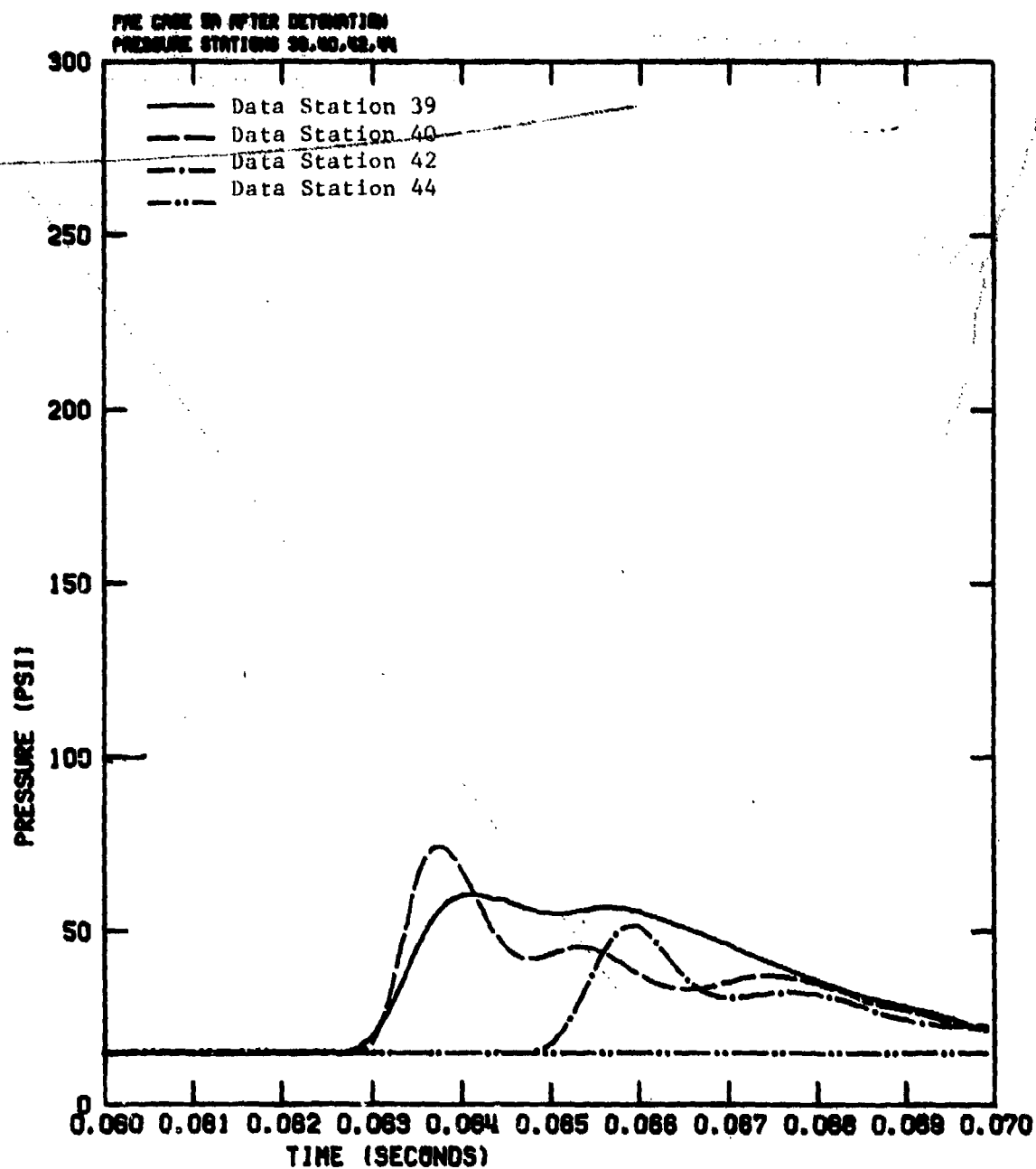


Figure E-5. Pressure versus Time at Data Stations 39, 40, 42, and 44

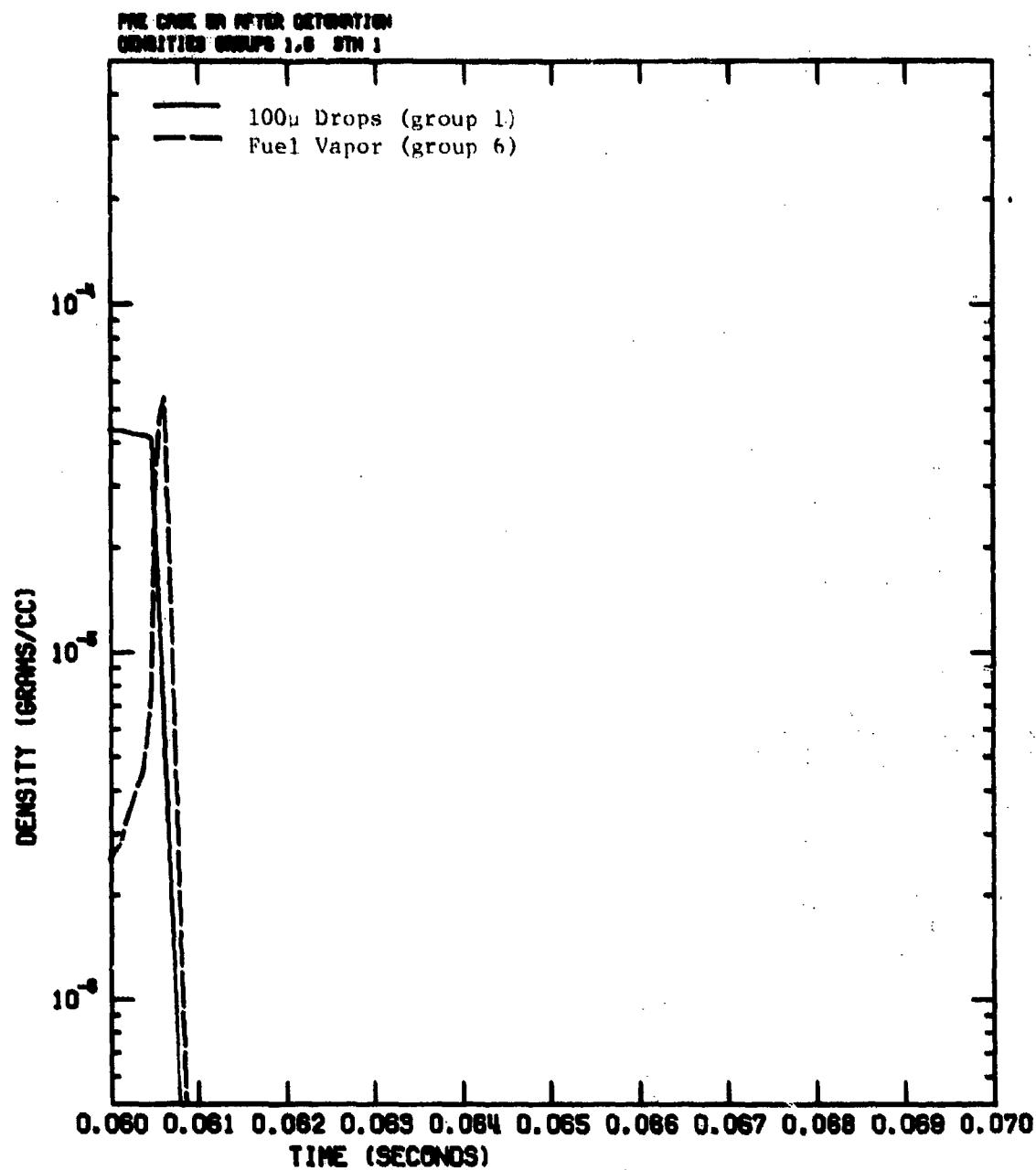


Figure E-6. Density versus Time for 100μ Drops (group 1) and Fuel Vapor (group 6) at Data Station 1

PRE CASE ON AFTER DETENTION
 DENSITIES GROUPS 1.6 STN 2

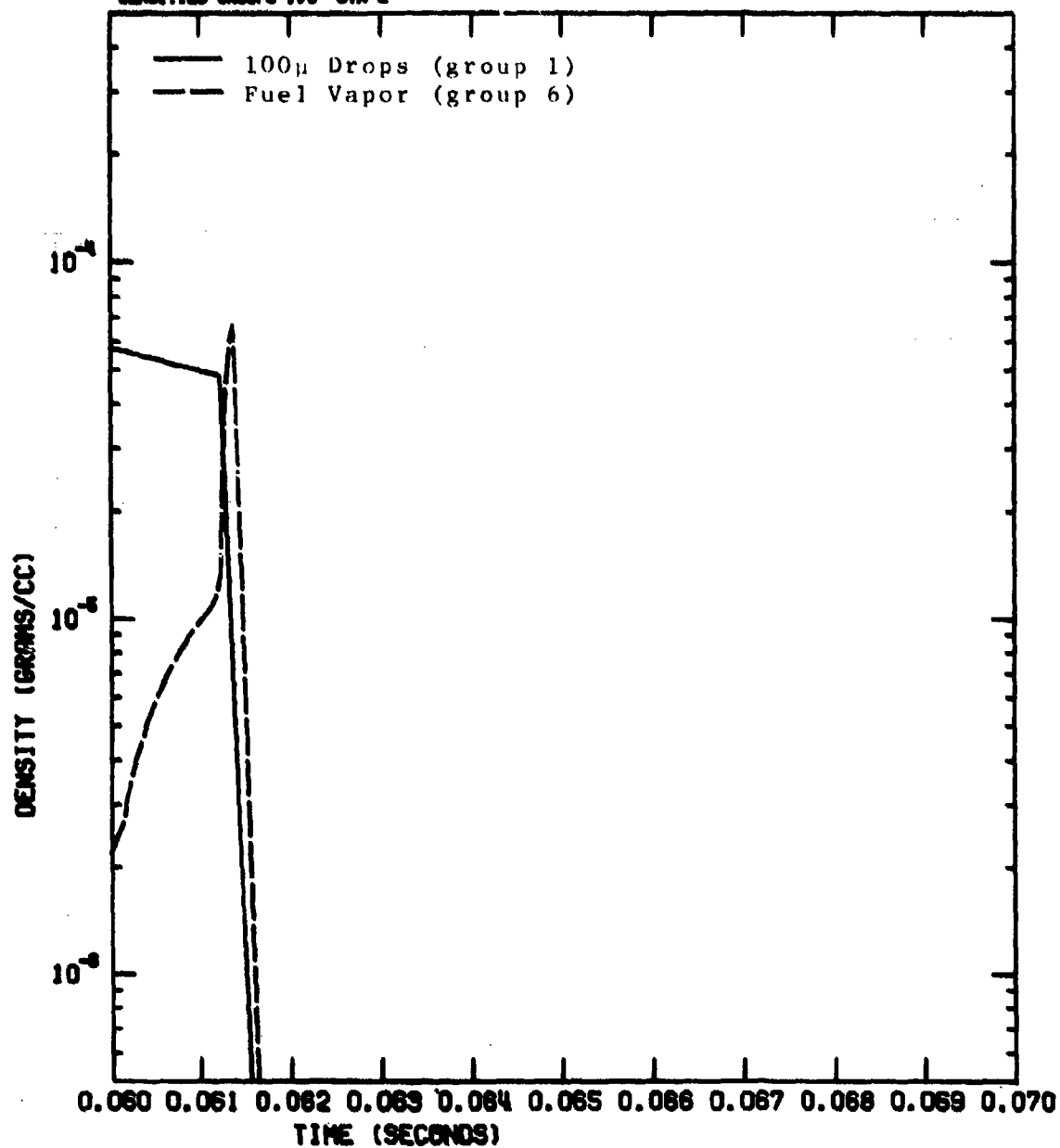


Figure E-7. Density versus Time for 100μ Drops (Group 1) and Fuel Vapor (Group 6) at Data Station 2

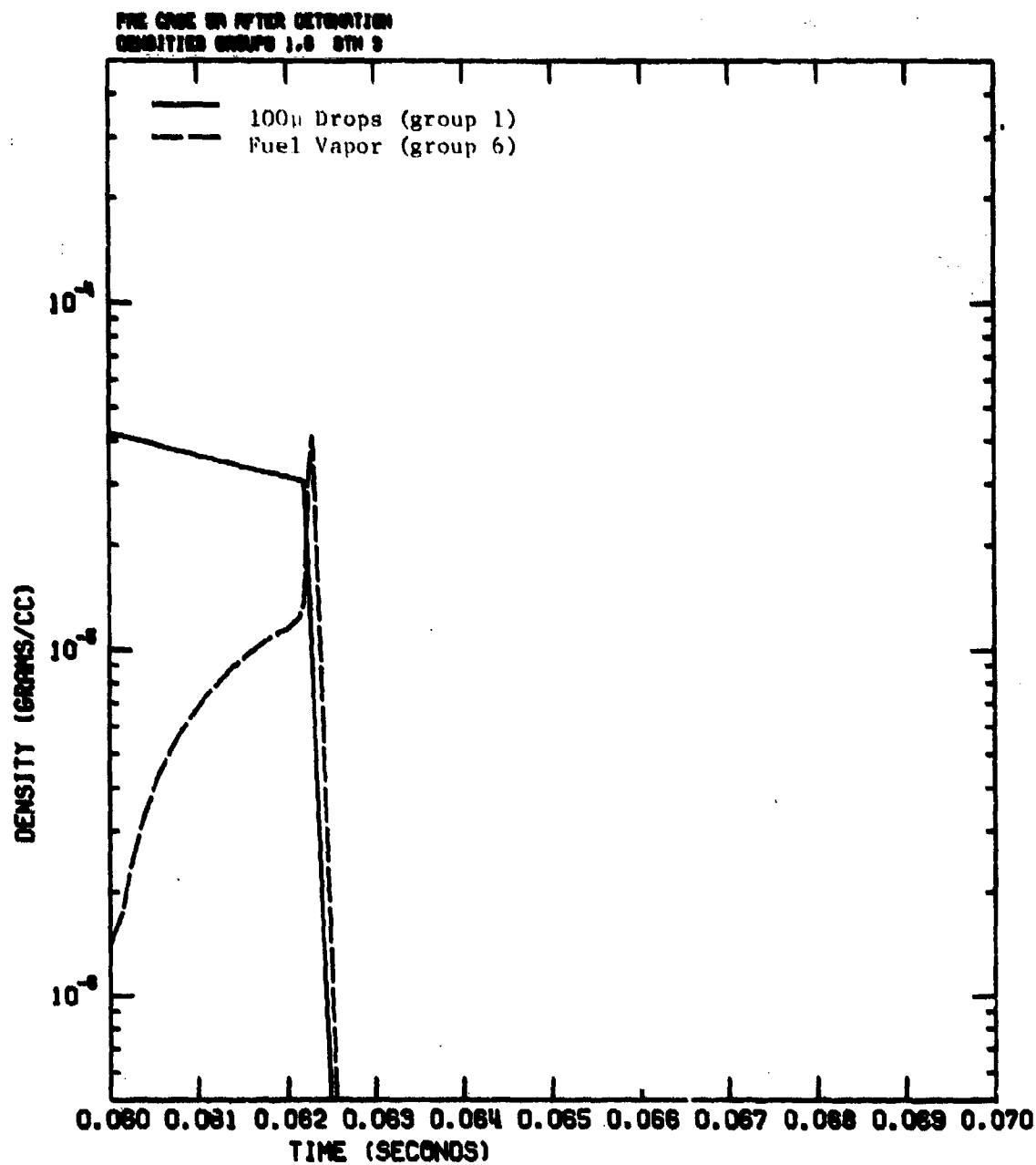


Figure E-8. Density versus Time for 100 μ Drops (group 1) and Fuel Vapor (group 6) at Data Station 3

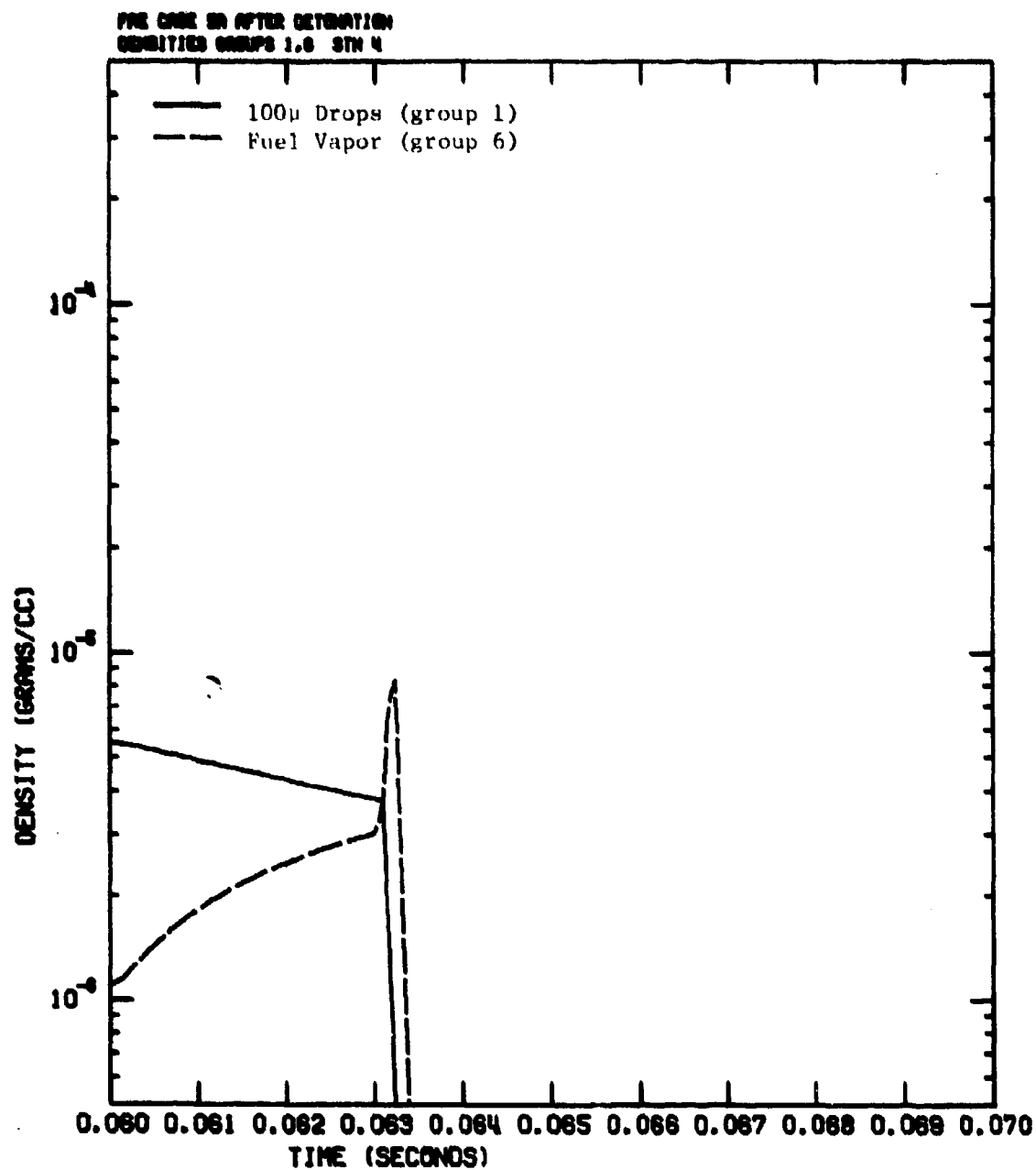


Figure E-9. Density versus Time for 100 μ Drops (group 1) and Fuel Vapor (group 6) at Data Station 4

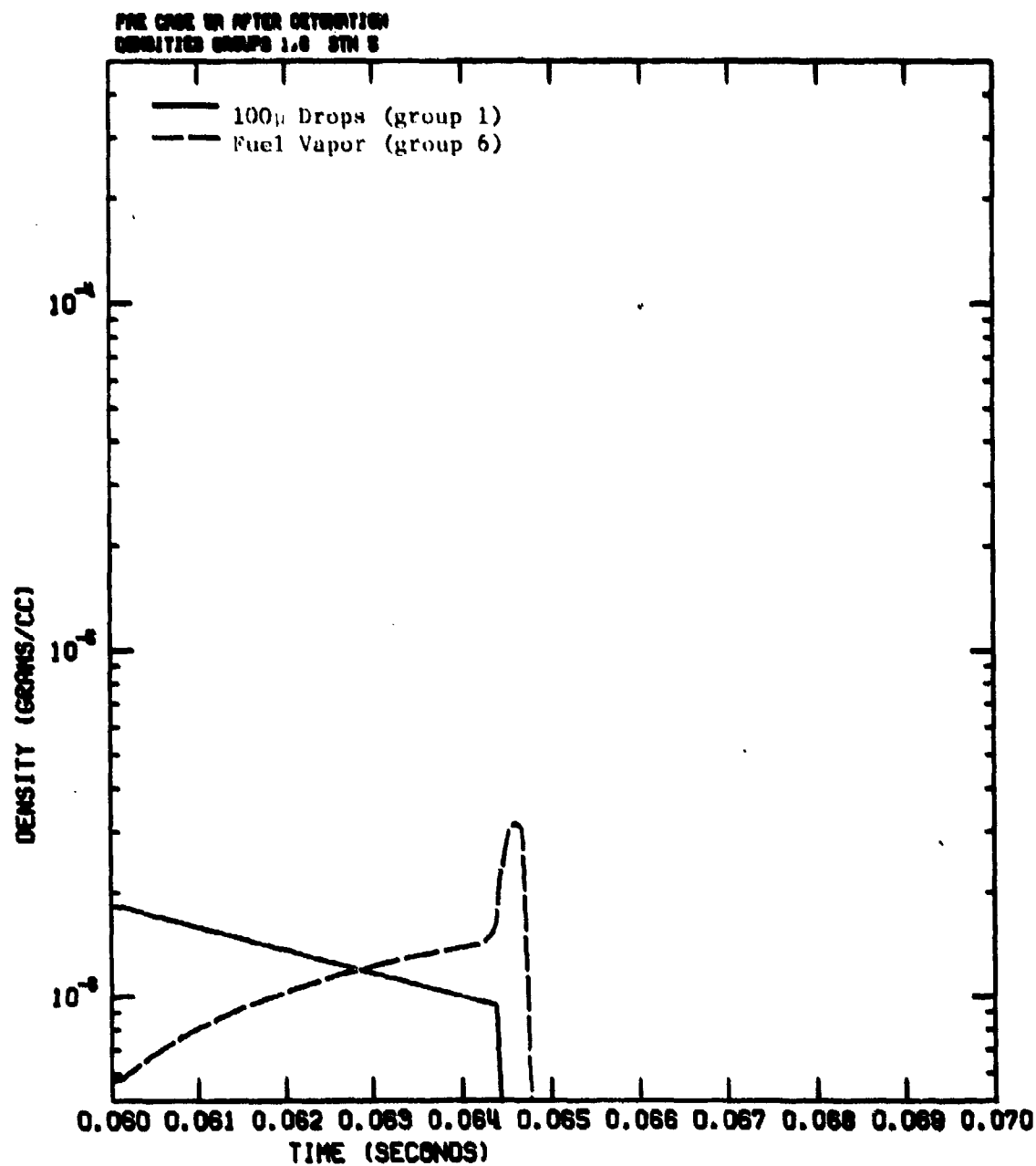


Figure E-10. Density versus Time for 100 μ Drops (group 1)
and Fuel Vapor (group 6) at Data Station 5

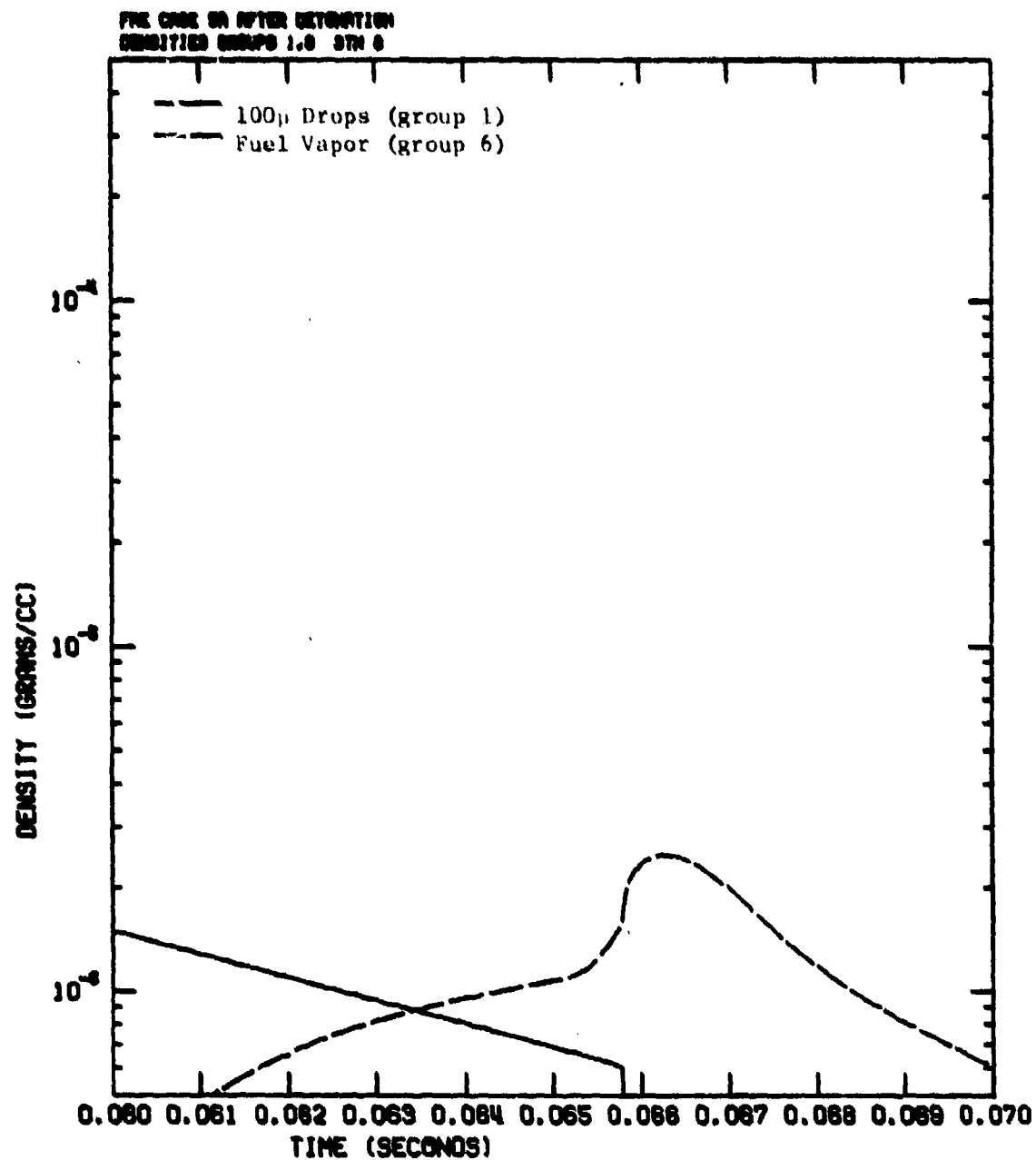


Figure E-11. Density versus Time for 100 μ Drops (group 1) and Fuel Vapor (group 6) at Data Station 6

PAGE ONE IN AFTER DETONATION
DENSITIES GROUPS 1-6 STA 7

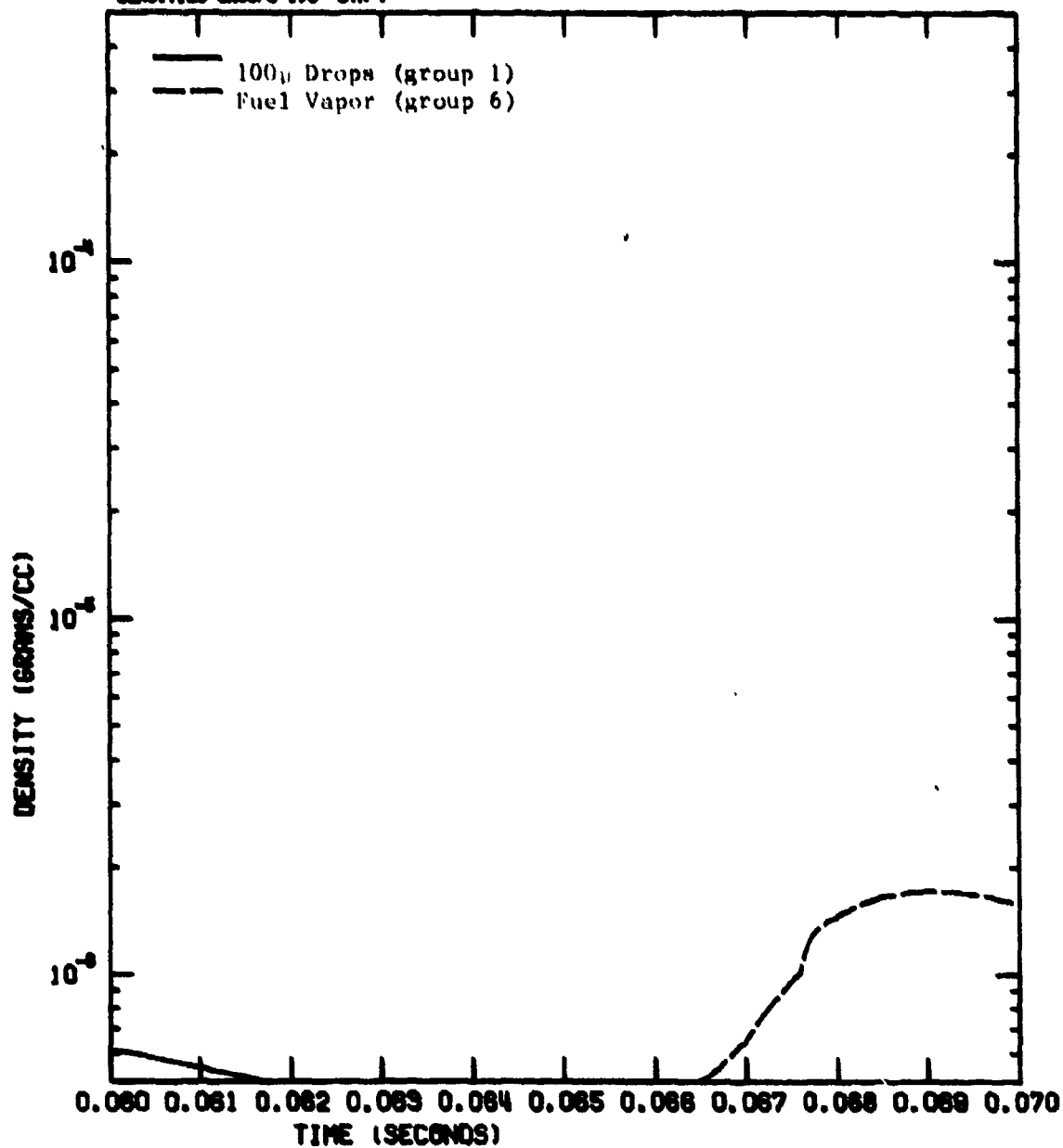


Figure E-12. Density versus Time for 100 μ Drops (group 1) and Fuel Vapor (group 6) at Data Station 7

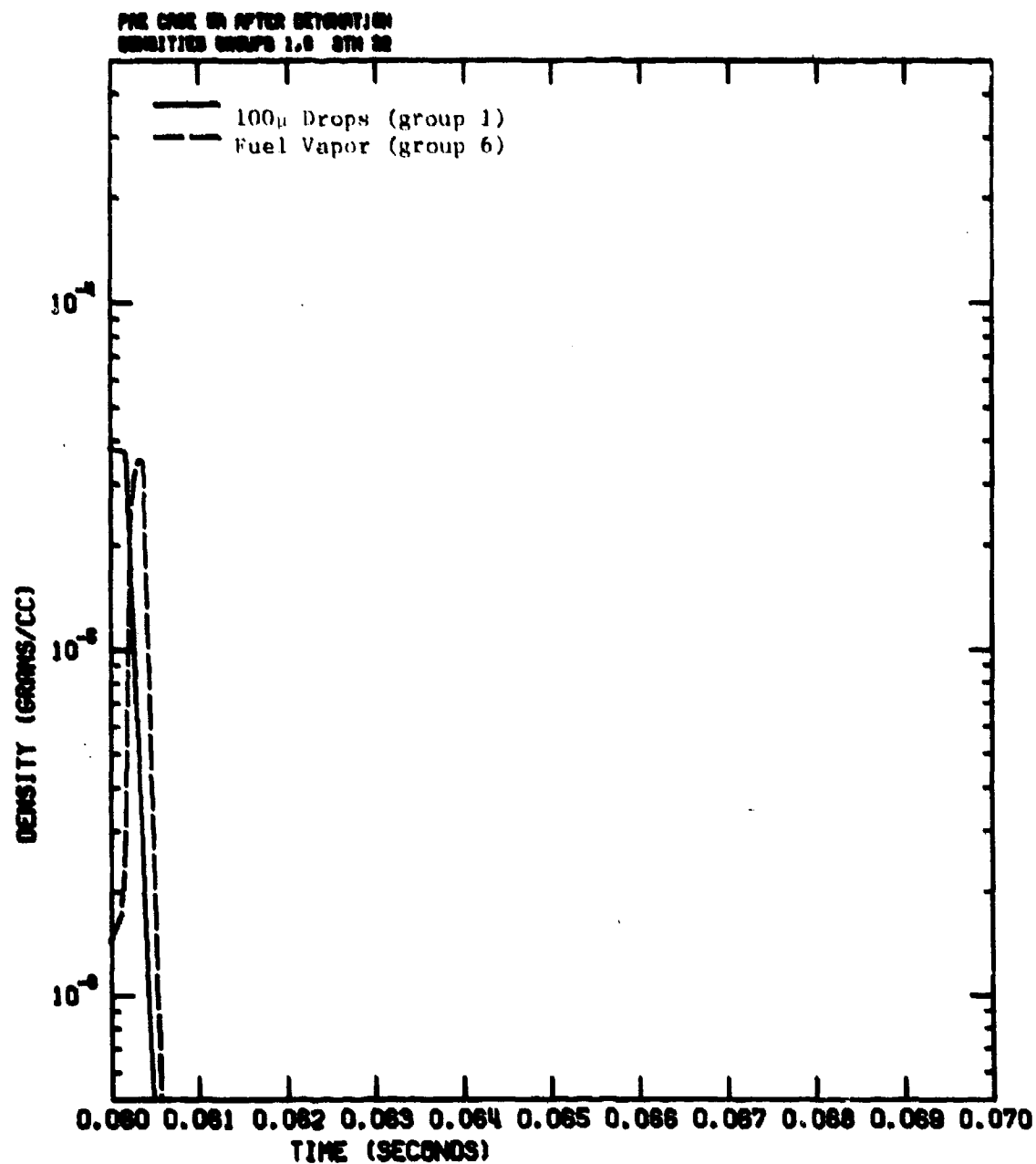


Figure E-13. Density versus Time for 100 μ Drops (group 1) and Fuel Vapor (group 6) at Data Station 22

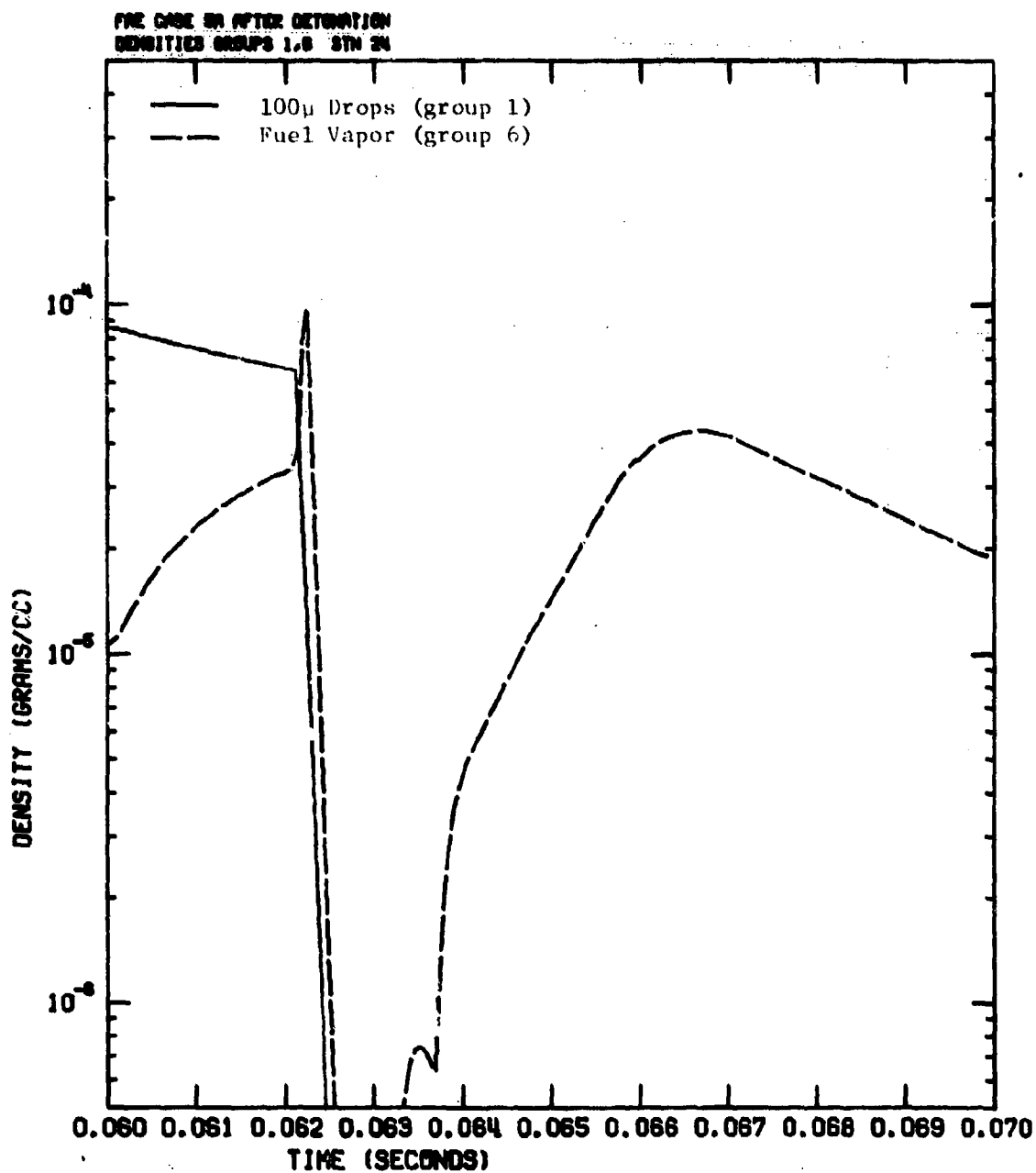


Figure E-14. Density versus Time for 100 μ Drops (group 1) and Fuel Vapor (group 6) at Data Station 24

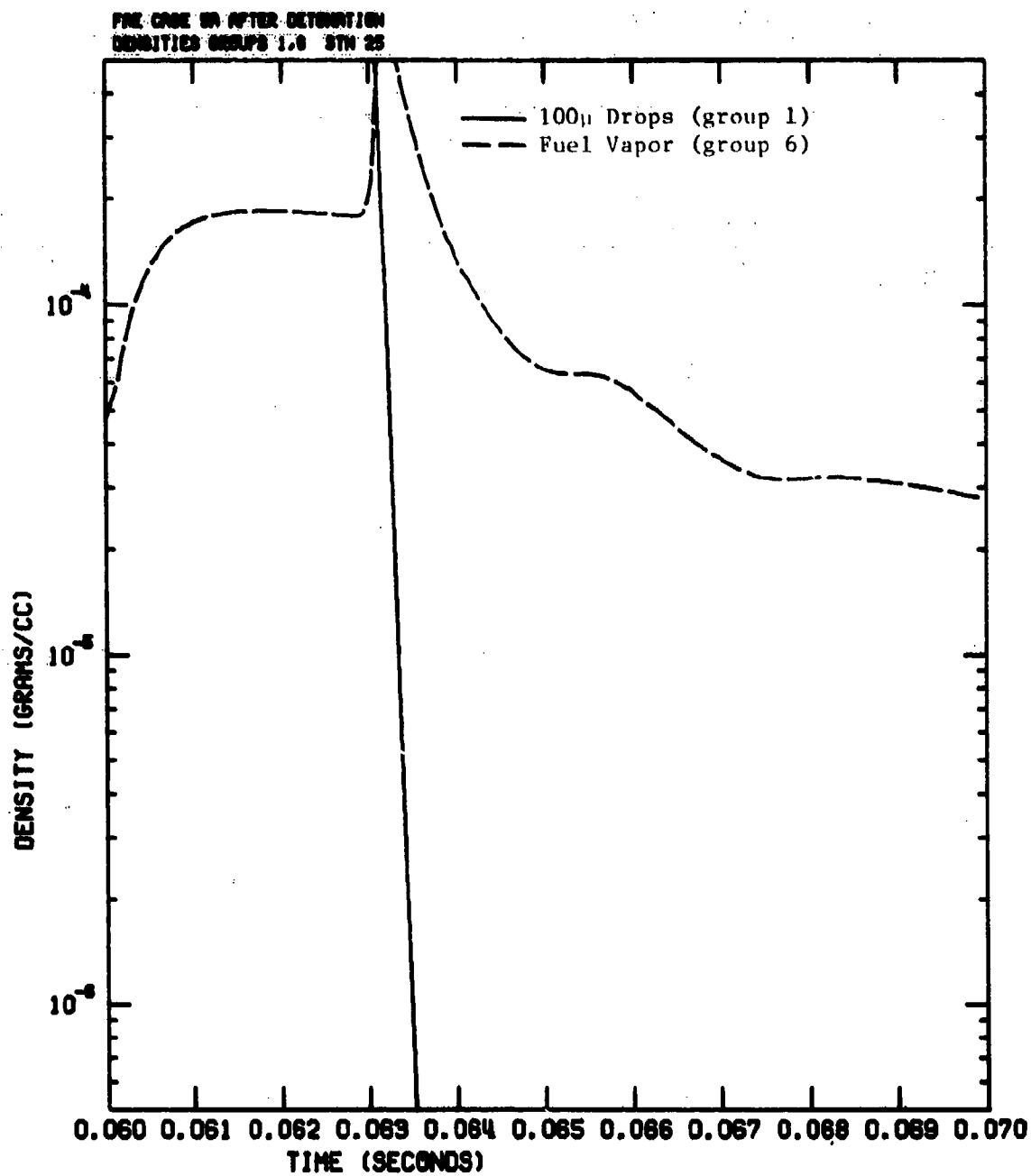


Figure E-15. Density versus Time for 100 μ Drops (group 1) and Fuel Vapor (group 6) at Data Station 25

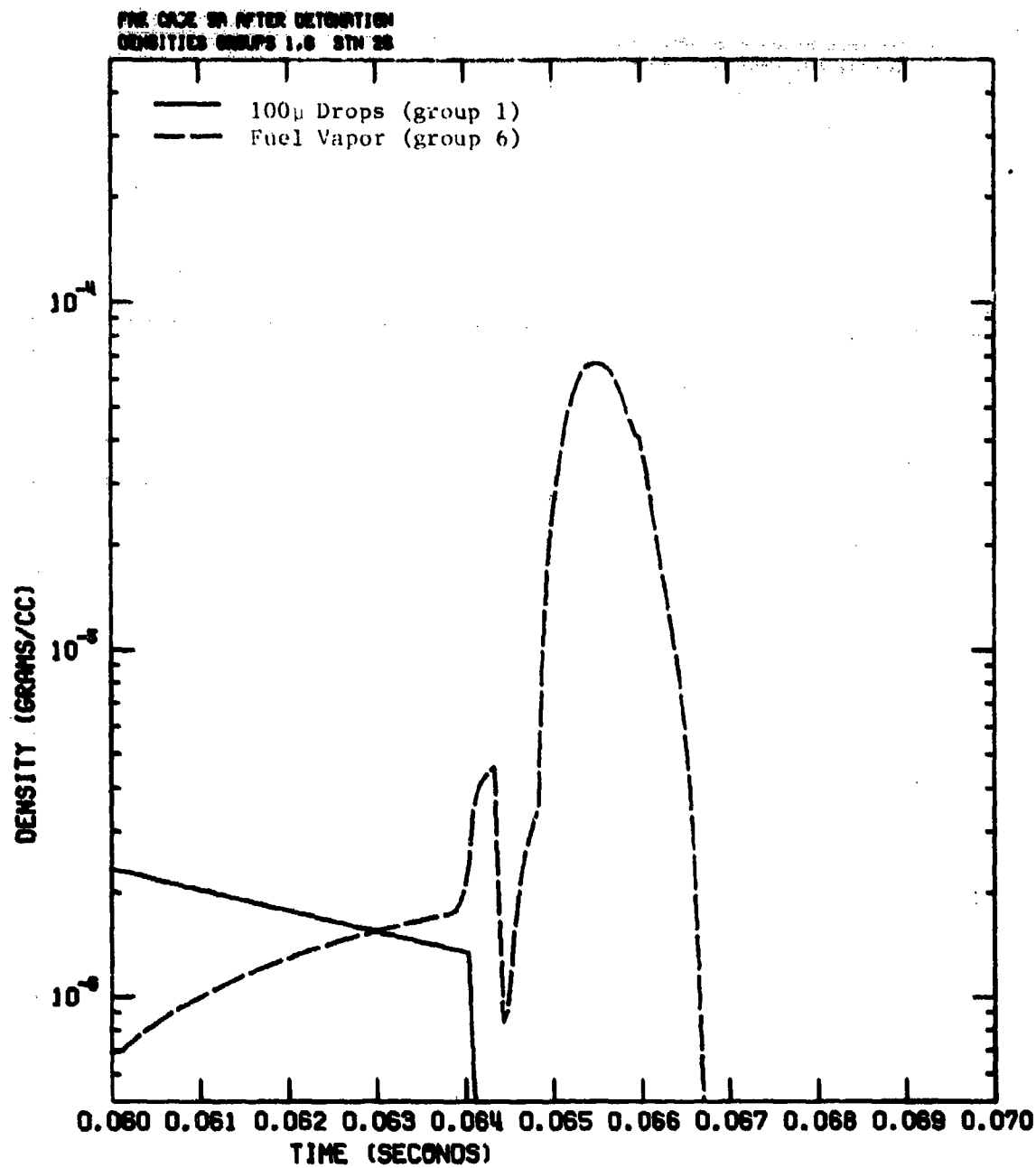


Figure E-16. Density versus Time for 100 μ Drops (group 1) and Fuel Vapor (group 6) at Data Station 26

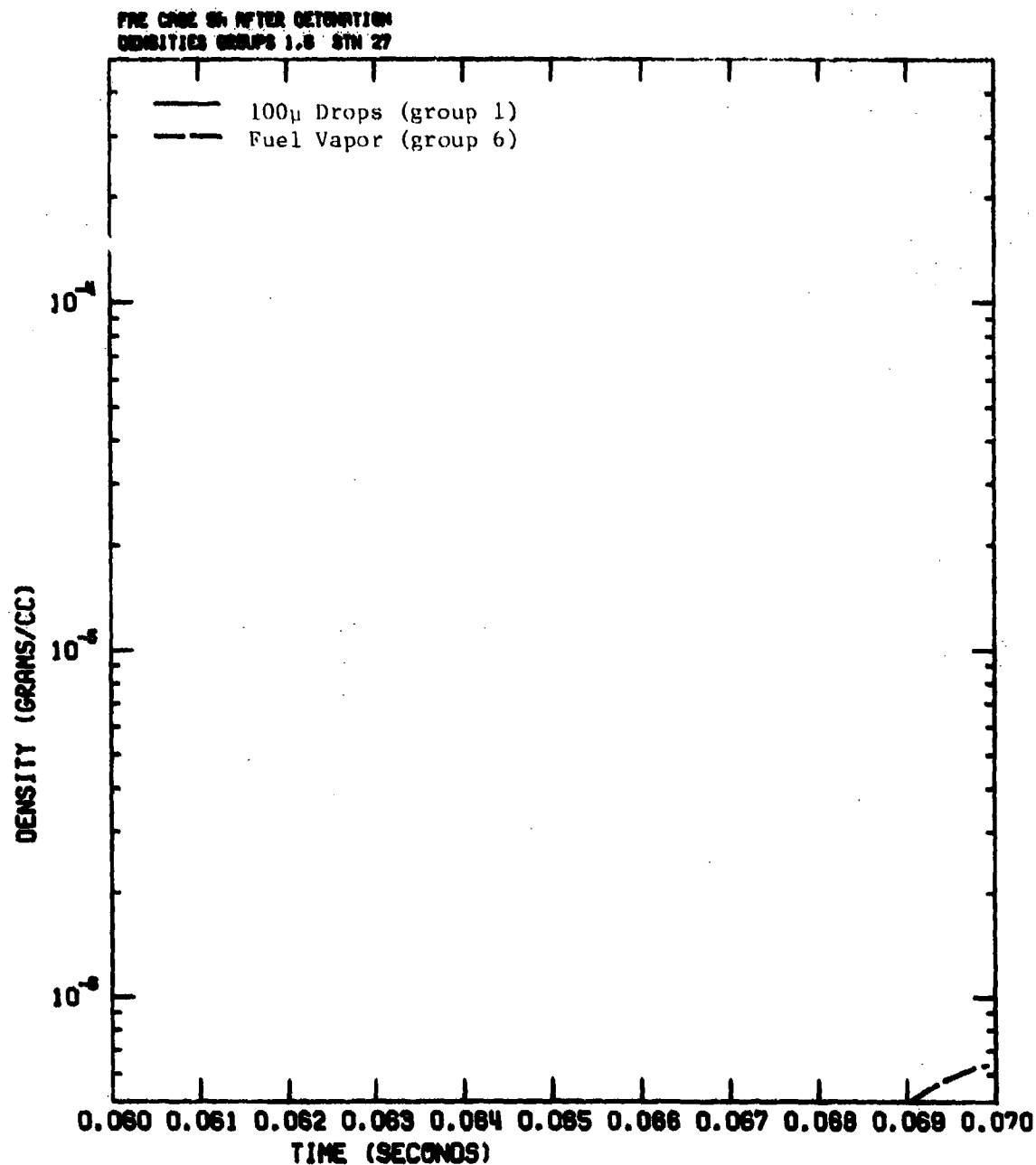


Figure E-17. Density versus Time for 100 μ Drops (group 1) and Fuel Vapor (group 6) at Data Station 27

PRE CASE OR AFTER DETONATION
DENSITIES GROUPS 1,6 STN 30

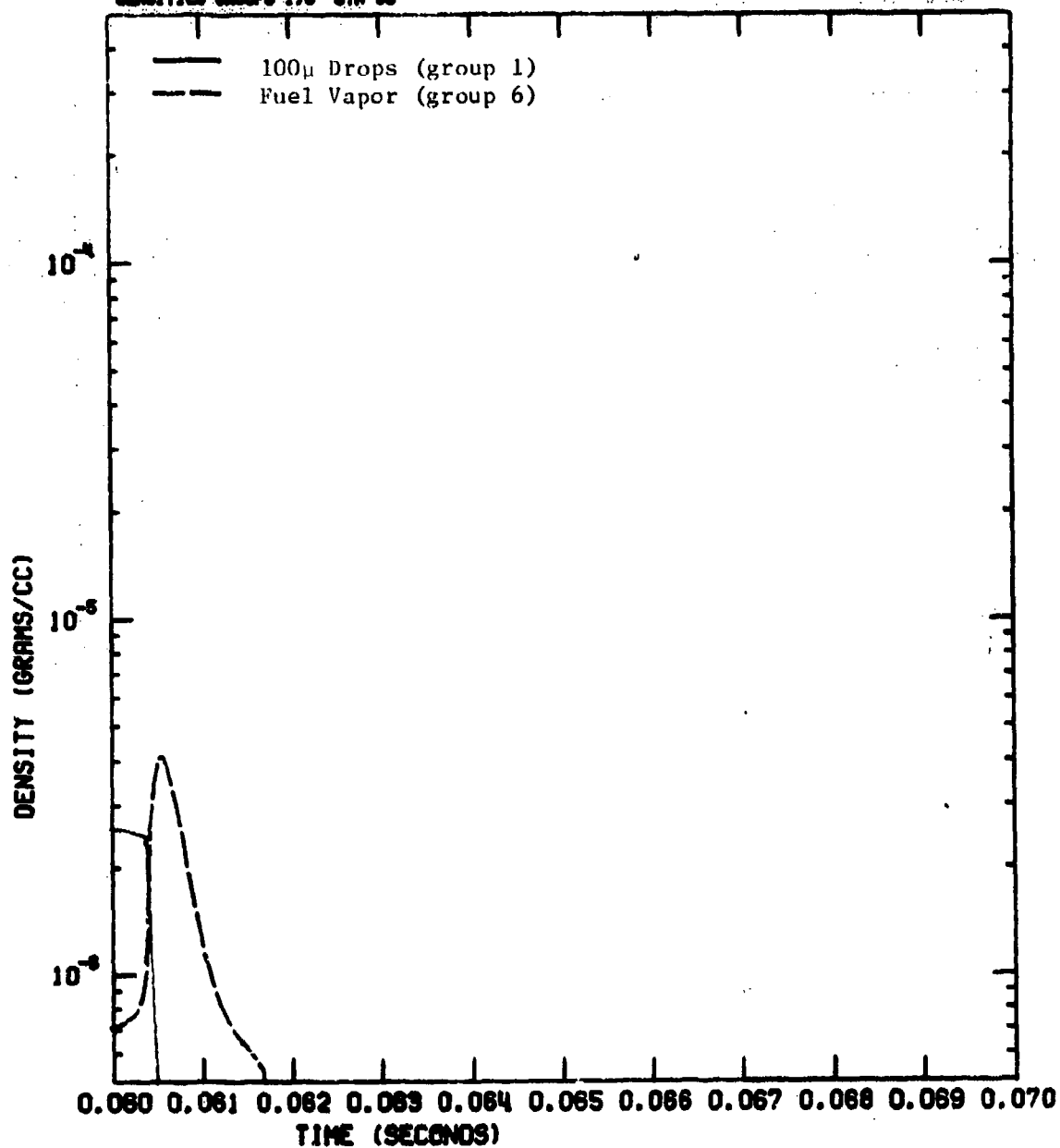


Figure E-18. Density versus Time for 100 μ Drops (group 1) and Fuel Vapor (group 6) at Data Station 30

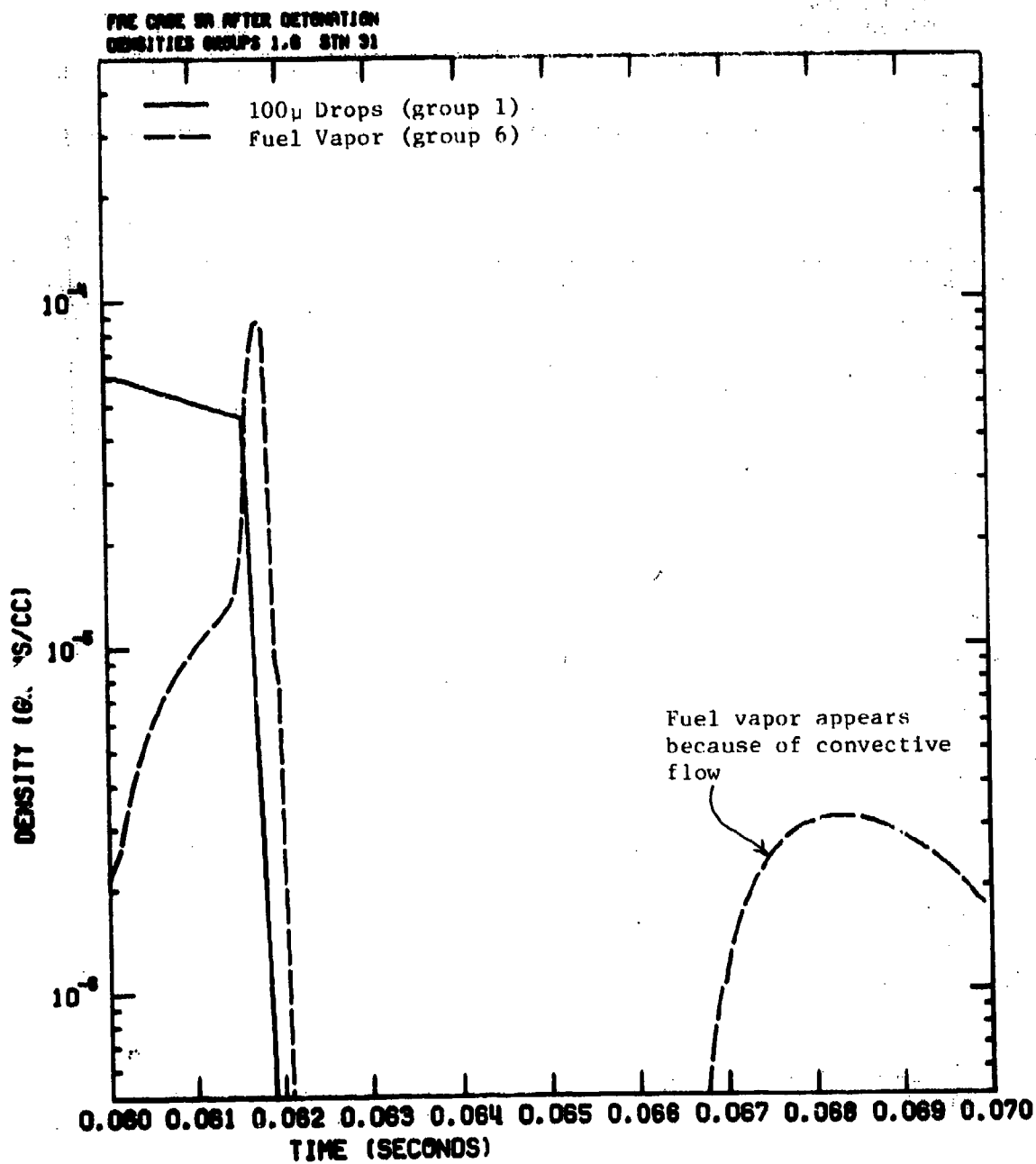


Figure E-19. Density versus Time for 100 μ Drops (group 1) and Fuel Vapor (group 6) at Data Station 31

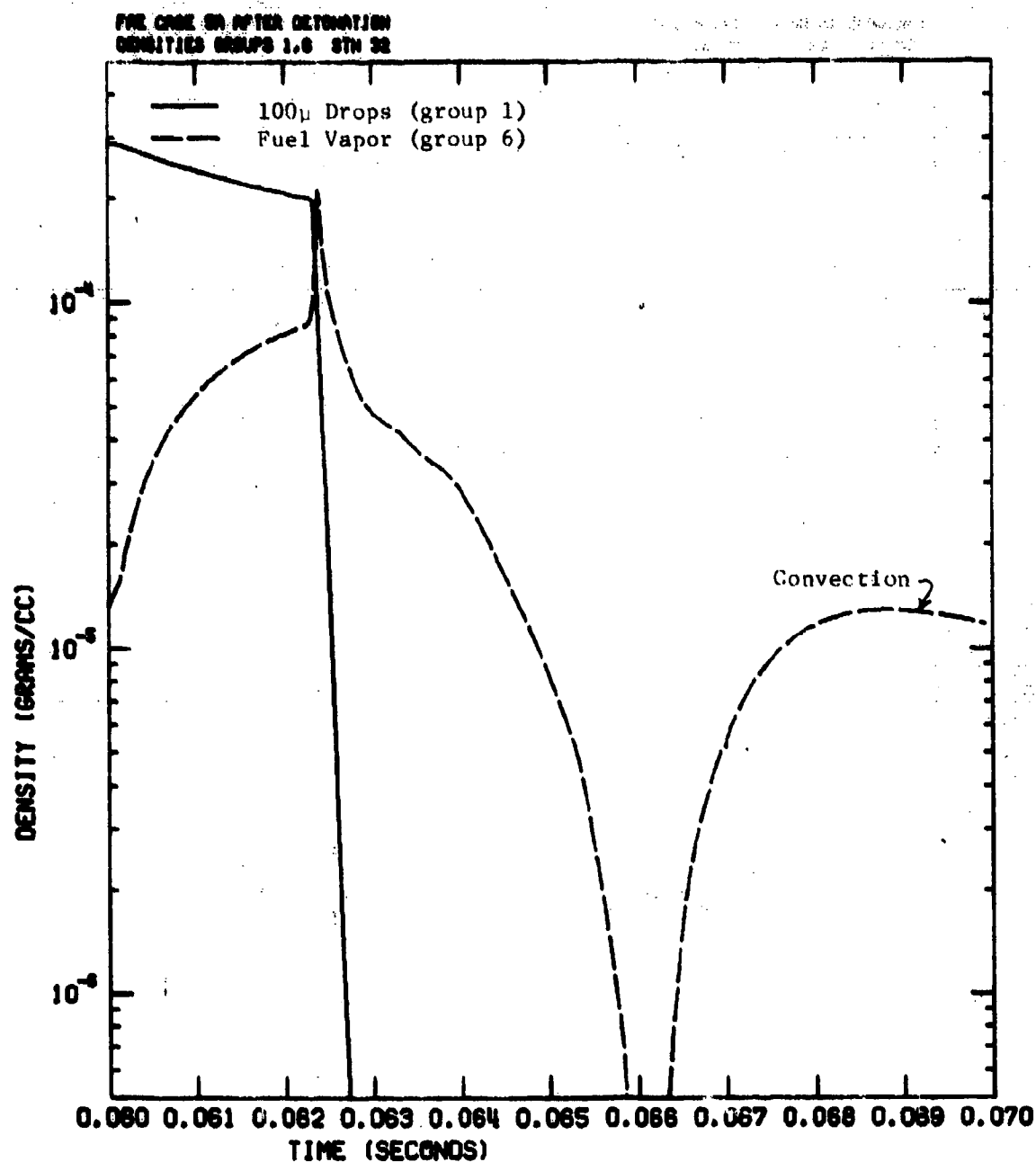


Figure E-20. Density versus Time for 100 μ Drops (group 1) and Fuel Vapor (group 6) at Data Station 32

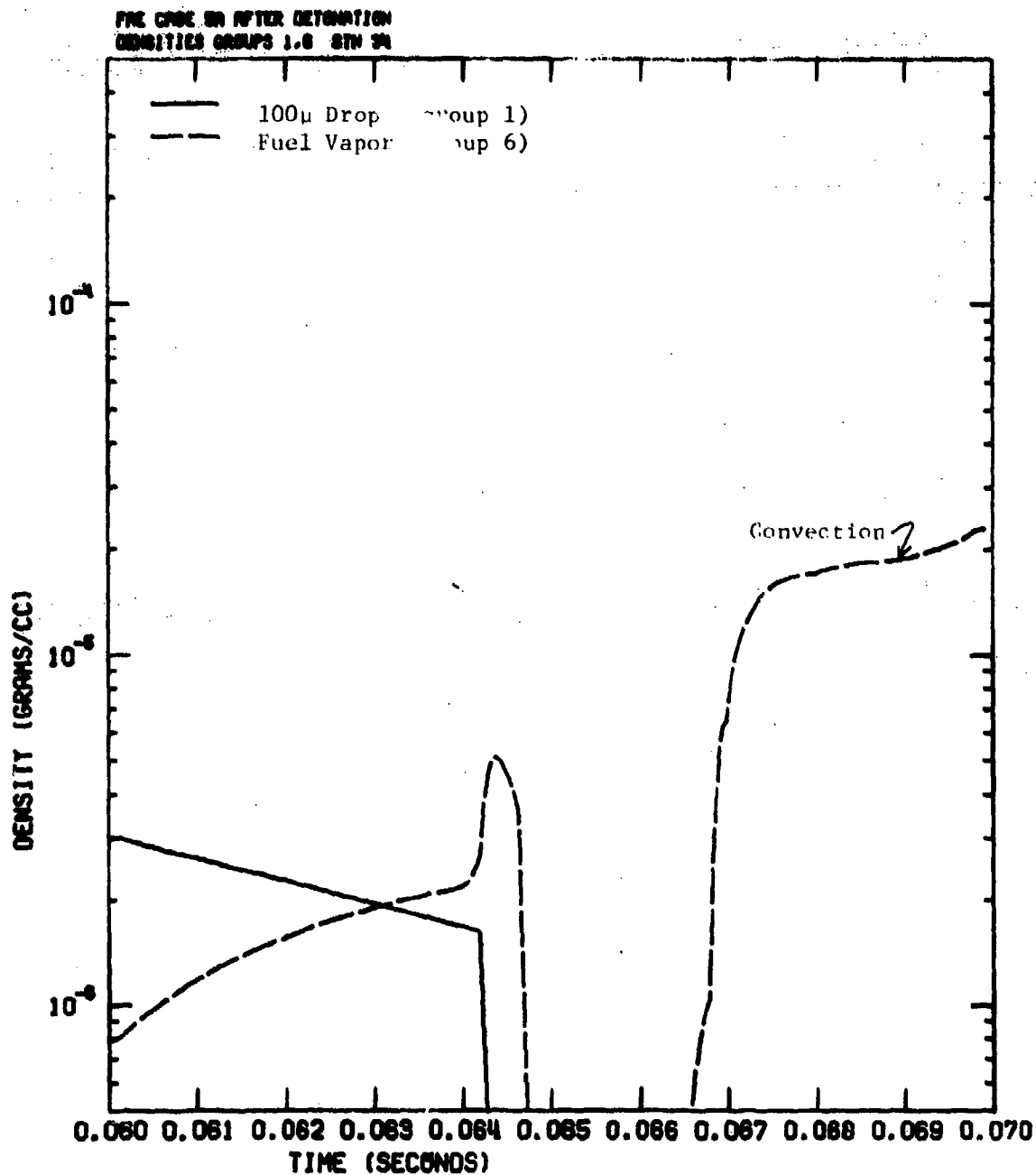


Figure E-21. Density versus Time for 100 μ Drops (group 1) and Fuel Vapor (group 6) at Data Station 34

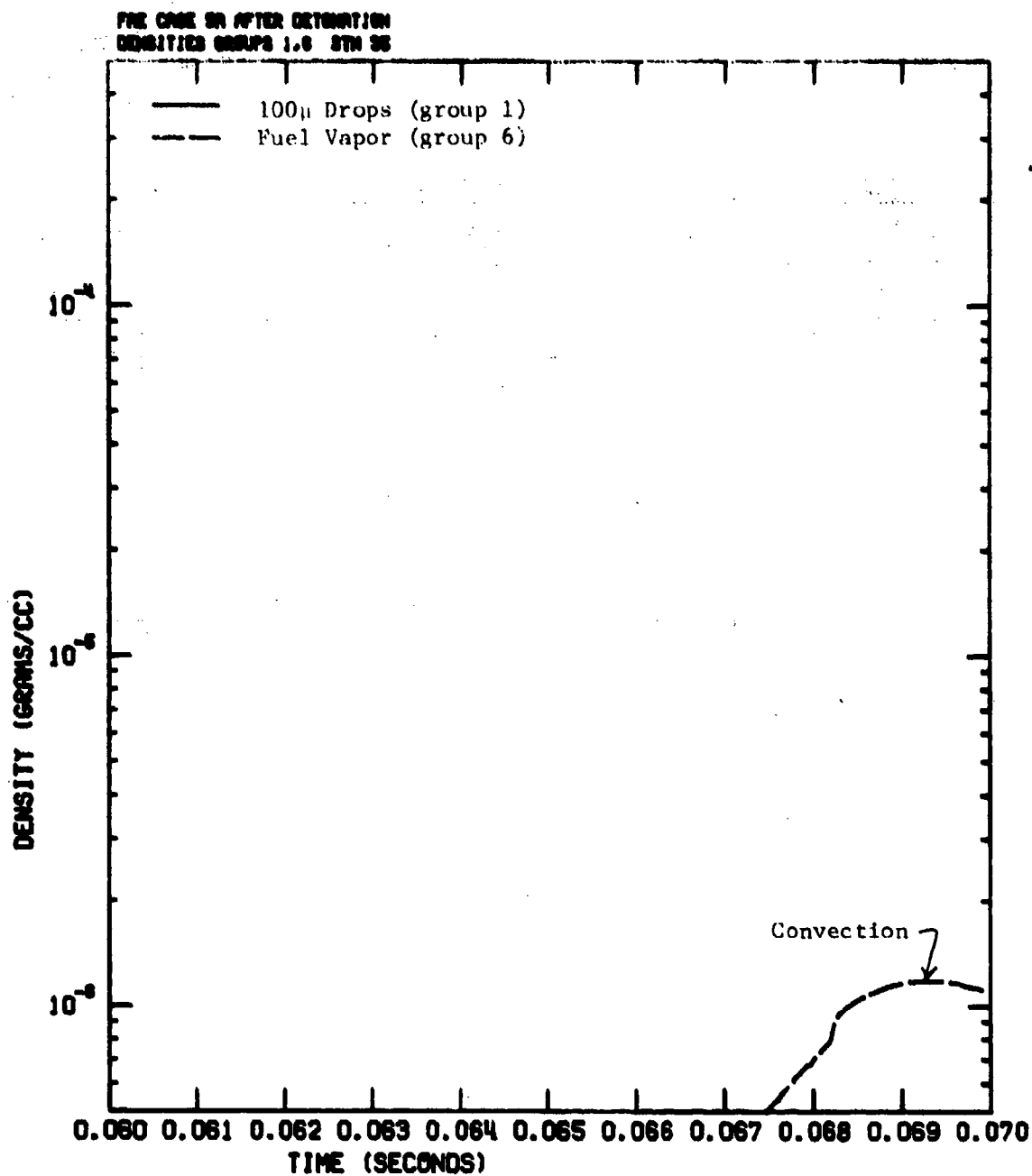


Figure E-22. Density versus Time for 100 μ Drops (group 1) and Fuel Vapor (group 6) at Data Station 35

$V = 10.0000E-05$, $\omega = 10.0000E-06$, $\tau = 10.0000E-07$,

Figure E-23. Fuel Drop Density Contours for DICE-FAE Case 5A at 61.5 msec

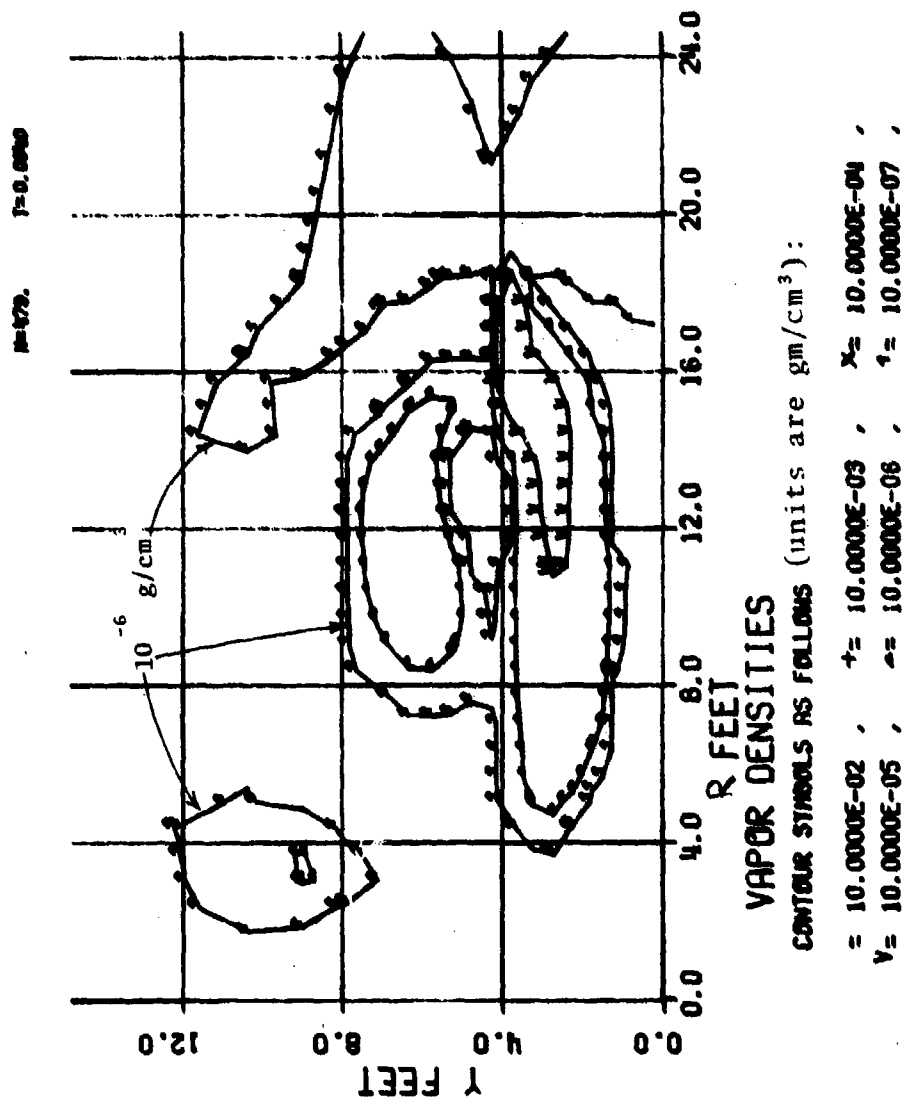
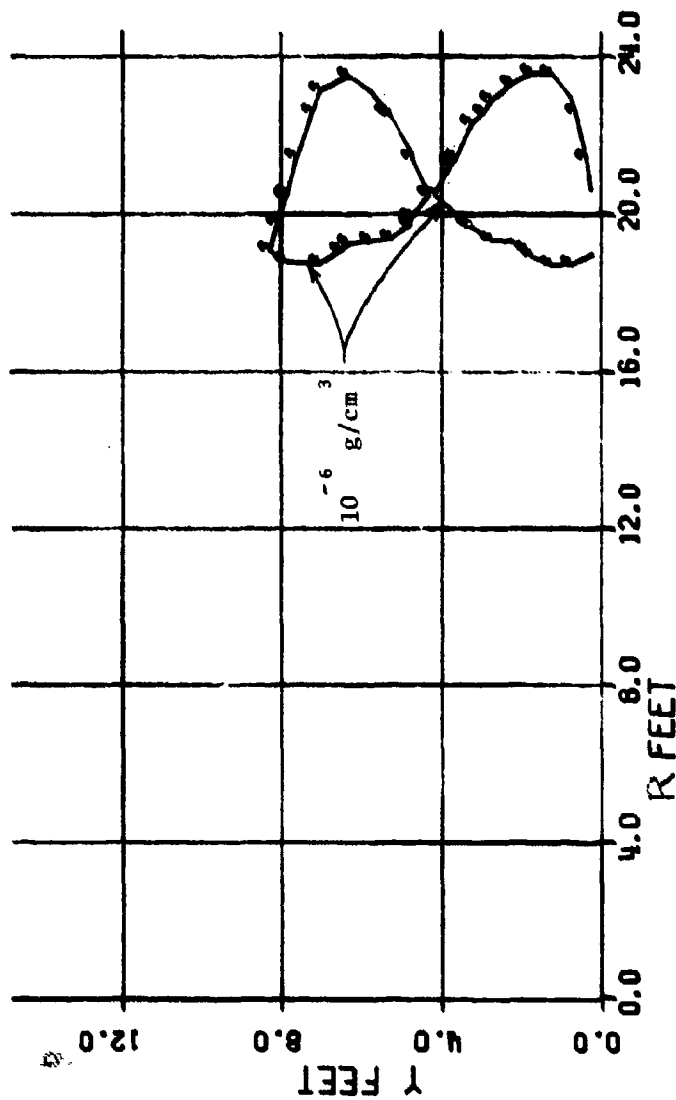


Figure E-24. Fuel Vapor Density Contours for DICE-FAE
Case 5A at 64.0 msec

D=100μ T=6.00000



DENSITY CONTOURS, GROUP 1

CONTOUR SYMBOLS AS FOLLOWS (units are gm/cm³):

+ = 10.0000E-02 , † = 10.0000E-03 , × = 10.0000E-04 ,
 v = 10.0000E-05 , * = 10.0000E-06 , † = 10.0000E-07 ,

Figure E-25. 100μ Fuel Drop Density Contours for DICE-FAE
 Case 5A at 64.0 msec

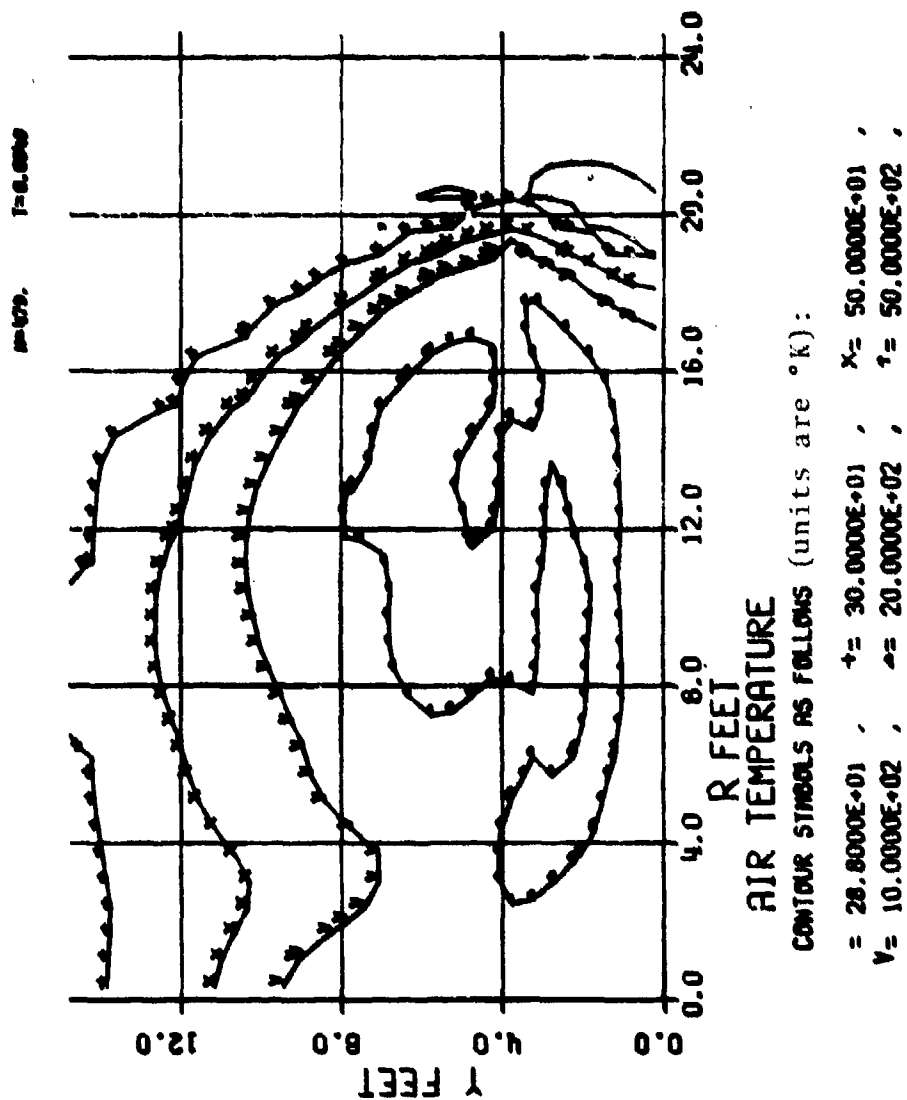


Figure E-26. Air Temperature Contours for DICE-FAE
 Case 5A at 64.0 msec

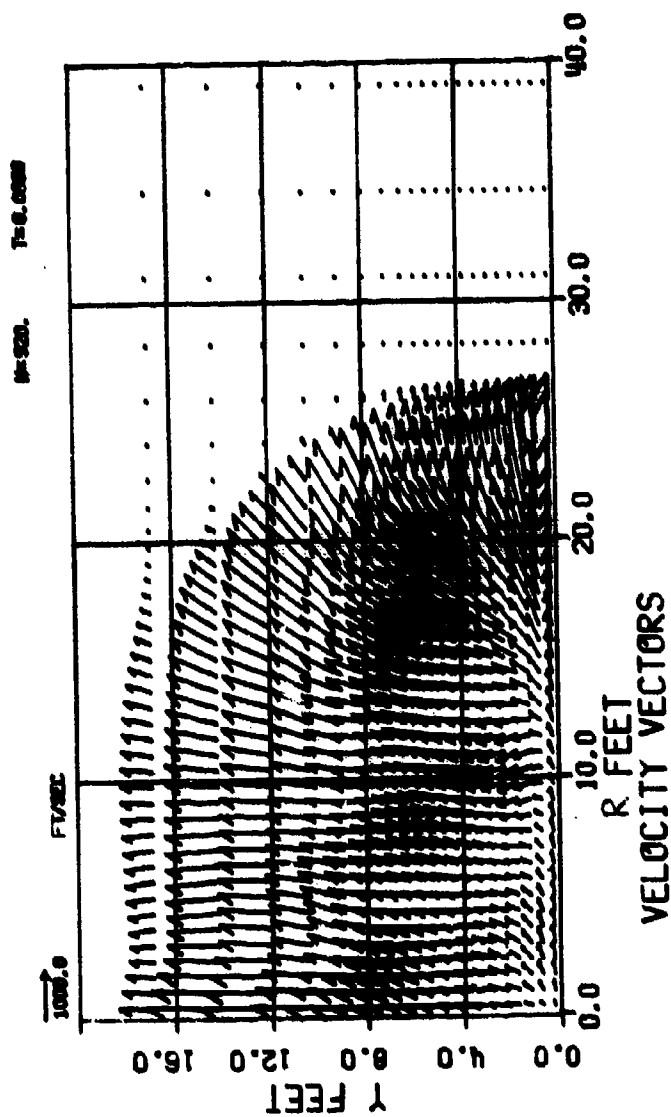
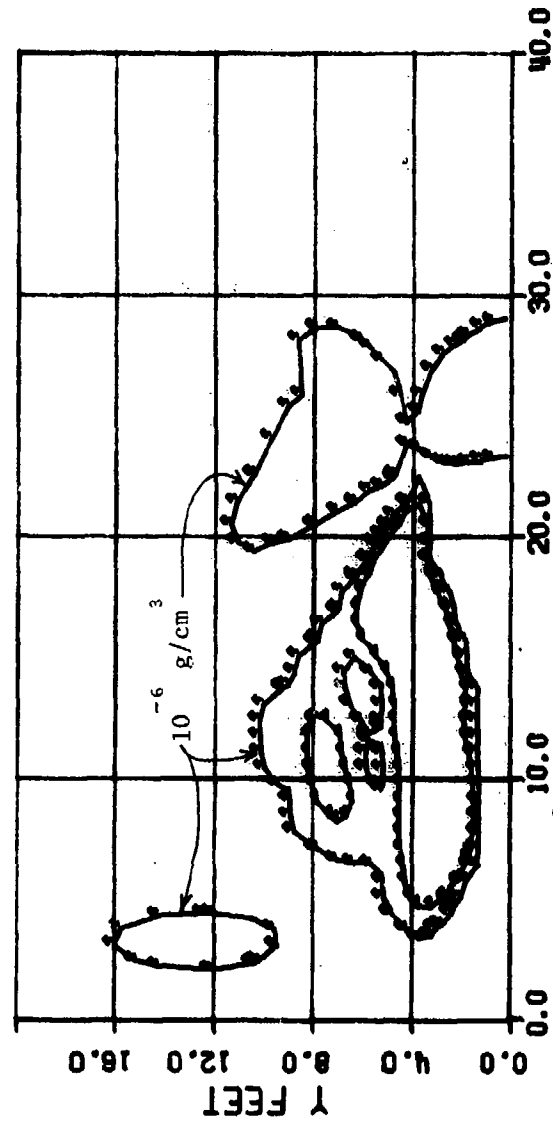


Figure E-27. Air Velocity Vectors for DICE-FAE
Case 5A at 66.0 msec

M=520. $\tau=0.0000$



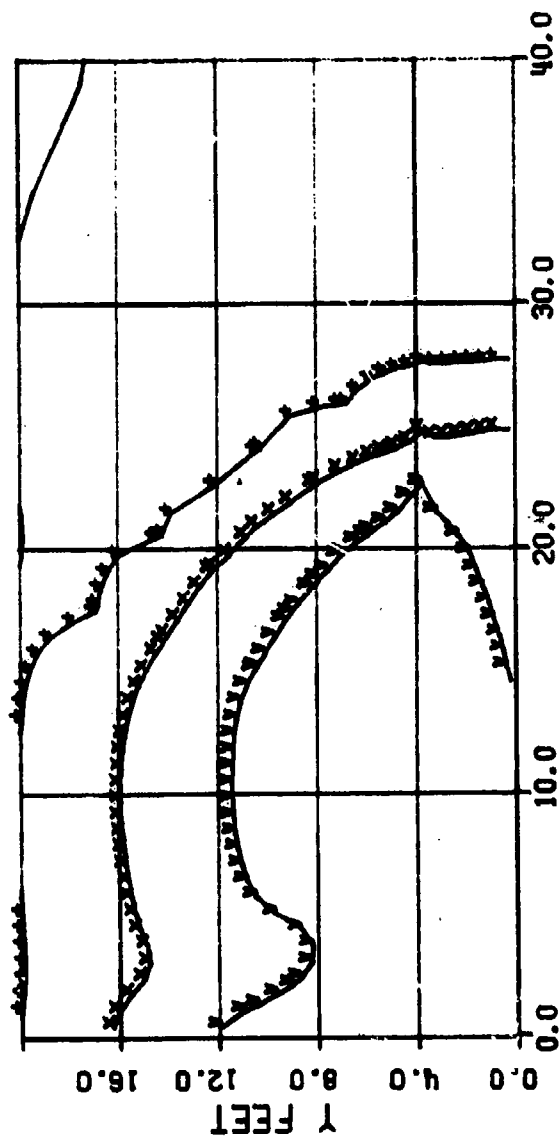
VAPOR DENSITIES

CONTOUR SYMBOLS AS FOLLOWS (units are gm/cm^3):

$\circ = 10.0000\text{E}-02$, $\times = 10.0000\text{E}-03$, $\star = 10.0000\text{E}-04$,
 $\nabla = 10.0000\text{E}-05$; $\triangle = 10.0000\text{E}-06$, $\square = 10.0000\text{E}-07$,

Figure E-28. Fuel Vapor Density Contours for DICE-FAE
 Case 5A at 66.0 msec

Re 520. $\gamma = 0.0050$



AIR TEMPERATURE

CONTOUR SYMBOLS AS FOLLOWS (units are °K):

$\bullet = 28.8000E+01$, $\times = 30.0000E+01$, $\times = 50.0000E+01$,
 $\nabla = 10.0000E+02$, $\triangle = 20.0000E+02$, $\nabla = 50.0000E+02$,

Figure E-29. Air Temperature Contours for DICE-FAE
 Case 5A at 66.0 msec

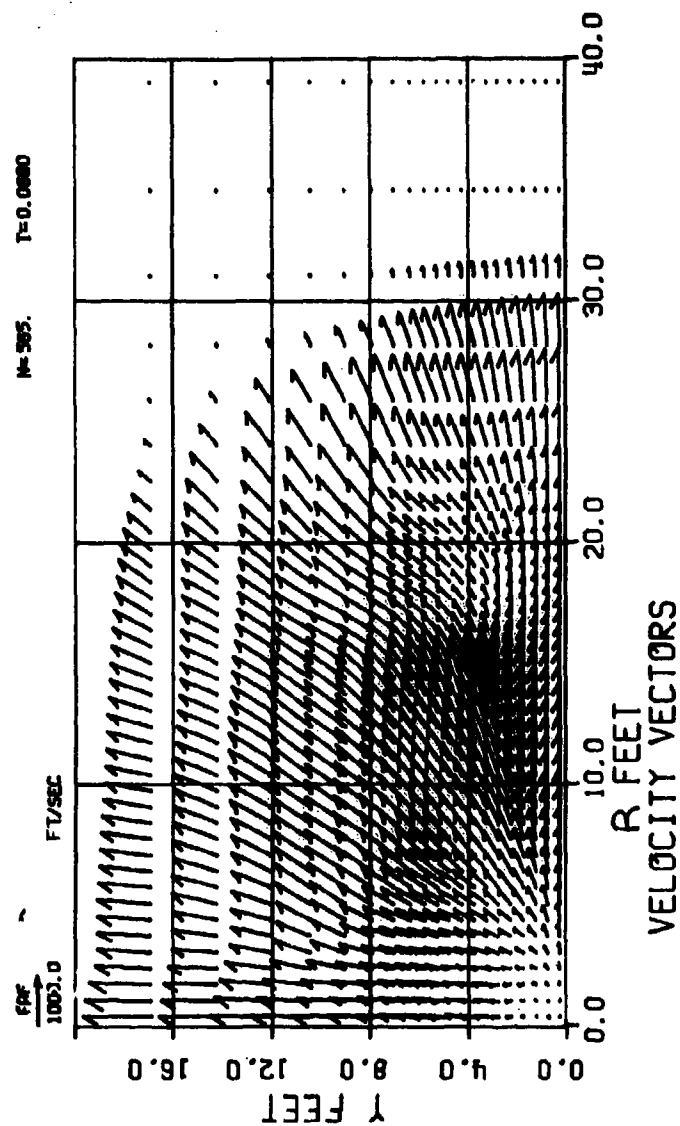


Figure E-30. Air Velocity Vectors for DICE-FAE Case 5A at 68.0 msec

BEST AVAILABLE COPY

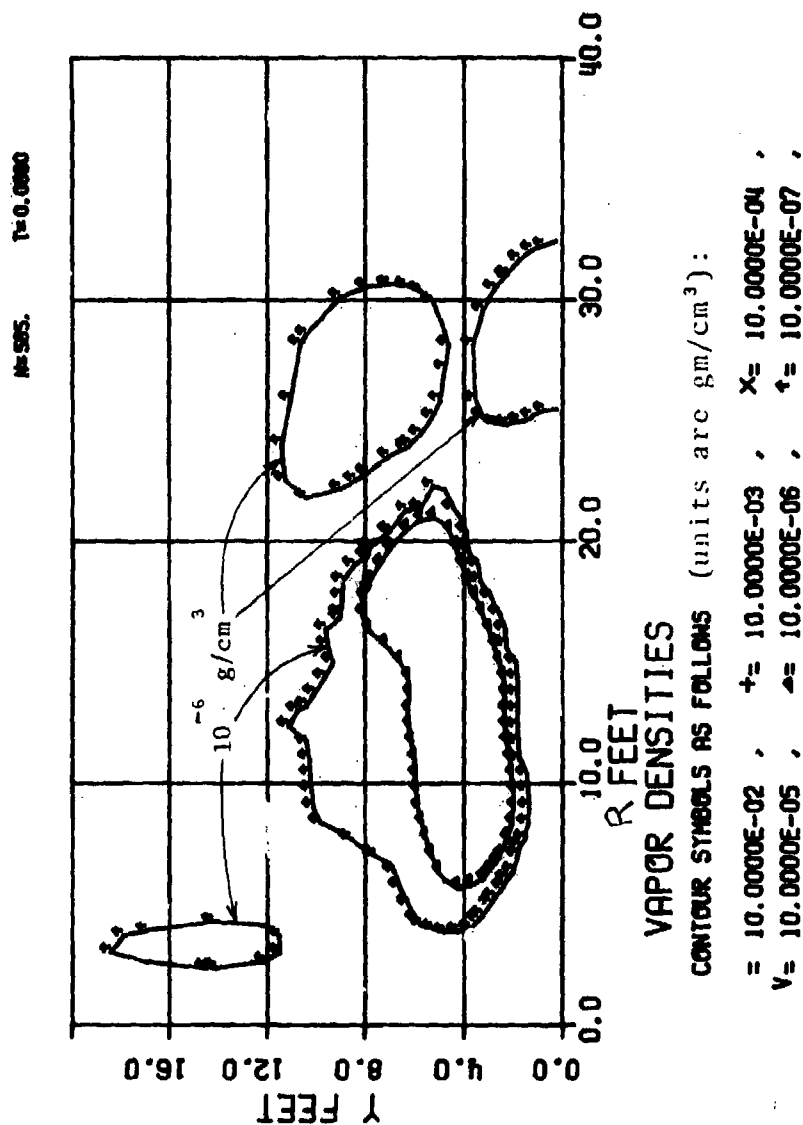


Figure E-31. Fuel Vapor Density Contours for DICE-FAE
Case 5A at 68.0 msec

BEST AVAILABLE COPY

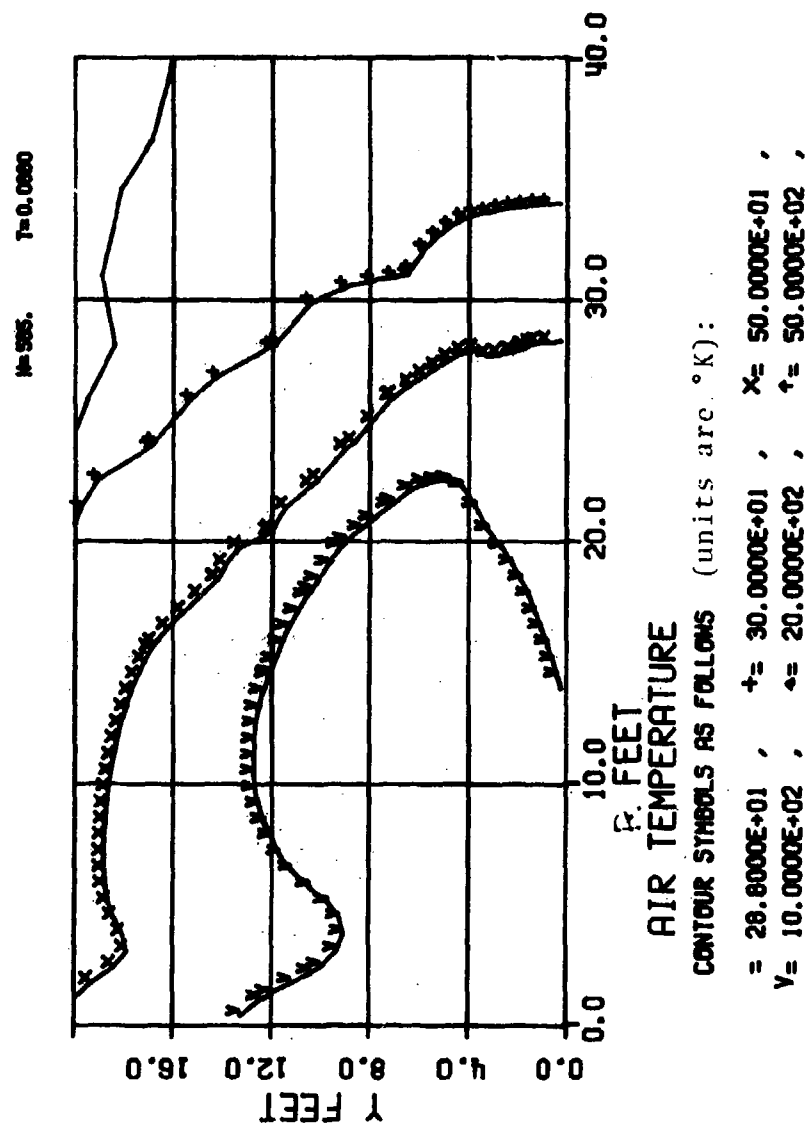


Figure E-32. Air Temperature Contours for DICE-FAE
Case 5A at 68.0 msec

BEST AVAILABLE COPY

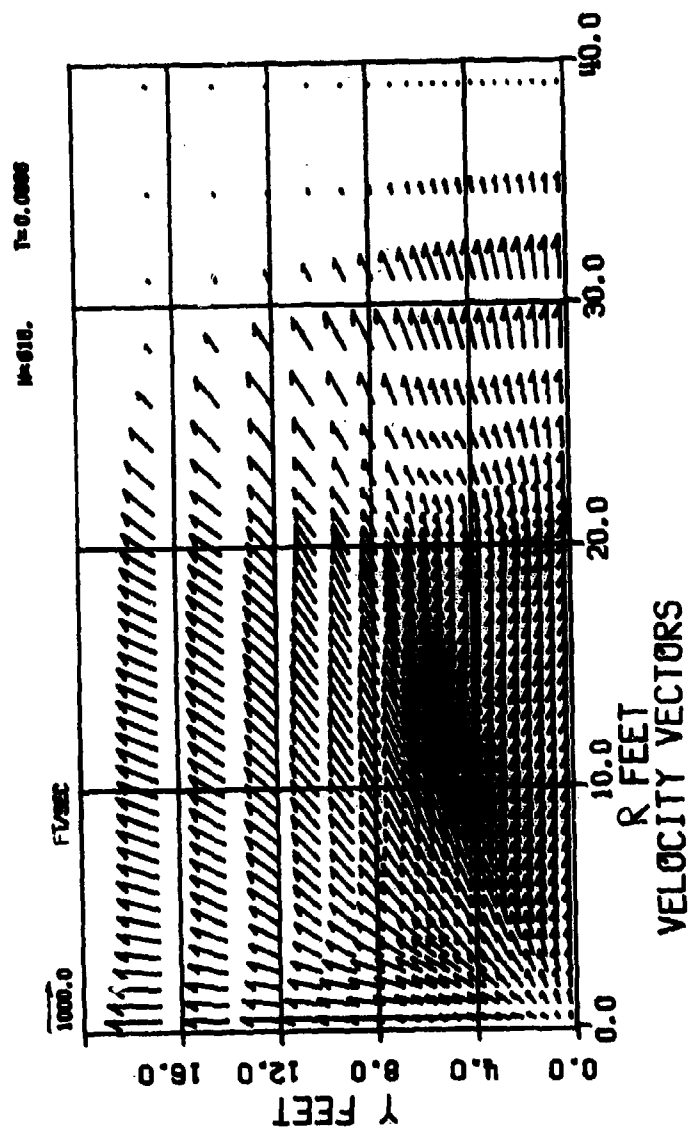


Figure E-33. Air Velocity Vectors for DICE-FAE
Case 5A at 69.6 msec

BEST AVAILABLE COPY

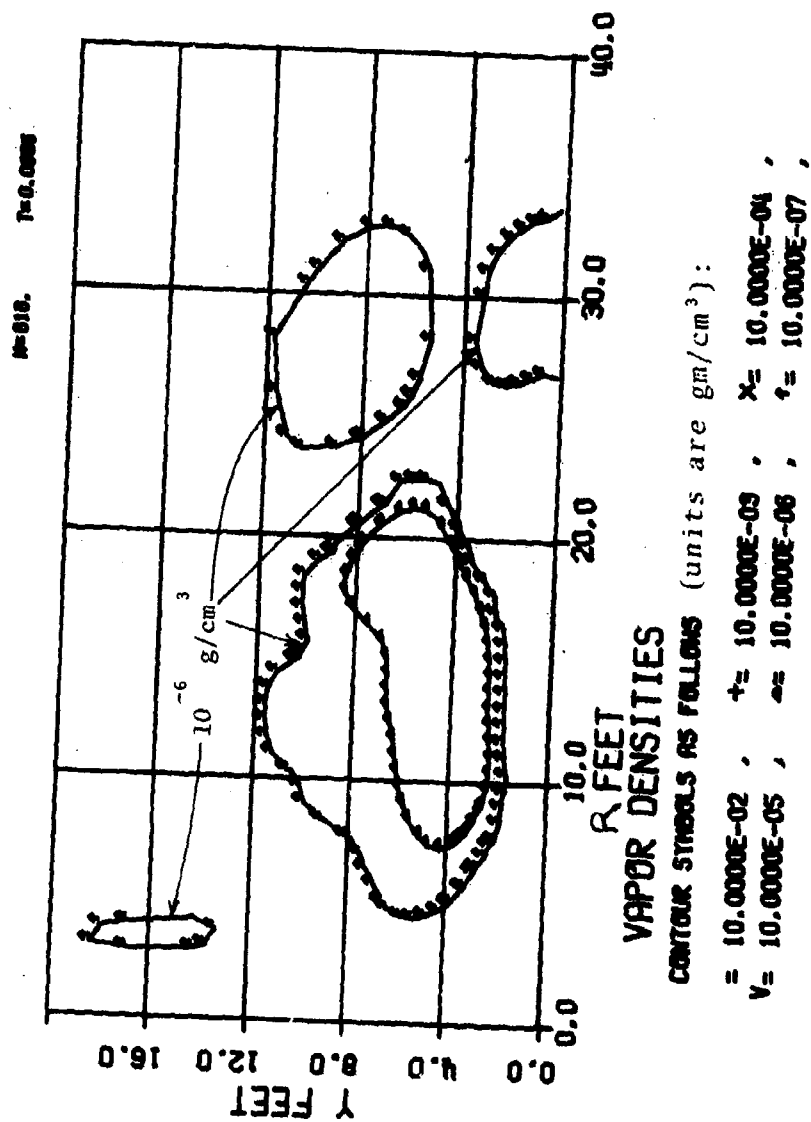


Figure E-34. Fuel Vapor Density Contours for DICE-FAE
Case 5A at 69.6 msec

BEST AVAILABLE COPY

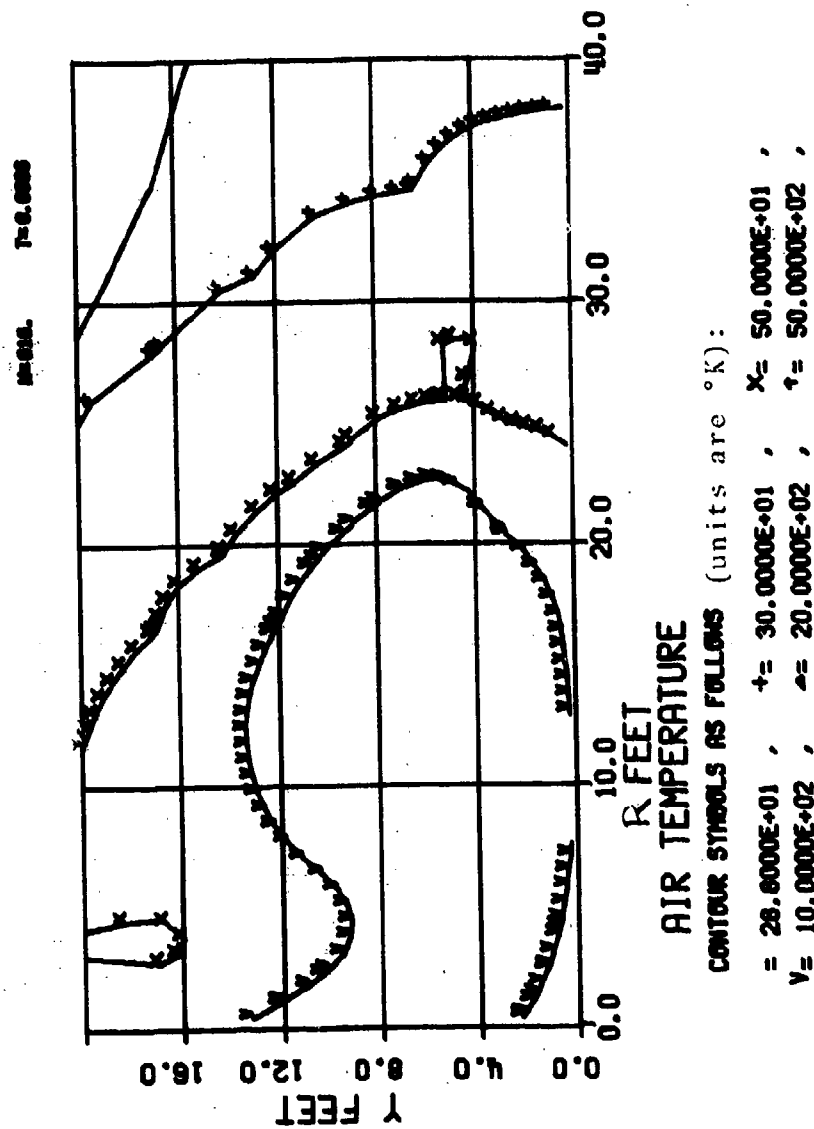
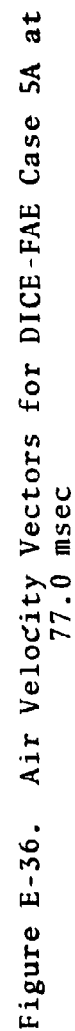


Figure E-35. Air Temperature Contours for DICE-FAE
Case 5A at 69.6 msec

123



BEST AVAILABLE COPY

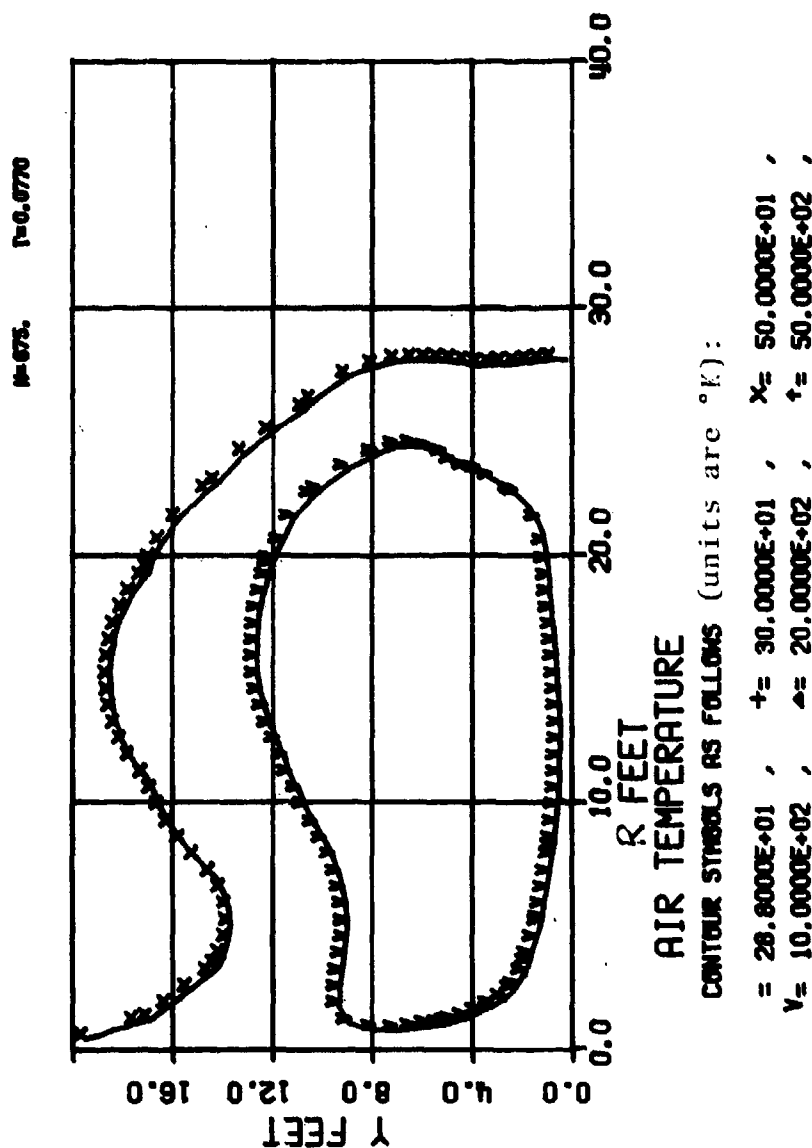


Figure E-37. Air Temperature Contours for DICE-FAE
Case 5A at 77.0 msec

APPENDIX F

DICE-FAE SOLUTION 5B:
SECOND EVENT INITIATION
BY 70G CHARGE

APPENDIX F

DICE-FAE SOLUTION 5B

DICE solution 5B is an attempt to ignite the dispersed fuel cloud of solution 5A with a SE initiator containing 70 gr of explosive, rather than the 350 gr of explosive used in solution 5A. The velocity field for solution 5B at 62 msec is shown in Figure F-1, in which the influence of the shock wave generated by the SE initiator is superimposed on the burster-induced velocities in the fuel cloud. Contours of fuel vapor density, fuel drop density, and air temperature at 62 msec are shown in Figures F-2 to F-4, where it is apparent that the *qualitative* phenomena associated with the propagation of a detonation wave are present, i.e., fuel drops within the detonating region are boiling to form fuel vapor, the fuel vapor is burning, and the temperature is elevated.

Qualitatively, these figures indicate that a propagating detonation wave has been generated. However, the detonation wave *does not propagate* through the dispersed FAE cloud. This fact is illustrated in Figure F-5 which shows the Case 5B velocity field at 66 msec. (This figure should be compared with Figure E-27 from Case 5A.) The detonation wave in Case 5B has died out because the region of initiation was lean and the shock wave generated by the initiator did not have sufficient strength to ignite the fuel when regions of more favorable fuel/air ratios were reached (even when reinforced by the energy from the fuel which did burn). This solution demonstrates the capability of the DICE-FAE code to predict the suitability of various SE ignition schemes and devices.

BEST AVAILABLE COPY

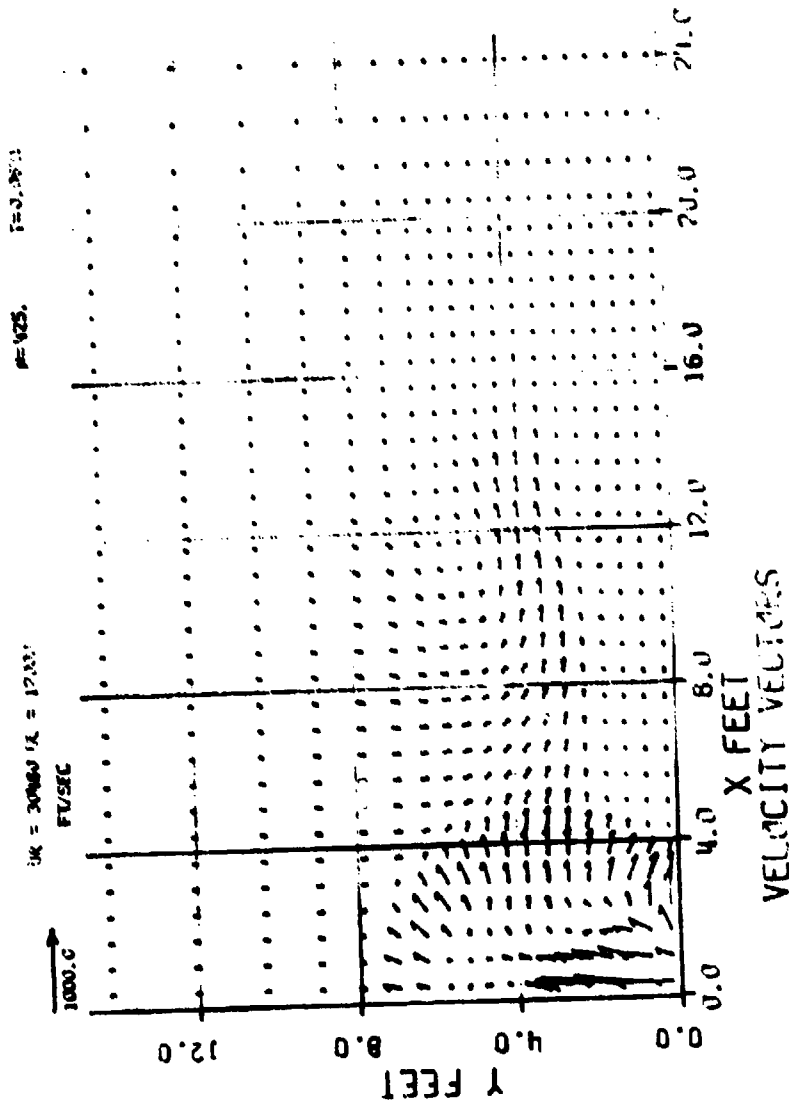
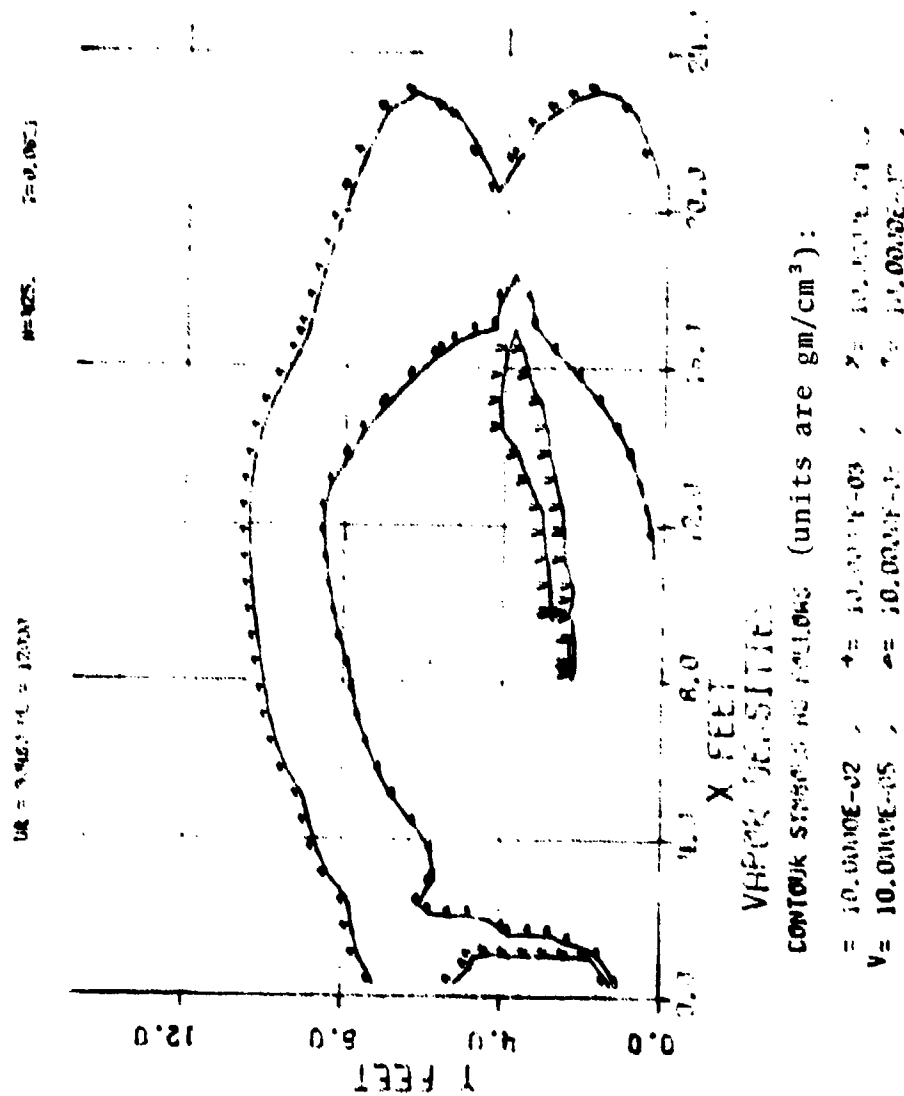


Figure F-1. Air Velocity Vectors for DICE-FAE Case 5B at 62.1 msec

BEST AVAILABLE COPY



BEST AVAILABLE COPY

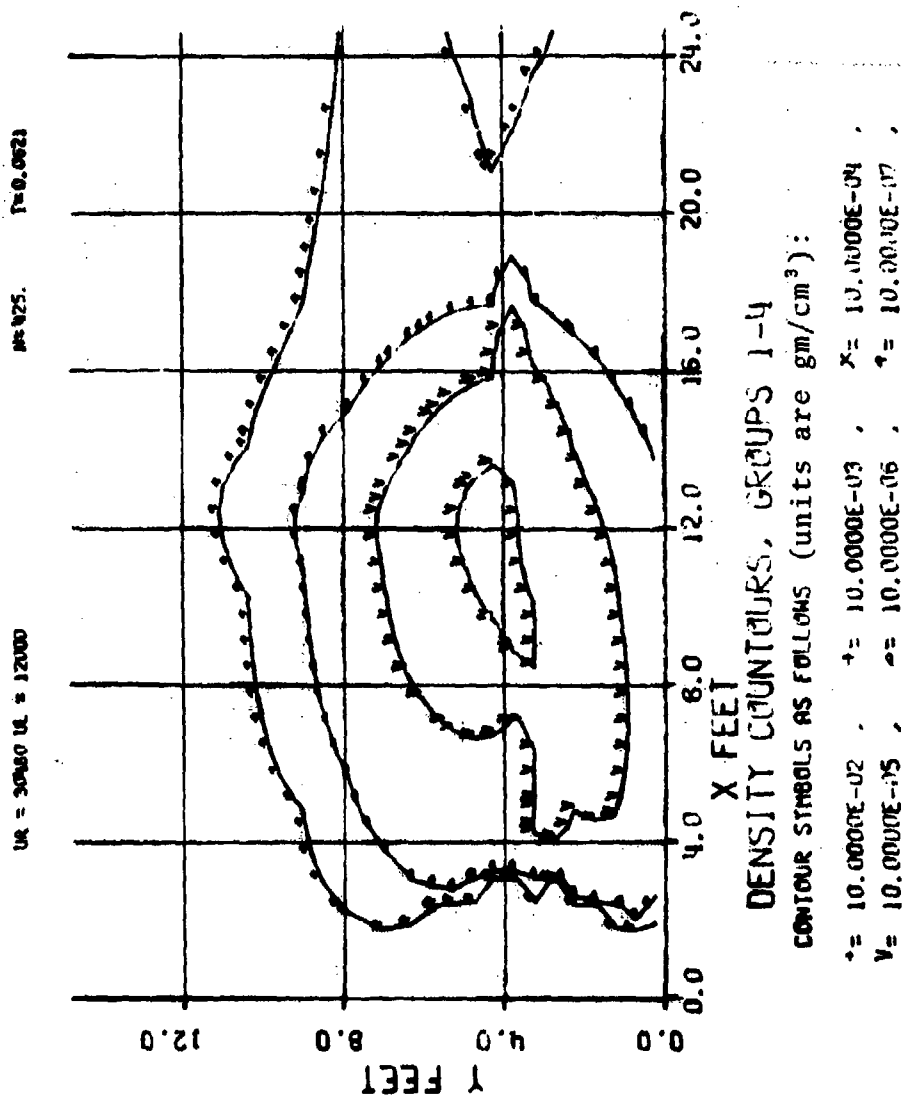


Figure F-3. Fuel Drop Density Contours for DICE-FAE
Case 5B at 62.1 msec

BEST AVAILABLE COPY

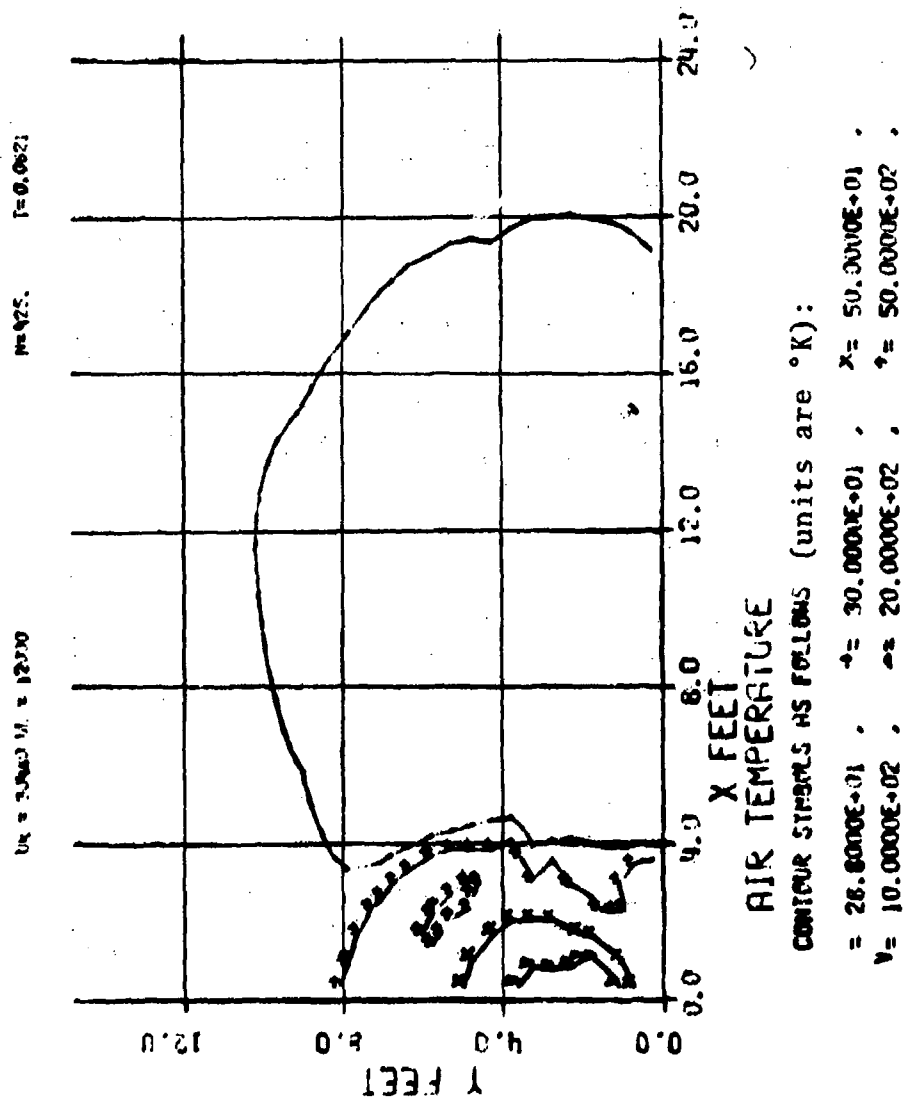


Figure F-4. Air Temperature Contours for DICE-FAE
Case 5B at 62.1 msec

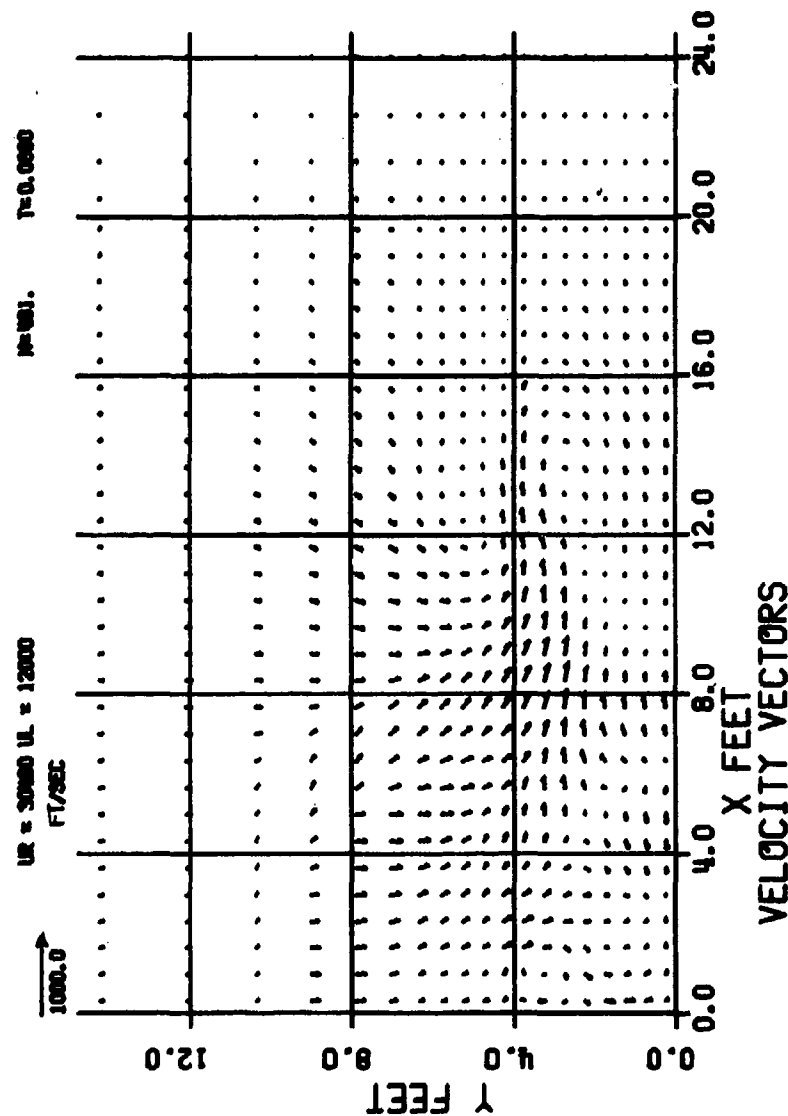


Figure F-5. Air Velocity Vectors for DICE-FAE
Case 5B at 66.0 msec

APPENDIX G

DICE-FAE SOLUTION 5C:
CLOUD EXPANSION ANALYSIS
USING SECOND-ORDER DIFFERENCING

APPENDIX G

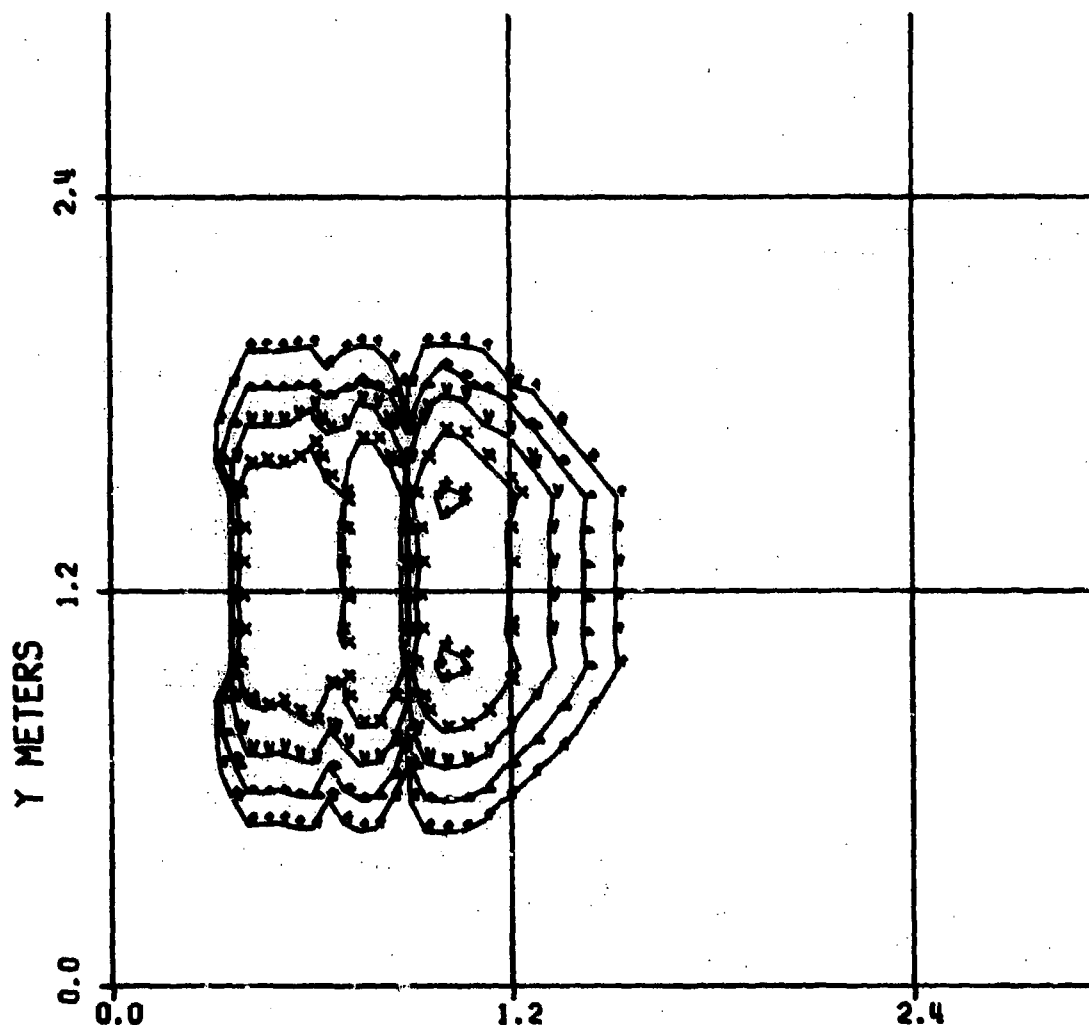
DICE-FAE SOLUTION 5C

The equations which govern the dynamics of the fuel drops in the DICE code are solved using one of two optional finite difference techniques. The first of these techniques uses a donor cell method and provides a solution which is stable under almost all conditions, but which under some circumstances may exhibit an objectionable amount of numerical diffusion. The second technique includes higher order terms in the finite difference equations, and thereby controls numerical diffusion; but requires more stringent conditions for stability. Stability here refers to the condition in which some parameter in the solution begins to "run away", reaching unrealistic values within only a few integration cycles. DICE-FAE solution 5C was an attempt to treat the fuel cloud expansion of the FAE device using second order finite differencing, rather than the donor cell approach which was used in solution 5A.

The results of solution 5C are shown in Figure G-1, where total density contours for fuel drop groups 1-4 at 2.0 msec are plotted. A vertical region at a radius of 0.9 meter in which the fuel drop density is zero appears in the figure, and is a result of the solution having gone unstable. The instability is the result of the large spatial density gradients in the fuel in the early stages of the solution. The higher order technique works best for problems characterized by relatively small spatial gradients, and could probably have been used at later times in the FAE cloud analysis when the large initial gradients had been reduced.

FRE CASE 502 UR = 30400 UL = 12000

T=0.0



X METERS
DENSITY COUNTOURS, GROUPS 1-4

CONTOUR SYMBOLS AS FOLLOWS

$\cdot = 10.0000E-02$, $\times = 10.0000E-03$, $\times = 10.0000E-04$,
 $\nabla = 10.0000E-05$, $\Delta = 10.0000E-06$, $\dagger = 10.0000E-07$.

Figure G-1. Fuel Drop Density Contours for DICE-FAE
Case 5C at 2.0 msec

BEST AVAILABLE COPY

REFERENCES

1. R. J. Zabelka and L. H. Smith, "Explosively Dispersed Liquids Part I Dispersion Model," NWC TP 4702-1, December 1969.
2. C. Kot et al, "Liquid Fuel-Air-Explosive Technology, Program," Vols. I and II, AFATL-TR-72-224, December 1972.
3. G. R. Abrahamson, et al, "Explosive Dissemination," SRI Technical Report No. 18, November 1967.
4. M. Cowperthwaite and W. H. Zwisler, "Tiger Computer Code Documentation," SRI Publication No Z106, January 1973.
5. T. H. Pierce, C. W. Kauffman, and J. A. Nicholls, "Mechanism of Ignition in Shock Wave Interactions with Reactive Liquid Droplet AIAA 13th Aerospace Sciences Meeting, AIAA Paper No 750163, Pasadena, CA January 20-22, 1975.
6. AFWL Air Equation of State, December 1971.
7. C. Marsden, "Solvents Guide," Interscience Publishers, 1963.
8. E. Condon and H. Odishaw, "Handbook of Physics," McGraw-Hill, 1958.
9. W. C. Kauffman, "Shock Wave Ignition of Liquid Fuel Drops," PhD Thesis, University of Michigan, 1971.
10. W. G. Reinecke and G. D. Waldman, "An Investigation of Water Drop Disintegration in the Region Behind Strong Shock Waves," Third International Conference on Rain Erosion and Related Phenomena, August 1970.
11. J. E. Nicholson and B. D. Figler, "Complimentary Aerodynamic Test Techniques for Rain Erosion Alleviation Studies, AIAA Aerodynamic Testing Conference, Los Angeles, California, September 21-23, 1966. AIAA Paper No. 66-766.
12. H. E. Wolfe and W. H. Andersen, "Kinetics, Mechanisms and Resultant Droplet Sizes of the Aerodynamic Breakup of Liquid Drops," Aerojet-General Corporation Report No. 0395-04 (18)-SP, Contract DA-18-108-405-CML-829, 1964.

INITIAL DISTRIBUTION

Hq USAF/RDQRM	1	Air Force Office of Scientific	
Hq USAF/SAMI	1	Research/NA	1
AFIS/INTA	1	IIT Research Inst	1
AFSC/DLCA	1	ASD/ENESS	1
AFSC/IGFG	1	California Research & Tech, Inc	10
AFWAL/Tech Lib/FL2802	1		
ASD/ENFEA	1		
FTD/PDXA-2	1		
AFWL/NSC	1		
AFWL/NSE	1		
AFWL/SUL	1		
AUL/AUL/LSE-70-239	2		
DDC	2		
Ogden ALC/MMWM	2		
TAC/DRA	1		
6510 ABG/SSD	1		
Hq USAFE/DOQ	1		
Hq PACAF/DOO	1		
Rock Island Ars/SARRI-LW	1		
Picatinny Ars/SARPA-TS-S#59	1		
Redstone Sci Info Ctr/Doc Sec	2		
USAF Waterways Experiment Stn			
WESFE	1		
Naval Rsch Lab/Code 2627	1		
NAVAIR SYS COMD/Code 530C	1		
NAVAIR SYS COMD/Tech Lib	1		
Naval Surface Wpn Ctr/Tech Lib	2		
Naval Ord Stn/Tech Lib	1		
Naval Air Test Ctr/Tech Pubs	2		
USNWC (Code 533)/Tech Lib	1		
Sandia Lab/Tech Lib Div 3141	1		
The Rand Corp	1		
TACTEC	1		
TAWC/TRADOCLO	1		
AFATL/DL	1		
AFATL/DLOSL	9		
AFATL/DLJ	1		
AFATL/DLJW	5		
USNWC/Code 326	1		
Naval Wpns Eval Fac/Wpns	1		
Univ of Mich/Dept of Aerospace			
Engineering	1		
Univ of Ill/Dept of Aeronautical			
Engineering	1		
Ohio State Univ/Dept of Aero-			
nautical Sciences	1		